

Calcium Dynamics and Intercellular Communication in Arterial Smooth Muscle Cells in Vitro

THÈSE N° 4957 (2011)

PRÉSENTÉE LE 17 FÉVRIER 2011
À LA FACULTÉ SCIENCES DE BASE
LABORATOIRE DE BIOPHYSIQUE CELLULAIRE
PROGRAMME DOCTORAL EN PHYSIQUE

ÉCOLE POLYTECHNIQUE FÉDÉRALE DE LAUSANNE

POUR L'OBTENTION DU GRADE DE DOCTEUR ÈS SCIENCES

PAR

Nadia HALIDI

acceptée sur proposition du jury:

Prof. O. Schneider, président du jury
Prof. J.-J. Meister, directeur de thèse
Prof. J.-L. Bény, rapporteur
Prof. G. Dietler, rapporteur
Prof. B. Hinz, rapporteur



ÉCOLE POLYTECHNIQUE
FÉDÉRALE DE LAUSANNE

Suisse
2011

Résumé

Le flux sanguin dans les tissus est contrôlé par les variations du diamètre des artères et des artérioles, lui-même coordonné par les contractions et relaxations des cellules musculaires lisses (SMCs) de la paroi artérielle. L'état de contraction des SMCs est principalement régulé par leur concentration intracellulaire de Ca^{2+} ($[\text{Ca}^{2+}]_i$). Une augmentation de la $[\text{Ca}^{2+}]_i$, en réponse à des stimuli, peut se propager de cellule en cellule, comme une vague intercellulaire de Ca^{2+} le long de la paroi artérielle et peut activer les processus de contraction. Le but de cette thèse est d'élucider les mécanismes sous-jacents à la propagation de la vague intercellulaire de Ca^{2+} entre les SMCs.

Dans la première partie, nous avons utilisé une lignée de SMCs issues de l'aorte du rat, les cellules A7r5, chargées avec un marqueur fluorescent, le Fluo-4, afin d'étudier la propagation de la vague intercellulaire de Ca^{2+} . Une stimulation mécanique locale a produit une vague de Ca^{2+} intracellulaire dans la cellule stimulée qui n'est pas parvenue à se propager aux cellules avoisinantes. En utilisant des cellules de culture primaire provenant d'artères méésentériques de rat (pSMCs) à la place des cellules A7r5, une propagation de la vague intercellulaire de Ca^{2+} a été observée. Afin de comprendre la différence de communication intercellulaire à travers les jonctions communicantes existantes entre les cellules A7r5 et les pSMCs, nous avons analysé l'expression des connexines37 (Cx37), Cx40, Cx43 et Cx45. Des analyses de protéines et d'ARN ont démontré que la Cx40 - contrairement aux cellules A7r5 - n'est pas exprimée dans les pSMCs. Pour confirmer que la co-expression des Cx40 et Cx43 interférait avec la communication intercellulaire, nous avons utilisé des cellules 6B5N, un clone des cellules A7r5 exprimant un rapport Cx43:Cx40 plus élevé. Cette communication intercellulaire, évaluée par le transfert du Jaune Lucifer ainsi que par la propagation des vagues calciques, était similaire entre les cellules 6B5N et les pSMCs. La propagation de la vague de Ca^{2+} était inhibée avec le peptide connexine-mimétique ⁴³Gap 26, qui cible la Cx43. Nos résultats démontrent que les jonctions communicantes formées de Cx43 sont principalement impliquées dans la médiation des vagues intercellulaires de Ca^{2+} entre les pSMCs et que la co-expression de la Cx43 avec la Cx40 peut interférer avec la formation des jonctions communicantes uniquement constituées de Cx43, affectant ainsi la communication cellulaire.

Dans la seconde partie, nous avons utilisé une technique d'impression par microcontacts pour cultiver des pSMCs sur des bandes de collagène. Cet alignement de cellules facilite l'observation de la propagation de la vague de Ca^{2+} entre cellules voisines. Afin d'induire une vague de Ca^{2+} , une pSMCs a été stimulée localement à l'aide d'une micropipette (simulation mécanique transitoire) ou par stimulation local de KCl. Une stimulation mécanique a produit deux vagues de Ca^{2+} distinctes: 1) une vague rapide (~ 2 mm/s) se propageant à toutes les cellules avoisinantes observées et 2) une vague lente (~ 20 $\mu\text{m/s}$) dont la propagation est limitée spatialement. Le KCl a induit seulement des vagues de Ca^{2+} rapides de même vitesse que les vagues rapides induites par stimulation mécanique. L'inhibition des jonctions communicantes, des canaux calciques dépendant du potentiel membranaire, des récepteurs à l'inositol 1,4,5-trisphosphate (IP_3) et des récepteurs à la ryanodine, montrent que la vague rapide est provoquée par une dépolarisation de la membrane cellulaire se propageant à travers les jonctions communicantes et induisant une entrée de Ca^{2+} dans la cellule, alors que la vague lente est principalement due à une libération de Ca^{2+} à travers les récepteurs IP_3 . Ensemble, ces résultats suggèrent un mécanisme par lequel les vagues intercellulaires de Ca^{2+} peuvent se propager le long des SMCs de la paroi artérielle.

Mots-clés: cellules musculaires lisses, connexin43, jonctions communicantes, vagues calciques, canaux calciques dépendant du potentiel membranaire, inositol 1,4,5-trisphosphate

Abstract

Tissue blood flow is controlled by changes in the diameter of the arteries and arterioles through coordinated contraction and relaxation of smooth muscle cells (SMCs) within the vascular wall. The contraction of SMCs is primarily regulated by the intracellular Ca^{2+} concentration ($[\text{Ca}^{2+}]_i$). An increase in $[\text{Ca}^{2+}]_i$, in response to stimuli, can propagate from cell to cell, as an intercellular Ca^{2+} wave along the vessel wall and can activate the process of contraction. The aim of this thesis is to elucidate the mechanisms underlying intercellular Ca^{2+} wave propagation between SMCs.

In the first part of this thesis, we used A7r5 cells, a rat aortic SMC line, loaded with the fluorescent Ca^{2+} dye Fluo-4 to study intercellular Ca^{2+} wave propagation. Local mechanical stimulation evoked a Ca^{2+} wave in the stimulated cell that failed to propagate to neighboring cells. Using primary cultured rat mesenteric smooth muscle cells (pSMCs) instead, intercellular Ca^{2+} wave propagation was observed. To understand the difference in junctional communication between A7r5 and pSMCs, we investigated the expression of connexin37 (Cx37), Cx40, Cx43 and Cx45. RNA and protein analysis demonstrated that Cx40 – in contrast to A7r5 cells – is not expressed in pSMCs. To confirm that coexpression of Cx40 and Cx43 interfered with junctional communication, we used 6B5N cells, a clone of A7r5 cells with a higher Cx43:Cx40 expression ratio. Junctional communication, assessed by transfer of Lucifer Yellow and propagation of Ca^{2+} waves, was comparable between 6B5N cells and pSMCs. In addition, Ca^{2+} wave propagation was inhibited with the connexin-mimetic peptide $^{43}\text{Gap} 26$, that targets Cx43. Our results demonstrate that Cx43 gap junctions are primarily involved in mediating intercellular Ca^{2+} waves between pSMCs, and the coexpression of Cx43 with Cx40 may interfere with Cx43 gap junction formation, affecting cell-cell communication.

In the second part of this thesis, we applied the microcontact printing technique to culture pSMCs on collagen lines. The aligned arrangement of the cells facilitates the observation of Ca^{2+} wave progression from one cell to another. To induce a Ca^{2+} wave, a single pSMC was locally stimulated with a micropipette (transient mechanical stimulation) or by microinjection of KCl. Mechanical stimulation evoked two distinct Ca^{2+} waves: 1) a fast wave (~ 2 mm/s) that propagated to all observed neighbouring cells, and 2) a slow wave (~ 20 $\mu\text{m/s}$), that was most often limited in propagation

to the first cell. KCl induced only fast Ca^{2+} waves of the same velocity as the mechanically-induced fast waves. Inhibition of gap junctions, voltage-operated calcium channels, inositol 1,4,5-trisphosphate (IP_3) and ryanodine receptors, showed that the fast wave was due to gap junction mediated membrane depolarization and subsequent Ca^{2+} influx, whereas, the slow wave was due to Ca^{2+} release primarily through IP_3 receptors. Together, these results suggest a mechanism by which intercellular Ca^{2+} waves can propagate between SMCs of the arterial wall.

Keywords: smooth muscle cells, connexin43, gap junctions, calcium waves, voltage-operated calcium channels, inositol 1,4,5-trisphosphate

Acknowledgments

Je tiens à remercier mon directeur de thèse, le Professeur Jean-Jacques Meister pour la confiance et la liberté qu'il m'a accordées, ainsi que pour ses conseils et encouragements.

Je remercie également le Professeur Jean-louis Bénny et le Dr. François-Xavier Boittin de l'Université de Genève pour leur collaboration, nos nombreuses discussions, leur passion et leurs encouragements.

Je remercie le Professeur Jacques-Antoine Haefliger et Florian Alonso de l'Université de Lausanne pour leur collaboration au chapitre 4, ainsi que les discussions, leur amitié et leur soutien.

Un grand merci au Dr. Michèle Koenigsberger et Dr. Dominique Seppey pour leur disponibilité et toutes les discussions que nous avons eu. Merci à toi, Aurélie pour m'avoir tout appris sur le monde des cultures primaires.

I am grateful to Dr. Lysianne Follonier Castella, Dr. Lara Buscemi and Dr. Alexander B. Verkhovsky for their selfless help, their suggestions and the discussions.

Je tiens aussi à remercier vivement Josiane Smith-Clerc pour son aide technique, mais surtout pour son amitié et pour m'encourager à apprendre le français. Sans toi Josiane, j'aurais perdu toute motivation.

I would like to thank all the members of the Laboratory of Cell Biophysics, in particular our secretary Brigitte Ramuz, as well as my open space officemate Rubin Berek Pisarek for their friendship and the nice atmosphere. Un grande grazie a Chiara Gabella e al neo dottore Maxime Fournier per aver portato un raggio di sole nel laboratorio.

Je remercie l'équipe du BIOP et les animaliers du CAV pour leur disponibilité et leur aide.

I thank the members of the jury for their constructive remarks.

Hálás vagyok szüleimnek és testvéremnek, Humannak, azaz Mr. Humi the Great-nek. Hálás vagyok nektek, hogy mindvégig támogattatok és bízattatok.

Gábor! Neked külön köszönettel tartozom, a türelemért, a támogatásért, a kéziratok és e disszertációhoz fűzött értékes megjegyzésekért és a rengeteg segítségért, de főleg azért mert mindig mosolyt varázsolsz az arcomra.

The work in this thesis was supported by the Swiss National Science Foundation.

Contents

Résumé	iii
Abstract	v
Acknowledgments	vii
1 Aim of this research	1
1.1 Introduction	1
1.2 Outline	2
2 Biophysical background	3
2.1 The arterial wall	3
2.1.1 Structure	3
2.1.2 Regulation of blood flow	4
2.1.3 Mechanical properties	5
2.1.4 Contraction of the arterial wall	7
2.2 Intracellular calcium signaling	7
2.2.1 Cellular calcium homeostasis	7
2.2.2 Intracellular calcium waves	8
2.3 Intercellular communication	10
2.3.1 Gap junction channels	10
2.3.2 Intercellular calcium waves	11
2.4 Vasomotion	12
2.4.1 Cellular background	13
2.4.2 Physiological importance	17
3 Materials and Methods	19

3.1	Explant preparation and cell culture	19
3.2	Microcontact printing	21
3.3	Fluorescence techniques	22
3.3.1	Fluorescent Ca ²⁺ dye	23
3.3.2	Fluorescence microscopy	24
3.4	Experimental setup for calcium imaging	27
3.4.1	Local mechanical stimulation	28
3.4.2	Local chemical stimulation	28
3.5	Image processing and data analysis	29
3.5.1	Ca ²⁺ wave velocity measurements	30
3.6	Scrape-loading and dye transfer with Lucifer Yellow	30
3.7	Protein analysis	31
3.7.1	RNA isolation, and quantitative RT-PCR	31
3.7.2	Western blot analysis	31
3.7.3	Immunofluorescence staining	32
3.8	Statistics	32
3.9	Chemicals and drugs	33
4	Connexin43 mediates intercellular Ca²⁺ waves	35
4.1	Introduction	35
4.2	Results	36
4.2.1	Intercellular communication in A7r5 cells and in pSMCs	36
4.2.2	Connexin expression in A7r5 cells and in pSMCs	42
4.2.3	Intercellular communication in 6B5N cells	44
4.2.4	Effects of connexin-mimetic peptides on Ca ²⁺ wave propagation	45
4.3	Discussion	47
4.4	Conclusion	49
5	Fast and slow intercellular Ca²⁺ waves	51
5.1	Introduction	51
5.2	Results	52
5.2.1	Characteristics of mechanically-induced Ca ²⁺ response in pSMCs: propagation of fast and slow Ca ²⁺ waves	52
5.2.2	Role of L-type voltage-operated Ca ²⁺ channels in the propagation of fast Ca ²⁺ waves	56

5.2.3	Role of extracellular calcium in the propagation of slow Ca^{2+} waves	58
5.2.4	Local KCl-induced Ca^{2+} response	59
5.2.5	Calcium release from intracellular stores; IP_3 receptors and Ryanodine receptors	59
5.2.6	Effects of multiple stimuli	60
5.3	Discussion	64
5.3.1	Propagation of fast and slow Ca^{2+} waves: a general characterization	64
5.3.2	Propagation of fast Ca^{2+} waves depends on the propagation of membrane depolarization	65
5.3.3	Propagation of the slow Ca^{2+} waves requires functional IP_3 receptors	65
5.3.4	Transmission of the slow Ca^{2+} waves to neighboring cells through gap junctions: transjunctional delay	66
5.3.5	Role of the second stimulation in enhancing the range of slow Ca^{2+} wave propagation	67
5.4	Conclusion	68
6	Conclusions	69
7	Perspectives	71
7.1	Experimental perspectives	71
7.1.1	Characterization of Cx43 and Cx40 protein interaction	71
7.1.2	Regulation of Cx43 gap junction assembly by cAMP .	72
7.1.3	Expression of Cx43 in pSMCs at different passages and implication on function	73
7.1.4	Propagation of depolarization and its influence on the slow Ca^{2+} waves	74
7.1.5	Ca^{2+} release in arterial segments: IP_3 Rs vs. RyRs . .	75
7.1.6	The effect of temperature	75
7.1.7	PSMCs can contract if cultured on deformable substrates	75
7.2	Model perspectives	76
	Appendices	79
A	Chemical stimulation	79

A.1	Background stimulation	79
A.2	Local AVP stimulation	80
B	Model equations	83
B.1	A model for Ca^{2+} waves	83
B.2	Gap junctional communication	85
B.3	Parameters	86
	Bibliography	89
	Curriculum Vitæ	105

1.1 Introduction

Most muscular arteries and arterioles undergo rhythmic diameter variations which appear to be uncorrelated with external influence, e.g., heart-beat. This phenomenon, termed vasomotion, is due to the coordinated contraction and relaxation of smooth muscle cells (SMCs) present in the arterial wall. Contraction of SMCs plays a key role in the control of hemodynamic resistance, and thus blood circulation.

The contractile state of SMCs is regulated primarily by cytosolic Ca^{2+} concentration ($[\text{Ca}^{2+}]_i$). An increase in $[\text{Ca}^{2+}]_i$ can propagate between the SMCs, as an intercellular Ca^{2+} wave. This has been reported to be associated with the propagation of contraction along a vessel segment. The mechanisms underlying the propagation of intercellular Ca^{2+} waves, however, are yet to be clarified.

The aim of this thesis is to investigate cell-cell communication between vascular SMCs *in vitro* at the cellular level, with a particular focus on intercellular Ca^{2+} wave propagation. One main advantage of cellular studies is that the methods and spatiotemporal resolution used could be quite difficult, if not impossible, to perform on the whole tissue. Cellular studies can provide tremendous insights into the cellular events that modulate tissue physiology.

In the first part of this thesis, we characterize the gap junction proteins involved in mediating intercellular Ca^{2+} waves, whereas in the second part, we study the mechanisms underlying the propagation of intercellular Ca^{2+} waves between SMCs.

1.2 Outline

This thesis is structured as follows:

Chapter 2 provides an introduction to the research work presented in later chapters. It describes the research background and explains the motivation for pursuing this work. In addition it provides an overview of the approach taken.

Chapter 3 gives a detailed account of the procedure that was followed in completing the experiments discussed in this thesis. A list of chemicals and drugs used, including their preparation is provided at the end of this chapter.

Chapter 4 presents results on the characterization of the vascular SMCs used in terms of connexin expression and the involvement of connexin43 gap junction channels in mediating intercellular calcium waves in primary cultured rat mesenteric smooth muscle cells. This work was performed in collaboration with the group of Prof. Jacques-Antoine Haefliger, Department of Internal Medicine, CHUV, Lausanne, Switzerland, and Prof. Janis M. Burt, Department of Physiology, University of Arizona, Tucson, AZ, USA.

Chapter 5 presents results of our analysis on mechanically-induced intercellular calcium wave propagation in primary cultured smooth muscle cells. In these experiments, cells were aligned along a collagen line using the microcontact printing technique.

Chapter 6 presents general conclusions of this thesis.

Finally, Chapter 7 suggests some possible directions for future experimental and theoretical research.

Appendix A contains supplementary data on chemical stimulation, and Appendix B contains the description of the mathematical model that was referred to in Chapter 7.

2.1 The arterial wall

The vascular system is composed of three subsystems: arteries, capillaries and veins. The arteries conduct oxygenated blood from the heart to the peripheral tissue and consist of various generations of arteries including elastic arteries, muscular arteries and arterioles. In this thesis we study muscular arteries.

2.1.1 Structure

Muscular arteries are composed of three distinct layers: tunica intima, tunica media and tunica adventitia. The proportion and structure for each layer varies with the size and function of the particular artery. The structure of a muscular artery is shown in Fig. 2.1.

The inner layer, the tunica intima, consists of a single layer of endothelial cells (ECs), internal elastic lamina and fibrocollagenous tissue. The ECs are in direct contact with the blood and aligned along the direction of the blood flow. ECs sense, integrate hemodynamic and hormonal stimuli and regulate vascular function through the secretion of various mediator proteins and molecules. The middle layer, the tunica media, is the thickest layer in muscular arteries and consists of almost entirely of smooth muscle cells (SMCs) arranged in multiple layers, and of external elastic lamina. SMCs are primarily aligned in the circumferential direction of the vessel axes. These cells are highly contractile, hence, the tunica media predominantly determines the mechanical properties of the arterial wall. The outermost layer of the arterial wall is the tunica adventitia, which consists of collagen fibers and elastic tissue. This layer provides structural support,

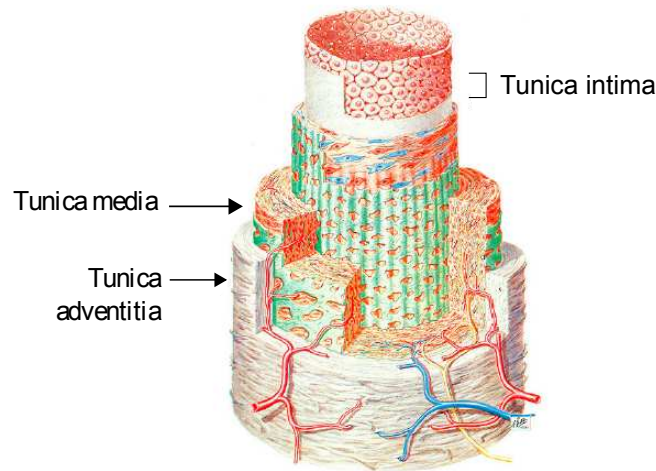


Figure 2.1: Scheme of the arterial wall structure (adapted from Kangasniemi and Opas (1997)). The artery wall consists of three layers: 1) Tunica intima: contains a single layer of endothelial cells, 2) Tunica media: composed of mainly smooth muscle cells, 3) Tunica adventitia: composed of connective tissue, collagen and elastic fibers.

mechanical strength and elasticity to the arterial wall, it also anchors the vessel to nearby organs.

The muscular arteries studied in this thesis were of first- and second-order rat superior mesenteric arteries originating from the anterior surface of the abdominal aorta. These arteries supply the intestine from the lower part of the duodenum through two-thirds of the transverse colon, as well as the pancreas. Their diameter is $\sim 300/400 \mu\text{m}$ (inner/outer) and they are composed of two to three concentric layers of SMCs (Walker-Caprioglio et al., 1991).

2.1.2 Regulation of blood flow

The primary function of the vascular system is to conduct oxygenated blood from the heart to tissues and return the deoxygenated blood from the tissues to the heart. To ensure functioning of this circulatory system, coordinated control of regional blood flow is required. Blood flow is determined by two factors. First, the force that pushes the blood through the vessel i.e., blood pressure, and second, the resistance of the vessels to

the blood flow i.e., vascular resistance. Mathematically, blood flow, Q , is described by Poiseuille's Law:

$$Q = \frac{\pi(P_i - P_o)r^4}{8\eta l} \quad (2.1)$$

Q is linearly proportional to the pressure difference, $P_i - P_o$, and the fourth power of the radius, r , of the vessel tube, and it varies inversely with the vessel length l and the viscosity, η , of the blood. P_i and P_o are the pressures at the inflow and outflow ends, respectively. Eq. 2.1 shows, that even small changes in artery diameter have significant impacts on flow regulation.

The rate of blood flow is measured in milliliters or liters per minute. The blood flow in the entire human circulation is about 5000 ml/min at rest in an average sized adult, but can reach 5 – 6 fold greater values during heavy exercise, when the body needs more oxygen.

Vascular resistance could be viewed as the electrical resistance R in electromagnetism, where, in accordance with Ohm's law, the resistance R is defined as the ratio of voltage drop, U , to current flow, I ($R = U/I$). Similarly, in fluid mechanics the hydraulic resistance R , could be defined by the ratio of pressure drop $P_i - P_o$, to flow, Q . By rearranging Poiseuille's law, the hydraulic resistance equation yields:

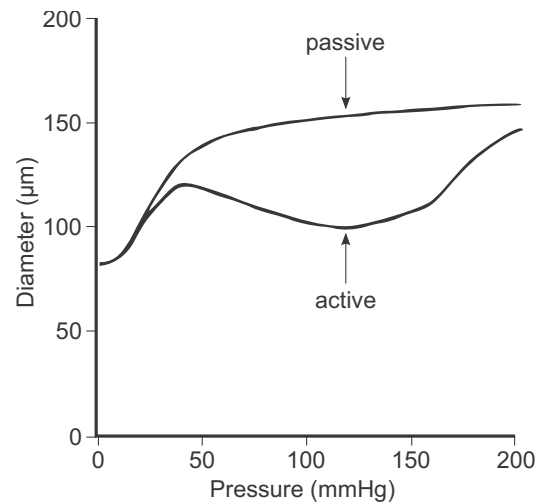
$$R = \frac{P_i - P_o}{Q} = \frac{8\eta l}{\pi r^4} \quad (2.2)$$

Thus, the resistance to flow depends only on the dimensions of the vessel and on the characteristics of the fluid.

2.1.3 Mechanical properties

Changes in vascular resistance induced by natural stimuli, e.g., hormones, occur through changes in radius. This is achieved by alterations in the contraction of the SMCs in the vessel wall. However, changes in internal pressure also alters the caliber of the blood vessel, and therefore alters the resistance to blood flow. Vessels are elastic tubes, the greater the difference between the internal and external pressure, i.e., transmural pressure, the greater will be the caliber of the vessel, and the less will be its hydraulic resistance. Transmural pressure acts perpendicularly to the layers of ECs

Figure 2.2: Pressure-diameter relationships for rat mesenteric arteries *in vitro* under passive and active conditions (adapted from Bund (2001)). The passive condition (absence of muscular tone) was mimicked by performing the experiment in a calcium free physiological solution.



and SMCs and creates a circumferential stress, and to shear stress resulting from friction of blood flow with the EC layer. Both types of mechanical stress modulate vascular tone.

Studies of pressure-diameter relationships permitted the analysis of the passive and active mechanical properties of the arterial wall. Passive mechanical properties are directly related to the intrinsic properties of the arterial wall, such as its elastic modulus; its value varies in function of stress or pressure (Fig. 2.2, upper curve). Another mechanical property is the viscoelasticity, i.e., when a force is applied there exists a time lag before the arterial wall responds with diameter variation. This indicates that the mechanical properties depend also on the rate of change of stress.

Active mechanical properties, on the other hand, are strongly affected by the smooth muscle tone. In an active condition, the diameter of the arterial wall at a given pressure is smaller than that in the passive condition due to the contraction of SMCs (Fig. 2.2, lower curve). An increase in pressure causes an increase in circumferential stress. This stress causes the SMCs in arterial wall to contract. A decrease in pressure induces a relaxation of the SMCs, which may lead to vessel dilatation. The contractile response of the SMCs in response to pressure rise is termed myogenic response and is shown in Fig. 2.2. The first report of this phenomenon is credited to William Bayliss in 1902 (Bayliss, 1902). The myogenic response is well established as a control mechanism for regulating both flow and pressure in the vascular system.

2.1.4 Contraction of the arterial wall

Arterial contraction is caused by the contraction of SMCs layered circumferentially in the tunica media of the arterial wall, playing an important role in the control of hemodynamic resistance. When made to contract, the SMCs shorten and change the diameter of the vessel.

Regardless of the stimulus, all SMCs produce force and contraction through cross-bridge cycling, when actin filaments slide past myosin filaments, without changing their length. The muscle shortens as the myosin phosphorylation makes the myosin heads interact cyclically with active sites on actin. The energy required for this process is provided by the hydrolysis of ATP. This process is regulated by the cytosolic Ca^{2+} concentration which determines the degree of myosin phosphorylation (Hilgers and Webb, 2005; Wynne et al., 2009).

2.2 Intracellular calcium signaling

Cytosolic Ca^{2+} is a versatile cellular signal. It is involved in many different cellular functions ranging from fertilization, proliferation and differentiation to secretion and contraction (for reviews see Berridge et al. (2000) and Clapham (2007)). In this section, we briefly discuss intracellular calcium signaling in SMCs.

2.2.1 Cellular calcium homeostasis

Calcium homeostasis refers to the regulation of Ca^{2+} concentration in the cell. This parameter is tightly controlled. Precise maintenance of the physiological levels of both extracellular and intracellular ionized calcium is essential to life.

The cytosolic free calcium ion concentration ($[\text{Ca}^{2+}]_i$) in cells at rest is around 100 nM, which is 10 000 times lower than the extracellular concentration. In addition to this steep concentration gradient, there is an electrical gradient because of the negative resting membrane potential. In the cell, Ca^{2+} is either in free form in the cytosol, bound to proteins or other molecules or trapped in huge concentrations (~1 mM) within cellular compartments such as the sarcoplasmic reticulum (SR) and the mitochondria (M). Fig. 2.3 presents the most important cellular components involved

in Ca^{2+} dynamics in a single SMC. Almost all Ca^{2+} signaling systems have one thing in common – upon stimulation (e.g., agonist, mechanical or electrical stimulation) they generate brief pulses of Ca^{2+} . Ca^{2+} is either derived from internal stores or from the external medium through several types of Ca^{2+} channels. Receptor-operated channels (ROCs) open directly upon interaction with their ligand (e.g., glutamate receptor and purinergic receptors). Voltage-operated calcium channels (VOCCs) open upon membrane depolarization. Stretch-activated channels (SACs) open upon mechanical stress. Store-operated channels (SOCs), that open upon the depletion of SR have been also suggested. Ca^{2+} can be released from the SR via two families of receptor-channels: inositol 1,4,5-trisphosphate (IP_3) receptor (IP_3R) channels (Foskett et al., 2007) and ryanodine (Ry) receptor (RyR) channels (Fill and Copello, 2002). The activation of IP_3Rs requires the binding of both second messengers, Ca^{2+} and IP_3 , whereas, RyRs are activated by binding of Ca^{2+} . The formation of IP_3 is initiated by a family of G-protein linked receptors on the cell membrane which activate phospholipase C (PLC) to generate IP_3 (Berridge, 2009).

The basal $[\text{Ca}^{2+}]_i$ is kept low by pumps and exchangers that move Ca^{2+} from the cytosol to internal stores or across the cell membrane. The membrane $\text{Na}^+/\text{Ca}^{2+}$ exchanger (NCX) is able to exchange 3 Na^+ for 1 Ca^{2+} . It uses the electrochemical gradient of Na^+ to extrude Ca^{2+} . The mitochondria (M) also play an important role in Ca^{2+} dynamics. The released Ca^{2+} from the SR activates the low affinity electrophoretic uniporters on the mitochondria membrane for rapid Ca^{2+} uptake. Ca^{2+} can exit the mitochondria through the NCX (Berridge et al., 2003). The plasma membrane Ca^{2+} -ATPase (PMCA) and the SR Ca^{2+} -ATPase (SERCA) requires energy from the hydrolysis of ATP to extrude Ca^{2+} against its concentration gradient.

Other ionic channels or pumps (e.g., Cl^- and K^+ channels, Na^+/K^+ exchangers) also regulate ionic fluxes. These fluxes regulate membrane potential and thus $[\text{Ca}^{2+}]_i$.

2.2.2 Intracellular calcium waves

Using digital imaging techniques, fluorescence microscopy and fluorescent Ca^{2+} indicators, it is possible to examine the spatial and temporal distribution of Ca^{2+} in the cell. At the cellular level, agonist or mechani-

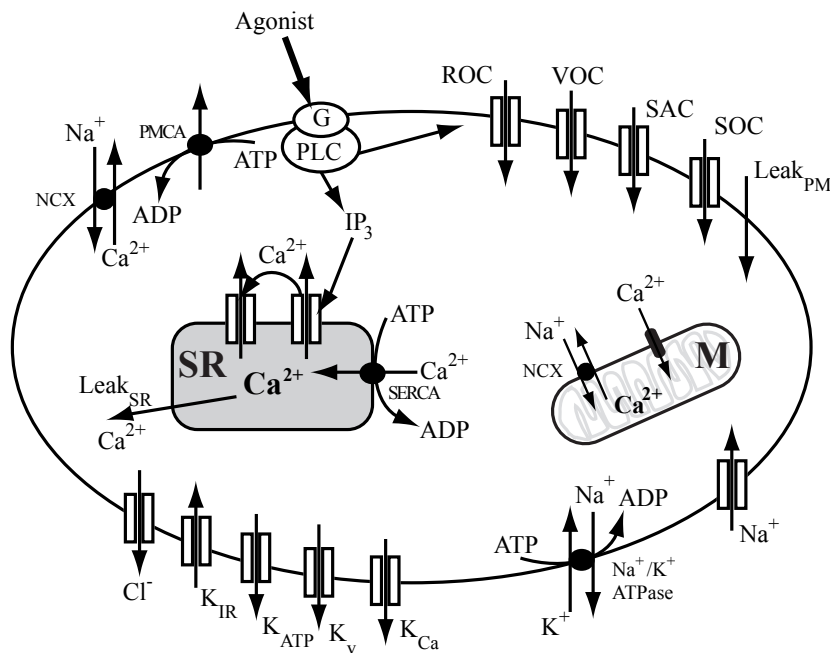


Figure 2.3: Calcium homeostasis in a single smooth muscle cell (adapted from Porret (1997)). *G*: G protein; *PLC*: phospholipase C; *ROC*: receptor-operated channel; *VOC*: voltage-operated calcium channel; *SAC*: stretch-activated channel; *SOC*: store-operated channel; *NCX*: $\text{Na}^+/\text{Ca}^{2+}$ exchanger; *Leak_{PM}*: leak currents through the plasma membrane; *K_{Ca}*: calcium-activated potassium channel; *K_v*: voltage-gated potassium channel; *K_{ATP}*: ATP-activated potassium channel; *K_{IR}*: inward-rectifier potassium channel.

cal stimulation initiates an increase in $[\text{Ca}^{2+}]_i$ at a discrete sites in the cell. This local Ca^{2+} rise progresses as a traveling spatial gradient of Ca^{2+} , as an intracellular Ca^{2+} wave. A consistent characteristics of Ca^{2+} waves is that they do not represent simple diffusion of the released Ca^{2+} , but involve a regenerative release of Ca^{2+} . It is likely that wave propagation also involves diffusion of a trigger for Ca^{2+} release.

Two principal mechanisms have been proposed for Ca^{2+} wave propagation: 1) Following IP_3 generation, a primary release of Ca^{2+} via IP_3Rs initiates further Ca^{2+} release at RyRs , a process known as Ca^{2+} -induced Ca^{2+} -release (CICR); waves propagate independently of IP_3Rs , and RyRs act as the major channel responsible for further Ca^{2+} release and Ca^{2+} wave propagation (Boittin et al., 1999; Ruehlmann et al., 2000; Balemba et al., 2006). 2) IP_3Rs are activated first allowing primary release of Ca^{2+} .

Then IP₃Rs may serve as sites for CICR, being opened by released Ca²⁺ in a positive feedback process (Iino et al., 1994; McCarron et al., 2004; Bai et al., 2009). The precise mechanisms underlying Ca²⁺ wave propagation in SMCs are still being investigated. In Chapter 5 we discuss Ca²⁺ wave propagation mechanisms in primary cultured mesenteric smooth muscle cells and we test which of the receptors, IP₃Rs or RyRs are involved in the CICR mechanism.

2.3 Intercellular communication

In vascular SMCs Blatter and Wier (1992) were the first to demonstrate that [Ca²⁺]_i oscillations take the form of waves of Ca²⁺ travelling parallel to the long axis of the cells. Iino et al. (1994) reported a similar behavior of SMCs in the intact vascular wall. Following these observations, intercellular Ca²⁺ waves have been reported in SMCs from many different vessels (for a review see Lee et al. (2002)). Cell-cell communication, and intercellular Ca²⁺ wave propagation between SMCs in the vascular wall are mediated by gap junctions. Intercellular signalling through gap junctions contribute to coordination and synchronization of the connected cells' function (Segal and Kurjiaka, 1995; Bény, 1999; Figueroa and Duling, 2009).

2.3.1 Gap junction channels

Gap junctions are intercellular channels that allow the direct exchange of ions (e.g., Na⁺, K⁺, Ca²⁺, H⁺) and small molecules (e.g., nucleotides, IP₃, glucose) with molecular masses less than 1 kDa, thereby coupling the cells both electrically and metabolically (Evans et al., 2006; Meşe et al., 2007). Gap junctions are formed of a family of proteins termed connexin (Cx). Six connexin subunits form a connexon, a hemichannel that docks to another hemichannel of a neighboring cell, forming together a gap junction channel (Fig. 2.4 A, B & C).

More than 20 different Cx proteins have been identified of which four, connexin37 (Cx37), Cx40, Cx43 and Cx45, are predominantly expressed in the vascular system (the numerical suffixes refer to the connexin's molecular weight in kDa). Coexpression of certain types of connexins, e.g., Cx40 and Cx43, may lead to the formation of mixed gap junction channels

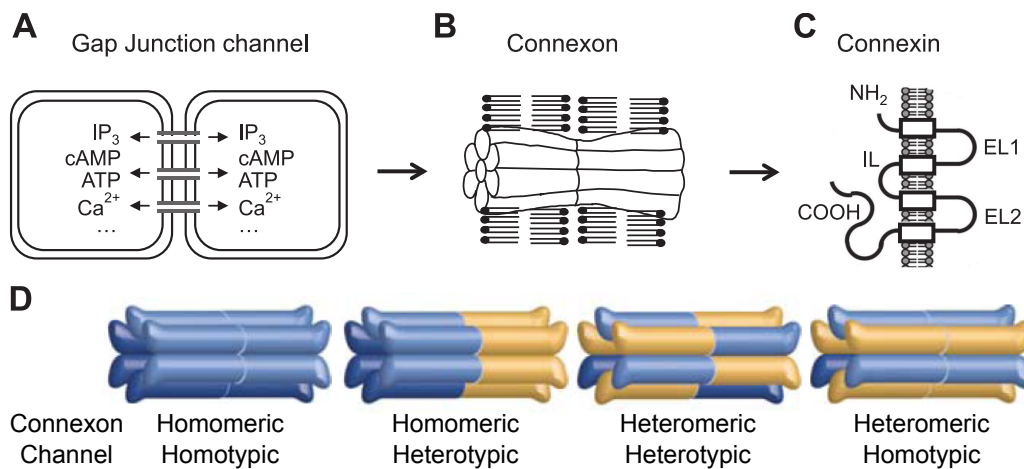


Figure 2.4: Schematic representation of connexins and gap junction channels. **A)** Gap junction channels mediate intercellular movement of cytoplasmic molecules. **B)** Gap junction channels are formed of two connexons (hemichannels) docked to another. A connexon is formed of six subunits, termed connexins. **C)** Connexins have four transmembrane domains, two extracellular loops (EL1 & EL2), an intracellular loop (IL), and cytoplasmic N- and C-termini (A, B & C adapted from Yao et al. (2009)). **D)** Possible arrangements of connexons to form gap junction channels (adapted from Meşe et al. (2007)).

(Fig. 2.4 D). Such mixed channels have distinct gating properties, possibly relevant to cell-cell communication. In Chapter 4, we study the influence of Cx40 and Cx43 coexpression on cell-cell communication.

In the vascular wall, ECs and SMCs are well coupled via gap junctions. In this context, they are termed myoendothelial gap junctions. For example, a signal of hyperpolarization in ECs is mediated to SMCs through gap junctions and induces a $[Ca^{2+}]_i$ decrease in the SMCs, leading to the dilation of the arterial wall (see Isakson et al. (2007), and Dora (2010) for a recent review).

2.3.2 Intercellular calcium waves

In multicellular systems, such as the SMCs in the vascular wall, Ca^{2+} waves are not restricted to the cytosol of one cell, but propagate to neighboring cells as intercellular Ca^{2+} waves. These intercellular Ca^{2+} signals could propagate either by paracrine effects of an extracellular diffusible messenger (e.g., ATP) or by diffusion of an intracellular messenger via gap junctions (e.g., Ca^{2+} , IP_3 , cADP-ribose). Mechanical stimulation of cells results

in Ca^{2+} release from the SR, as well as release of ATP to the extracellular medium. Extracellular diffusion of ATP activates purinergic receptors on neighboring cells (Chen et al., 1995; Young et al., 2002) and triggers the generation of IP_3 and the release of Ca^{2+} from internal stores. This Ca^{2+} release can also propagate as a wave. In this thesis, we study intercellular Ca^{2+} waves mediated exclusively by gap junction channels.

The cellular mechanisms involved in the propagation of intercellular Ca^{2+} waves in vascular SMCs are not yet clear, nor is the identity of the second messenger(s) involved in mediating these waves. In Chapter 5, we study the mechanism underlying the propagation of intercellular Ca^{2+} waves in primary cultured rat mesenteric SMCs.

2.4 Vasomotion

Many muscular vessels undergo rhythmic diameter oscillations, a phenomenon called vasomotion. Vasomotion is to some extent an intrinsic contractile behavior of the vascular SMCs generated from within the vascular wall and is independent of external input, e.g., heartbeat, respiration, or neuronal input (Aalkjaer and Nilsson, 2005). It has been first reported in detail by T. Wharton Jones in 1852 (Jones, 1852). He observed rhythmic contractions of the veins of a bat's wing, and that the blood flow was accelerated at each contraction. Since the first report, a number of experimental studies had been carried out both *in vivo* and *in vitro*, however, the cellular mechanisms responsible for the initiation of vasomotion and the physiological importance of vasomotion remain elusive.

Beside the direct demonstrations of diameter oscillations in the vessel, the presence of vasomotion had also been shown by measuring, e.g., blood-cell velocity (Fagrell et al., 1977), capillary pressure variations (Mahler et al., 1979), and laser-Doppler flow signals (Braverman et al., 1990). In human radial arteries *in vivo*, the pattern of arterial vasomotion appeared with either quasi-periodic peaks superimposed on a nearly steady component or, more often, with irregular variations (Fig. 2.5 A) (Porret et al., 1995). The high-amplitude (40 – 180 μm) and low-frequency oscillations (< 0.05 Hz) in the mean artery diameter resulted from changes in the SMC tone, i.e., from vasomotion. The insert in Fig. 2.5 A shows diameter variations due to pressure changes during the cardiac cycle. Oscillations in

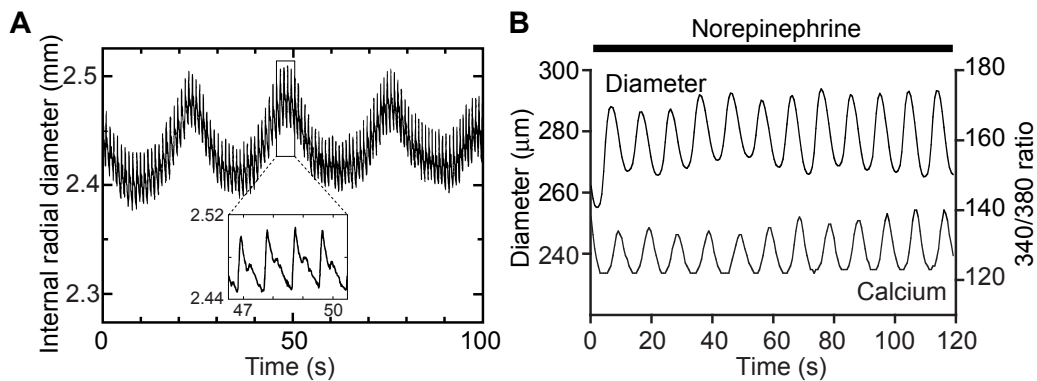


Figure 2.5: **A)** Noninvasive continuous recordings of radial artery diameter under resting conditions (from Porret et al. (Porret et al., 1995)). A prominent low-frequency oscillation in diameter is clearly seen (0.04 Hz) on which diameter variations due to pulse pressure (63 beats/min) were superimposed. **B)** Simultaneous measurement of external vessel diameter and Ca^{2+} (Fura-2 ratio 340/380 in arbitrary units) changes in rat mesenteric arteries *in vitro* during vasomotion induced by norepinephrine (adapted from Oishi et al. (2002)).

diameter and tone have been also demonstrated *in vitro* on a wide variety of isolated preparations from several animal tissues, such as rat and rabbit, in coronary artery, carotid artery, basilar artery, ear small arteries and rat mesenteric arteries. These preparations are used as models to understand the cellular mechanisms underlying vasomotion.

2.4.1 Cellular background

At the cellular level, vasomotion is associated with slow oscillations of SMCs membrane potential (Gustafsson et al., 1993) and of intracellular Ca^{2+} concentration (Peng et al., 1998; Oishi et al., 2002). Fig. 2.5 B shows that in pressurized rat mesenteric artery, application of norepinephrine induced rhythmic contractions and relaxations of the artery in parallel with $[\text{Ca}^{2+}]_i$ variations. A calcium increase in SMCs induced an arterial contraction, whereas a calcium decrease led to an arterial relaxation. Recent studies, however, showed that average vessel $[\text{Ca}^{2+}]_i$ does not represent calcium dynamics of individual SMCs within the vessel wall (Ruehlmann et al., 2000; Zang et al., 2001; Peng et al., 2001; Sell et al., 2002; Lamboley et al., 2003). In order to get a macroscopic oscillation of the vessel wall the Ca^{2+} oscillations in individual SMCs must be synchronized. Lambo-

ley et al. (2003) have demonstrated that synchronization occurs only if all SMCs are recruited, i.e., all the SMCs present Ca^{2+} changes. This could be achieved by stimulating all SMCs with a sufficiently high concentration of the vasoconstrictor agent. At low vasoconstrictor concentrations a small number of SMCs present unsynchronized Ca^{2+} transients. Increasing the vasoconstrictor concentration increases the frequency of Ca^{2+} oscillations (Ruehlmann et al., 2000; Lamboley et al., 2003), therefore, increases the probability that all SMCs display Ca^{2+} oscillations that are synchronized and vasomotion can be obtained. Very high concentrations would lead to a tonic contraction of the artery (Lamboley et al., 2003).

Calcium oscillations, waves and vasomotion

Ca^{2+} oscillations have been reported to take a form of a Ca^{2+} wave that propagates along SMCs (Blatter and Wier, 1992; Iino et al., 1994). Ca^{2+} waves are found to be associated to the propagation of contraction waves during arterial vasomotion (Seppey et al., 2010). Following these observations, it is important to understand the mechanisms underlying $[\text{Ca}^{2+}]_i$ oscillations and the propagation of Ca^{2+} waves.

The generation of Ca^{2+} oscillations is not completely understood. Inhibition of the SERCA strongly inhibited Ca^{2+} oscillations and waves, suggesting that they are caused by the release of Ca^{2+} from the SR (Miriell et al., 1999; Peng et al., 2001). This was also supported by the observation that Ca^{2+} waves were present in absence of extracellular Ca^{2+} (Iino et al., 1994; Ruehlmann et al., 2000; Peng et al., 2001). The next question is which of the receptors IP_3Rs or RyRs are primarily involved in the CICR mechanism? Acute blockade of the RyR blocks Ca^{2+} waves (Blatter and Wier, 1992; Iino et al., 1994; Boittin et al., 1999; Ruehlmann et al., 2000; Peng et al., 2001), indicating the involvement of RyR . Under some circumstances, however, CICR via the IP_3Rs is sufficient to produce Ca^{2+} waves. McCarron et al. (2004) showed that in isolated intestinal SMCs, IP_3 -induced Ca^{2+} waves are dependent on CICR, but they are only mediated via IP_3Rs and not via RyRs . It seems that CICR based Ca^{2+} waves in SMCs are mediated either via IP_3Rs or RyRs , or a combination. Whether IP_3Rs or RyRs are more important, may depend on the relative concentration of the receptors (Boittin et al., 1999), the expression and distribution of the receptor subtypes, on the SR Ca^{2+} concentration (McCarron et al., 2004), or a number of other pa-

rameters that determine sensitivity of the two receptors, but also on SMC type and condition.

Another suggested mechanism for the generation of Ca^{2+} oscillations is that $[\text{Ca}^{2+}]_i$ follows membrane potential oscillations that may be generated by membrane channels like VOCCs or Ca^{2+} activated potassium or chloride channels. However, the inhibition of VOCCs in some studies led to different results. In pulmonary artery SMCs, VOCCs are not required for Ca^{2+} oscillations (Hamada et al., 1997), neither required for vasomotion in irideal arterioles (Hill et al., 1999). In other studies, inhibition of VOCCs abolished vasomotion and reduced or abolished membrane potential oscillations (Bartlett and Segal, 2000; Oishi et al., 2002).

As mentioned earlier, changes in vasoconstrictor concentration changes Ca^{2+} oscillation frequency. This could also mean that the continuously-graded (analog) vasoconstrictor extracellular signal was converted to a frequency-encoded digital signal (number of Ca^{2+} transients). Similar dynamic behavior has been observed in several cell types. This suggests that Ca^{2+} transients and frequency encoding must have a physiological role. Recently, it had been suggested that the frequency information encoded in Ca^{2+} waves are decoded rather precisely by transcriptional factors so that different types of oscillations lead to the expression of different proteins (Lewis, 2003; Berridge et al., 2000).

Role of gap junctions

Peng et al. (2001) have demonstrated that applying a low vasoconstrictor agent, SMCs first displayed unsynchronized Ca^{2+} oscillations, but then Ca^{2+} oscillations were synchronized and vasomotion started. This result could only be obtained if the SMCs are coupled or linked together. A key element for the synchronization of the SMCs is the gap junction channels. Several studies have demonstrated that gap junction inhibitors abolished vasomotion (Tsai et al., 1995; Chaytor et al., 1997; Hill et al., 1999) and the synchronization of Ca^{2+} oscillations (Sell et al., 2002; Matchkov et al., 2004). Other experimental studies also support that the intercellular communication between SMCs is achieved through electrical communication and that the oscillations in membrane potential are responsible for the oscillations in vessel diameter (Peng et al., 2001; Aalkjaer and Nilsson, 2005). Electrical communication may be the only possible mechanism which is fast enough to coordinate responses over several millimeters of vessels.

Role of the endothelium

The role of the endothelium in vasomotion remains controversial. In some arteries, removal of the endothelium prevented vasomotion (Jackson, 1988; Gustafsson et al., 1993; Mauban et al., 2001; Peng et al., 2001; Akata et al., 1995; Kvandal et al., 2003; Okazaki et al., 2003; Haddock et al., 2006). Other studies have reported that vasomotion was observed when the endothelium was removed (Griffith and Edwards, 1993; Marchenko and Sage, 1994; Sell et al., 2002; Lamboley et al., 2003; Seppely et al., 2008). In some situations, the presence or absence of the endothelium did not have any effect on vasomotion (Chemtob et al., 1992; Freeman et al., 1995; Omote and Mizusawa, 1993; von der Weid and Bény, 1993). The studies that agree on the importance of endothelium for vasomotion, disagree on whether NO or endothelium-derived hyperpolarizing factor (EDHF) is required for the generation of vasomotion. Seppely et al. (2008) showed that vasomotion was still present in endothelium denuded arteries, however, three-fold higher agonist concentration was needed to induce vasomotion compared to arteries with intact endothelium, i.e., removal of the endothelium (or endothelium-derived factors), had to be compensated by increasing the agonist concentration. The variability of these results, even within the same tissue, may suggest that one or several factors from the endothelium are responsible for one or several pathways that are important to induce vasomotion.

Theoretical models of vasomotion

Several mathematical models have been proposed to study the mechanisms of Ca^{2+} dynamics, primarily in non-excitable cells. Only few attempts have been made to model the mechanisms of vasomotion. The model of Imtiaz et al. (2002), for instance, studied slow waves in gastrointestinal muscle, and found that IP_3 has an important role in mediating these waves. They suggested that membrane depolarization promotes IP_3 formation. In this model, membrane depolarization is assumed to propagate through gap junctions and to be responsible for synchronization.

Gonzalez-Fernandez and Ermentrout (1994) and Parthimos et al. (1999) have developed models describing the calcium dynamics of a single SMC without taking into account intercellular communication. In these models, vasomotion is caused by instabilities in ionic fluxes across the plasma

membrane or the SR. The model of Koenigsberger et al. (2004) is based on the model of Parthimos et al. (1999) expanded to a multicellular tissue by including gap junctions. Results were based on the experimental observations of Lamboley et al. (2003), and demonstrated that asynchronous Ca^{2+} transients result from stochastic opening of channels on the SR, and that arterial contraction and vasomotion emerge from a population of coupled SMCs. However, electrical coupling alone was not sufficient to induce synchronization of Ca^{2+} oscillations – a certain Ca^{2+} permeability via gap junctions was necessary.

The recent model presented by Jacobsen et al. (2007) also studies a population of coupled SMCs. They suggest that cGMP has a permissive role in the onset of vasomotion. Moreover, they show that intercellular diffusion of calcium or another second messenger is not necessary to explain synchronization, and that vasomotion frequency is strongly influenced by membrane potential.

2.4.2 Physiological importance

Although vasomotion has been seen in many studies for many years, the physiological consequences remain very unclear (Nilsson and Aalkjaer, 2003). A potential benefit of vasomotion is that it improves tissue oxygenation. This suggestion comes from results of theoretical modeling performed by Tsai and Intaglietta (1993). The authors suggested that periods of high flow at low oscillation frequency permit long-distance diffusion of oxygen to capillaries, therefore, at critical perfusion levels, oxygen becomes more homogeneously distributed, thus less of the tissue is exposed to very low levels of oxygen. Later, experimental studies have shown that as perfusion levels are reduced, vasomotion is induced in most muscle preparations (Rücker et al., 2000), likely as a protective mechanism against ischemia.

The prevalence of vasomotion may be altered under pathological conditions. Increased prevalence of vasomotion has been extensively studied in hypertension. For example, vasomotion was enhanced in hypertensive rats (e.g., Bandick and Sparks (1970)). Studies have shown that the prevalence of increased vasomotion positively correlates with increased blood pressure. There is also some evidence for enhanced vasomotion in human hypertension: isolated arteries from women with preeclampsia

(pregnancy-induced hypertension associated with significant amounts of protein in the urine) exhibit more vasomotion than normotensive pregnant women (Aalkjaer et al., 1985; Pascoal et al., 1998).

In diabetes, there is good evidence that vasomotion is less prevalent. Stansberry et al. (1996) found that in insulin-dependent and in insulin-independent diabetics the amplitude of vasomotion in the finger was reduced to about 20 %. Diabetes is often associated with atherosclerosis. Atherosclerosis, apart from being a major cause of death in diabetic patients, is the leading cause of human death. Given that all these diseases are associated with abnormalities in vasomotion, the understanding of the mechanisms underlying vasomotion is crucial.

3.1 Explant preparation and cell culture

Male Wistar rats (300 ± 50 g) were anesthetized with isoflurane (4 %) and then decapitated in agreement with the Care of Animals (edited by the Swiss Academy of Medical Sciences and the Helvetic Society of Natural Sciences). All experiments performed on rat mesenteric arteries were approved by the Cantonal Veterinary Office (authorization number 1799.1) in agreement with the law on animal protection in Switzerland. The mesenteric arcade was excised and placed in a physiological solution containing in mM: 145 NaCl, 5 KCl, 1 CaCl₂, 0.5 MgSO₄, 1 Na₂HPO₄, 20 HEPES, 23 Tris base, 10.1 glucose and pH was set to 7.4. The methods used for isolation and culture are similar to the protocol described by Golovina and Blaustein (2006). Briefly, the superior mesenteric artery was removed and placed in isolation solution (in mM: 137 NaCl, 5.4 KCl, 0.44 KH₂PO₄, 0.42 NaH₂PO₄, 0.2 MgCl₂, 4.2 NaHCO₃, 0.2 CaCl₂, 0.05 EGTA, and 10 HEPES, 10.1 glucose, pH 7.4). First- and second-order arteries were extensively cleaned of adventitial fat and connective tissue using fine forceps and vannas scissors. A partially cleaned artery within the superior mesenteric artery bed is shown in Fig. 3.1.

Blood was removed by injecting isolation solution into the lumen using a syringe with a 30 mm long gauge needle with outer diameter 0.30 mm, inner diameter 0.15 mm (Unimed S.A., Lausanne, Switzerland). Arteries were cut to 2 – 3 mm length and prepared for enzymatic digestion for 20 min at 37°C in isolation solution containing collagenase (2 mg/ml) and elastase (1 mg/ml). Arteries were then rinsed with isolation solution for 10 min at room temperature and transferred to 60 mm diameter culture dishes containing 5 ml culture medium (Dulbecco's modified Eagle's

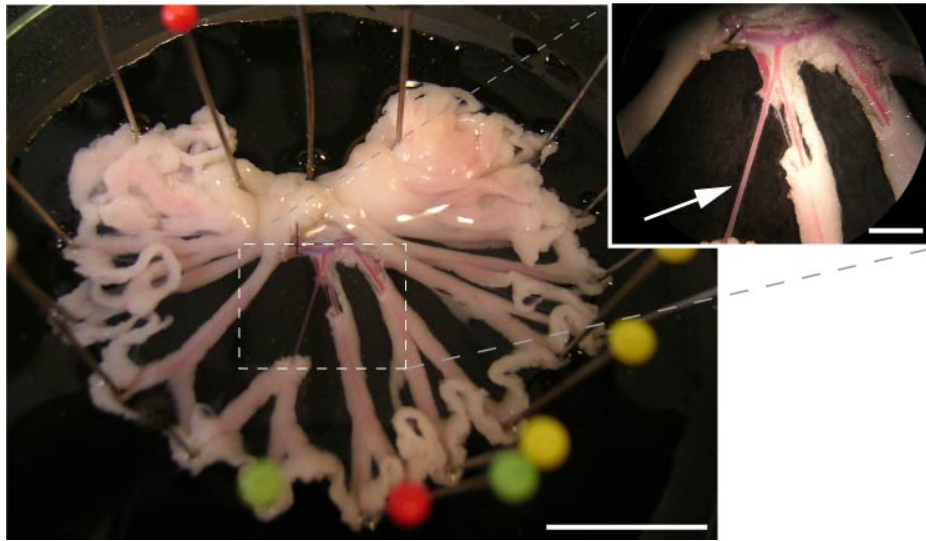


Figure 3.1: Dissection of the mesenteric artery. Artery branches with adjacent tissues (including veins and connective tissue) were pinned to facilitate fine dissection. The arrow in the zoom points to an artery dissected and discarded from adventitial fat and connective tissue. Scale bars: 1 cm, zoom: 2 mm

medium, DMEM, Invitrogen, Basel, Switzerland) supplemented with 10 % fetal calf serum (FCS) (BioConcept, Allschwil, Switzerland), 20 mM L-glutamine and 1000 U/ml penicillin/streptomycin (Invitrogen). Explants were cultured for 10 – 12 days and culture medium was refreshed every 2-3 days. Cells outgrowing from the explants (passage 0, P0, Fig. 3.2 A) were then treated with trypsin and seeded (passage 1, P1) on coverslips for experiments. The purity of the pSMCs in cultures was verified by positive staining with smooth muscle specific α -SMA and with desmin, a type III intermediate filament. As shown in Fig. 3.2 B, pSMCs express both α -SMA and desmin, however, not all pSMCs express desmin. This result was expected, since a study by Wede et al. (2002) demonstrated that there exists a gradient in desmin expression in the arterial tree towards more desmin in the microarteries compared to the large arteries.

A7r5 cells were obtained from the American Type Culture Collection and were used up to passage 15. 6B5N cells are a clone of the A7r5 cell line expressing higher Cx43:Cx40 ratio (Burt et al., 2001). 6B5N cells were obtained from Prof. Janis M. Burt (Department of Physiology, University of Arizona, Tuscon, AZ, USA). The same culture medium was used for all three cell types. For 6B5N cells, culture medium was supplemented

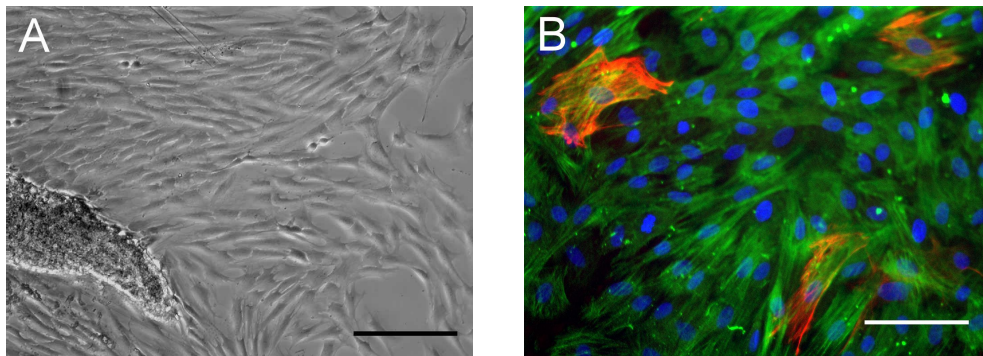


Figure 3.2: Primary culture of SMCs. **A)** Phase contrast image of SMCs derived from superior mesenteric artery explant after 9 days in culture. Scale bar 100 μm with 10x objective. **B)** Immunofluorescence staining characteristic of smooth muscle cells; Labels show typical α -SMA (in green) and desmin (in red) filaments in pSMCs (nucleus in blue). Scale bar: 100 μm with 20x objective.

with 10 mg/ml neomycin, which is an aminoglycoside antibiotic, a common agent for selecting stable transfection. For the calcium experiments in Chapter 4, cells were trypsinized and seeded on ibidi coverslips (Ibidi GmbH, Martinsried, Germany) or 35 mm diameter petri dishes and cultured for 2 days. Since the growth rate of these cells was different, the following seeding densities were used for calcium experiments to obtain small cell clusters: pSMCs: 2×10^4 /ml, A7r5 cells: 1.5×10^4 /ml and 6B5N cells: 1.7×10^4 /ml.

3.2 Microcontact printing of proteins for cell patterning

To facilitate local stimulation of one cell and the observation of Ca^{2+} wave propagation between SMCs, cells were grown on ibidi coverslips (Ibidi GmbH, Martinsried, Germany), patterned with collagen lines of 50 μm width, created by the microcontact printing (μCP) technique, described previously (Goffin et al., 2006). Briefly, optical lithography was used to etch the topography of interest on a silicon wafer, serving as a mould to produce silicone stamps (Dow Corning, Wiesbaden, Germany). Silicon stamps were cleaned with ethanol, treated for 30 seconds with plasma oxygen (Plasmaline, Tegal Corporation, Petaluma, CA) and incubated for

1 h with collagen type I. (50 $\mu\text{g}/\text{ml}$ in serum free culture medium) (Sigma-Aldrich, Buchs, Switzerland). Conformal contact was made for 4 minutes with the coverslip surface that were also activated for 30 s with plasma oxygen. The remaining gaps on the coverslip were passivated with Poly(L-lysine)(20)-graft(2)-poly(ethylene glycol)(3.5) (PLL-g-PEG; SuSoS AG, Dübendorf, Switzerland) to form areas resistant to cell adhesion. SMCs adhered only to the collagen lines and were cultured for 1 day before experiments. μCP was used for the experiments in Chapter 5.

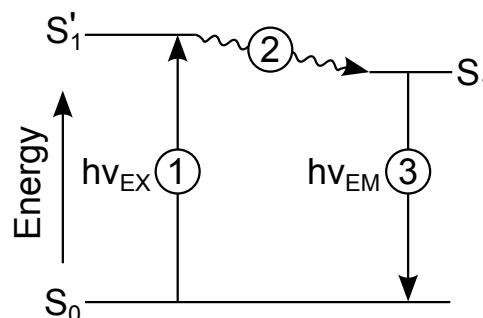
3.3 Fluorescence techniques

The process of fluorescence involves a three-stage process that occurs in certain molecules called fluorophores or fluorescent dyes. A fluorescent dye allows to monitor temporal and spatial variations of specific ions within a biological specimen. Throughout this thesis, we used a calcium ion-selective fluorescent dye to measure the changes of cytoplasmic free $[\text{Ca}^{2+}]_i$. We have also used fluorescence to detect proteins (e.g. connexins). The fluorescence process is illustrated in Fig. 3.3 and involves the following stages.

Stage 1: Excitation A photon of energy $h\nu_{\text{EX}}$, supplied by an external source (e.g. laser), is absorbed by the fluorophore, creating an excited electronic singlet state (S'_1).

Stage 2: Excited-State lifetime The excited state has a limited lifetime, typically 1-10 ns. During this time, the fluorophore undergoes conformational changes which leads to partial dissipation of the S'_1 energy. This yields a relaxed singlet excited state (S_1).

Figure 3.3: Jablonski diagram illustrating the processes involved in the creation of an excited electronic singlet state by optical absorption and subsequent emission of fluorescence. The labeled stages 1, 2 and 3 are explained in the adjoining text. (*Handbook of Fluorescent Probes and Research Products, Molecular Probes, 2002*)



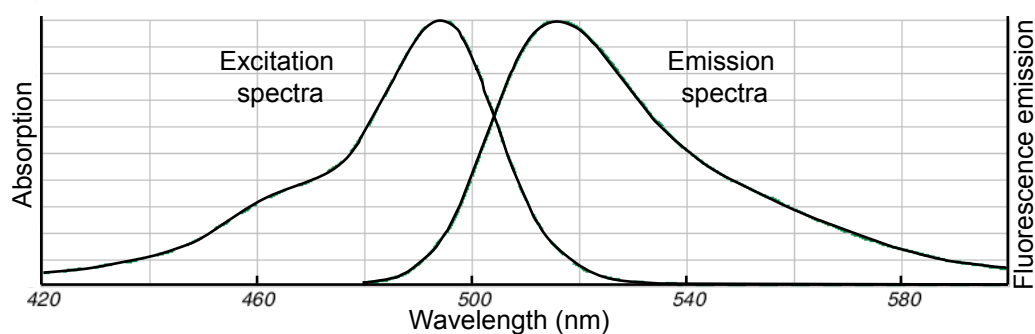


Figure 3.4: Fluorescence excitation and emission spectra of Fluo-4 AM. Spectra was prepared with Molecular Probes' Fluorescence SpectraViewer online application at www.invitrogen.com

Stage 3: Fluorescence emission A photon of energy $h\nu_{EM}$ is emitted, returning the fluorophore to its ground state (S_0). Due to energy dissipation during Stage 2, the energy of this photon is lower, thus it has a longer wavelength than the excitation photon $h\nu_{EX}$.

The fluorescence process is cyclical. The same fluorophore can be repeatedly excited and detected unless the fluorophore is irreversibly destroyed in the excited state. This process is known as photobleaching. A single fluorophore can generate many thousands of detectable photons. This is fundamental to the high sensitivity of fluorescence detection techniques.

3.3.1 Fluorescent Ca^{2+} dye

Fluorescent Ca^{2+} dyes are molecules whose optical properties change when they bind to Ca^{2+} . Usually either the excitation or emission spectrum (or both) are changed upon Ca^{2+} binding. A wide variety of Ca^{2+} dyes are available; the choice of dye is determined by several factors, e.g., excitation and emission wavelengths, the affinity of the dye (K_d), the dynamic range for Ca^{2+} detection and ease of use. Throughout this thesis, the fluorescent Ca^{2+} dye Fluo-4 AM (Molecular Probes) was used. Excitation and emission spectra for Fluo-4 are shown in Fig. 3.4.

Ca^{2+} dyes are, in their Ca^{2+} -sensitive forms, hydrophilic compounds (with $-COO^-$ groups), thus they cannot readily cross the plasma membrane. The ester derivative of Fluo-4 (Fluo-4 AM), however, is cell-perme-

ant. Since Fluo-4 AM is highly lipophilic, it was first dissolved to 1 mM in di-methylsulfoxide (DMSO). A7r5, pSMCs and 6B5N cells were loaded for 40 – 50 min in the dark, at room temperature in physiological solution containing 10 μ M Fluo-4 AM (the physiological solution in Chapter 5 contained 2 mM CaCl_2 instead of 1 mM), in presence of 2.5 % (v/v %) Pluronic F-127 (Molecular Probes). Including a detergent, such as Pluronic, prevents formation of dye micelles, whereas performing dye loading at room temperature reduces compartmentalization into organelles such as mitochondria and sarcoplasmic reticulum. Once the esters are in the cytoplasm, they are cleaved by endogenous esterases and released in their Ca^{2+} -sensitive form. After loading with the fluorescent dye, cells were washed for 30 minutes in the dark with physiological solution to allow complete de-esterification of the indicator.

3.3.2 Fluorescence microscopy

A fluorescence microscope is principally a conventional light microscope with added features and components that extend its capabilities. A conventional microscope uses light to illuminate the specimen and produce a magnified image of the specimen. A fluorescence microscope, however, uses a much higher intensity light to illuminate the specimen previously loaded with a fluorescent dye. A fluorescence microscope also produces a magnified image of the sample, but the image is based on the second light source – the light emanating from the fluorescent dye – rather than from the light originally used to illuminate, and excite, the sample. During this thesis two types of fluorescence microscopes were used, depending on the analysis: epifluorescence microscope and confocal microscope.

Epifluorescence microscopy

The type of excitation-emission configuration, in which both the excitation and emission light travel through the objective, is called epifluorescence. The key to the optics in an epifluorescence microscope is the separation of the excitation light from the fluorescence emission emanating from the sample with a dichroic mirror. A dichroic mirror is basically a beamsplitter. The dichroic mirror allows longer wavelengths (excitation light) to be transmitted through, while the shorter wavelengths (emitted light) will be

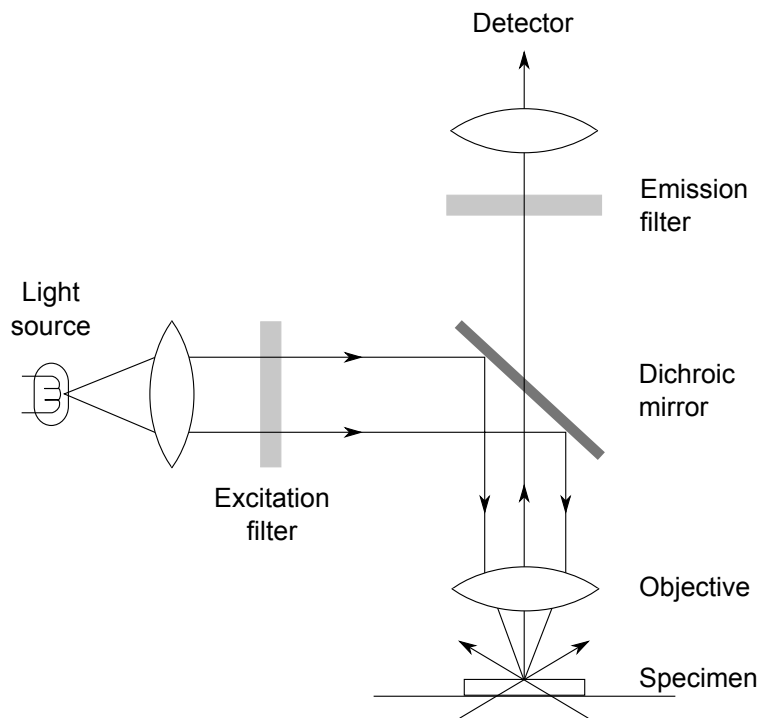


Figure 3.5: Illustration of the light path of an epifluorescence microscope. The light is first directed through the excitation filter. The dichroic mirror directs the light to the specimen. The fluorescent light emitted from the specimen is then directed through the dichroic mirror and will be even more selective after passing the emission filter. The fluorescent signal is then analyzed by eye at the microscope or recorded by a camera.

reflected. Two filters are used along with the dichroic mirror: 1) Excitation filter, in order to select the excitation wavelength, placed prior to the dichroic mirror. 2) Emission filter, in order to more specifically select the emission wavelength of the light emitted from the sample and to remove traces of excitation light. An emission filter is placed beneath the dichroic mirror. A schematic diagram in Fig. 3.5 illustrates the light path in an epifluorescence microscope.

This type of microscope was used for all calcium experiments, for analyzing the purity of pSMCs with α -SMA and desmin and for scrape-load and dye-transfer experiments in Chapter 4. The epifluorescence microscope composed of a Nikon (Tokyo, Japan) Eclipse TE300 inverted microscope and 40x, NA 1 objective lens. Mercury arc lamp (Nikon HMX-4 Mercury) was used as a light source. Light intensity was regulated by neutral

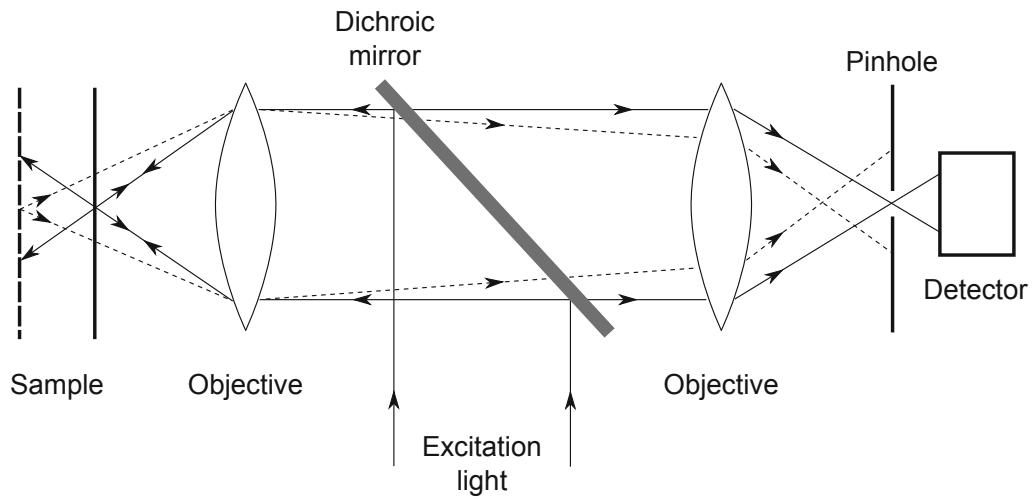


Figure 3.6: The principle of confocal microscopy. Light emitted by the sample passes through a pinhole aperture that is situated in front of the detector. Thus, the pinhole physically removes the out-of-focus light from the final image.

density filters (ND). Data were acquired with a Micromax PB1300 and a Micromax 512FT cooled charge-coupled device cameras (Roper Scientific, Trenton, NJ) controlled by Metamorph software. For Ca^{2+} experiments ND 4 + 8 was used. Light exposure time was 80 ms and acquisition rate was 12 Hz.

Confocal microscopy

Confocal microscopy offers several advantages over epifluorescence microscopy, including shallow depth of field, elimination of out-of-focus glare, and the ability to collect serial optical sections from thick samples. In confocal microscopy, fluorescence emission is directed through a pinhole aperture positioned near the image plane to exclude light from fluorescent structures located away from the objective focal plane. The word *confocal* means that the pinhole is *conjugate* to the *focal* point. The confocal principle is illustrated in Fig. 3.6.

Two types of confocal microscopes were used in this research, a laser scanning confocal microscope and a spinning-disk confocal microscope (also known as Nipkow disk system). In the latter, a spinning-disk with multiple small holes is installed between the light source and sample, to shed point-like illumination on the sample. The same hole serves as a de-

tecting pinhole to remove out-of-focus light (for a discription see Nakano (2002)).

The figures of this thesis were captured with a spinning-disk confocal microscope for a simple reason; the sensitivity of the camera used with the spinning-disk was much higher. Confocal microscopy was used for the immunofluorescence experiments in Chapter 4 to detect connexins and their distribution within the cell. The setup is composed of an Olympus IX 81 motorized inverted spinning-disk confocal microscope and oil-immersion objective 20x, NA 0.8. Light sources: Argon-ion and Argon-Krypton laser (488 nm and 568 nm respectively). Images were acquired with a Hamamatsu EMCCD C 9100 B/W controlled by UltraVIEW ERS 2005.

Since the spectra of each fluorophore is different, different excitation wavelengths, excitation-emission filters and dichroics were used. The name of the fluorophore, it's absorption-emission maximum wavelengths (λ , $\lambda_{ab}/\lambda_{em}$ in nm), target molecule or ion, excitation (ex), emission (em) filters and dichroic mirrors are summarized in Table 3.1.

Table 3.1: Fluorophors and filters for fluorescence microscopy

Fluorophore ($\lambda_{ab}/\lambda_{em}$)	Target	Filter _{ex}	Dichroic	Filter _{em}
DAPI (359/461)	Nucleus	365	395	445/50
FITC AB-c ^a (495/519)	α -SMA	490/20	510	–
TRITC AB-c ^a (557/576)	Desmin	565/30	585	620/60
Fluo-4 AM (494/516)	Ca ²⁺	490/20	510	–
Lucifer Yellow (LY) (428/540)	LY	470/40	495	525/50
Alexa Fluor 488 AB-c ^a (495/520)	Cx40	–	488	485/60
Alexa Fluor 568 AB-c ^a (578/603)	Cx43	–	568	615/70

^aThe exact type of antibody conjugates (AB-c) used are listed in Section 3.7.3.

3.4 Experimental setup for calcium imaging

For imaging intercellular Ca²⁺ wave propagation, SMCs loaded with the fluorescent Ca²⁺ dye Fluo-4 AM were stimulated by either local mechanical or local chemical stimulation.

3.4.1 Local mechanical stimulation

Local mechanical stimulus was applied by gently and transiently touching a single cell with a micropipette (1 μm tip diameter Eppendorf Femtotips I). Under visible light the micropipette was initially positioned just above the target cell. Then, during fluorescence image capture, the pipette was lowered to transiently (< 1 s) contact the cell with a transjector (transjector 5246, Eppendorf, Schönenbuch, Switzerland) attached to a micromanipulator (Leica Mikroskopie und Systeme GmbH). To exclude the possibility that paracrine signals diffuse to neighboring cells, we performed all calcium experiments in a homemade flow chamber. Perfusion flow (2 ml/min) was provided with a syringe pump (SP 210 IW, World Precision Instruments, Stevenage, UK). The direction of the flow was opposite to the pipette axis to ensure drifting of paracrine signals away from the examined neighboring cells. Without perfusion of the extracellular medium the onset Ca^{2+} signal slowly propagated from the target cell to all neighboring cells in all directions. At the end of each experiment the stimulated cell was observed under transmitted light to verify that the membrane depression was slight and had not visibly damaged the cell. Control experiments showed that the stimulated cell could be repetitively and reproducibly stimulated without change in the rate of Ca^{2+} increase for subsequent stimuli.

3.4.2 Local chemical stimulation

Chemicals were administered with local microejection of the drug. Microejection was performed by filling the micropipette (Eppendorf Femtotips I.) with ejection solution, placing the tip of the pipette near the cell surface opposite the perfusion flow (2 ml/min), and ejection of a small amount of fluid under controlled pressure and timing (80 hPa, for a duration of 1 s) with a controlling unit (FemtoJet Microinjector, Vaudaux-Eppendorf AG, Basel, Switzerland). Without perfusion of the extracellular medium, the onset Ca^{2+} signal propagated from the target cell to all neighbouring cells in all directions. Fig. 3.7 demonstrates an experiment where local chemical stimulation was applied in presence of flow and at the end of this experiment the counter flow was stopped. The area of stimulation was tested by ejecting lucifer yellow with the same ejection parameters in

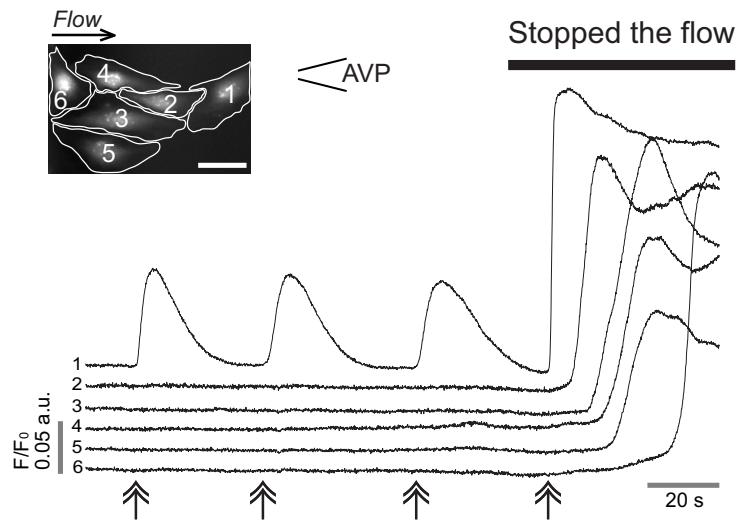


Figure 3.7: Local AVP stimulation of 6B5N cells in presence and absence of perfusion flow. This control experiment demonstrates that the counter flow effectively drifted away the ejected drug away from the neighboring cells. The same ejection parameters were used as in text. Note the difference in Ca^{2+} rise between with and without the presence of flow. The smaller Ca^{2+} increase indicates that the stimulation was local and only part of the cell was reached by the drug. When flow was stopped Ca^{2+} increase was order of magnitude bigger, indicating that the drug diffused to the entire cell surface and even to neighboring cells. Scale bar: 50 μm .

presence of perfusion flow. A high concentration of stimulus was used in order to compensate for the dilution that occurs before the drug reaches the target cell. In control experiments, where the micropipette was filled with physiological solution only, the applied pressure did not stimulate the cells mechanically, the stimulated cell did not respond to the ejected physiological solution.

3.5 Image processing and data analysis

Increase in $[\text{Ca}^{2+}]_i$ due to stimulation leads to an increase in the emitted fluorescence. Changes in $[\text{Ca}^{2+}]_i$ over time were presented as the relative fluorescence intensity change, which was calculated by dividing all images from the time series by the first image ($F/F_0 = \text{fluorescence}/(\text{fluorescence at rest})$). Changes in $[\text{Ca}^{2+}]_i$ were measured by taking the average fluorescence intensity of the regions of interest (ROIs) that included the

entire cell. All experiments were performed at room temperature. Image analysis was performed with ImageJ software (NIH Image, Bethesda, MD) and data processing was performed with MatLab software (MathWorks, MA, USA).

3.5.1 Ca^{2+} wave velocity measurements

Kymograph analysis was used to quantify Ca^{2+} wave velocity in Chapter 5. To obtain a kymograph, a long thin (1 pixel) trajectory, that passes along the cells (red trajectory in Fig. 5.1 A), is extracted from each image in the fluorescent time-lapse series and pasted sequentially side-by-side to make a montage of the trajectory over time (Fig. 5.1 B). Velocity of the Ca^{2+} wave was estimated from the slopes of the wave front seen on the kymograph in each individual cell for intracellular Ca^{2+} waves or starting from the stimulated cell until the end of the last observed cell for intercellular Ca^{2+} waves. The same color bar, shown in Fig. 5.1, was used in the kymograph images in Chapter 5, unless stated. Kymograph analysis was performed with ImageJ software (NIH Image, Bethesda, MD) and data processing was performed with MatLab software (MathWorks, MA, USA).

3.6 Scrape-loading and dye transfer with Lucifer Yellow

Gap junctional intercellular communication was evaluated by the diffusion of the fluorescent tracer Lucifer Yellow (LY) (Molecular Probes), as described by Follonier et al. (2008). A7r5, pSMCs and 6B5N cells grown to confluent monolayer were washed with Hank's buffered salt solution (HBSS, Invitrogen), loaded with 5 mg/ml LY and then injured along a line with a scalpel blade. Wounded cells were allowed to absorb and to intercellularly transmit LY for 5 min. Cells were then washed in HBSS, fixed for 10 minutes in 3 % paraformaldehyde and stained with DAPI for nuclei. Images were acquired using 10x Plan Neofluor Zeiss objective (NA 0.3) mounted on an upright Zeiss Axioplan microscope with a Zeiss Axio-Cam camera (HRm Rev.2) and were assembled and analyzed with ImageJ software (NIH Image, Bethesda, MD). Since, A7r5, pSMCs and 6B5N in

confluent cultures appeared to be different in size, the spread of LY was quantified relative to the cell width for each cell type. Cells had no specific orientation; consequently, cell width could be calculated as the square root of the average cell area. Average cell area was calculated by measuring the surface area of LY positive cells ($n = 50$ for each cell type). Average cell area for A7r5 cells: $1104 \pm 104 \mu\text{m}^2$, for pSMCs: $1216 \pm 154 \mu\text{m}^2$ and for 6B5N cells: $581 \pm 38 \mu\text{m}^2$.

3.7 Protein analysis

3.7.1 RNA isolation, and quantitative RT-PCR

Cells were homogenized in the Tripure Isolation Reagent (Roche Diagnostics) and total RNA was extracted using the kit procedure. Transcripts ($1 \mu\text{g}$) were reverse-transcribed using ImProm-2 Reverse transcription System (Promega). Quantitative PCR was performed using the SYBR[®] Premix ExTaq[™] (Takara) in a Lightcycler Instrument (Roche Diagnostics). cDNAs were amplified using the following primers: rat Cx43: 5'-CAACGACCTTCCAGCAGAG-3' (sense) and 5'-CTCCCTTATCCCCACCTGTT-3' (antisense). Rat Cx40 5'-AGGGTGAGGCAGGACAGAAG-3' (sense) and 5'-GGT TGGGGATTTGAGGAGTAG-3' (antisense). Rat Cx37 5'-GACCACCGAGGAGAGACTGA-3' (sense) and 5'-CCGAGAGGCATTCAAGGT-3' (antisense). Rat Cx45: 5'-GCTCTGGAAGAAACGGAAGA-3' (sense) 5'-AAAGCCCACCTCAAA CACAG-3' (antisense). Rat α -actin 5'-CGTTGACATCCGTAAAGACC-3' (sense) and 5'-TAGAGCCACCAATCCACACA-3' (antisense).

3.7.2 Western blot analysis

Cells were solubilised by sonication in SDS buffer (62.5 mM Tris-EDTA, pH 6.8, 5 % SDS). Protein content was measured using a detergent-compatible DC protein assay kit (Bio-Rad Laboratories, Reinach BL, Switzerland). Samples were equally loaded ($50 \mu\text{g}$) on a 12.5 % polyacrylamide gel followed by electrophoresis and transferred onto PVDF membrane (Immobilon-P; Millipore, Volketswil, Switzerland). Membranes were incubated for 1 hour in PBS containing 5 % milk and 0.1% Tween20 (blocking buffer). Saturated membranes were incubated overnight at 4°C with: rabbit polyclonal antibodies against Cx40 (1:250) (AB1726, Chemicon Inter-

national), Cx43 (1:5000) (AB1728, Chemicon International), Cx37 (1:2000) (Cx37A11-A, Biotrend Chemikalien GmbH), or with goat polyclonal antibody against Cx45 (1:1000) (AB1748, Chemicon International) or monoclonal antibody anti- α -tubulin (1:3000) (T5168, Sigma-Aldrich). After incubation at room temperature for 1 hour with a convenient secondary antibody conjugated to horseradish peroxidase (1:20,000) (Fluka Chemie), membranes were revealed by enhanced chemiluminescence (ECL) according to the manufacturer's instructions (Amersham Bioscience Europe). Densitometric analyses of immunolabeled proteins (western blots) were performed using the ImageQuant Software (Molecular Dynamics, Amersham BioscienceEurope).

3.7.3 Immunofluorescence staining

Cells were washed with serum free culture medium, then fixed for 10 minutes with 3 % paraformaldehyde in PBS. For primary antibodies, we applied: anti- α -SMA (mouse IgG2a, SM-1 (1:50)), a kind gift from G. Gabiani, University of Geneva, Switzerland), monoclonal anti-desmin D33 (mouse IgG1 (1:20), DAKO), anti-Cx43 (mouse IgG1 (1:100), BD Biosciences, Allschwill, Switzerland), anti-Cx40 (rabbit C-term (1:100), invitrogen, Carlsbad, CA, USA). For secondary antibodies, we applied: anti-mouse IgG2a-FITC (1:100) and anti-mouse IgG1-TRITC (1:100) (both from Southern Biotechnology, Birmingham, AL), anti-mouse Alexa Fluor 568 (1:250), anti-rabbit Alexa Fluor 488 (1:250) (both from Molecular Probes) and nuclei were stained with DAPI (1:50) (Fluka, Buchs, Switzerland). For control experiments cells were loaded with only secondary antibodies. Images were acquired using an oil-immersion objective 20x (NA 0.8), mounted on an Olympus IX 81 motorized inverted spinning disk confocal microscope (Perkin Elmer Ultra View ERS). Figures were assembled with ImageJ software (NIH Image, Bethesda, MD).

3.8 Statistics

Data are reported as the mean \pm standard error of the mean (S.E.M.). *n* indicates the number of independent experiments. Comparisons of means between groups were performed by paired or unpaired student's t-tests as

appropriate. * $P < 0.05$, ** $P < 0.01$, *** $P < 0.001$. $P < 0.05$ was considered as a statistically significant difference.

3.9 Chemicals and drugs

Bay K8664 (Sigma-Aldrich) Activates the L-type voltage operated calcium channels. Bay K8664 was stored as 10 mM stock solutions in DMSO. Before experiments the stock solution was diluted in buffer to 300 nM and cells were allowed to preincubate for 5 min before stimulation.

Ca²⁺ free buffer solution Calcium-free solution composed of physiological solution without calcium and supplemented with 0.5 mM EGTA.

Carbenoxolone (CBX) (Sigma-Aldrich) A gap junction inhibitor. CBX was first dissolved in distilled water to 100 mM, then diluted to 100 μ M in buffer. Cells were allowed to preincubate in CBX for 20 min at room temperature.

⁴³Gap 26 (Tocris Bioscience Bristol, UK) A synthetic connexin-mimetic peptide that specifically targets Cx43 (VCYDKSFPISHVR). ⁴³Gap 26 was dissolved directly in buffer to the final concentration of 300 μ M and allowed to preincubate for 40 min. For control experiments cells were preincubated in buffer solution for 40 min.

KCl (Sigma-Aldrich) A membrane depolarizing agent. A high concentration of KCl (3 M) was used in order to compensate for the dilution that occurs before the drug reaches the target cell.

Nifedipine (Sigma-Aldrich) Blocks the L-type voltage operated calcium channels. Nifedipine was stored as 10 mM stock solutions in DMSO. Before experiments the stock solution was diluted in buffer to 10 μ M and cells were allowed to preincubate for 5 min before stimulation.

1-Octanol (Sigma-Aldrich) A gap junction inhibitor. Octanol was first dissolved in 100 % ethanol at a concentration of 100 mM, and then diluted to 1 mM in buffer. It's action is rapid, therefore, no preincubation was needed.

Palmitoleic acid (PA)(Sigma-Aldrich) A gap junction inhibitor. PA was directly dissolved in the physiological medium, by sonication for 3 min, at the final concentration of 50 μM .

Ryanodine (Sigma-Aldrich) Blocks ryanodine receptors. Ryanodine was first dissolved in DMSO at 10 mM, and then diluted to 20 μM final concentration in the buffer solution. Cells were allowed to preincubate in ryanodine for 20 minutes.

Vasopressin (AVP) (Sigma-Aldrich) A vasoconstricting agent. A high concentration of AVP (3 μM) was used in order to compensate for the dilution that occurs before the drug reaches the target cell.

Xestospongine C (Xes C) (Tocris Bioscience, Bristol, UK) Blocks IP_3 receptors. Xes C was first dissolved at 1 mM in DMSO, and then diluted to 5 μM in buffer. Cells were allowed to preincubate in XesC for 15 minutes.

Chapter

4

Connexin43 mediates intercellular Ca^{2+} waves

4.1 Introduction

Intercellular Ca^{2+} waves have been shown to be mediated through gap junction (GJ) channels. GJs contain intercellular channels (connexins) that allow direct communication between the cytosolic compartments of adjacent cells (Evans et al., 2006; Harris, 2007). Four connexin (Cx) isoforms are predominantly expressed in vascular tissue: Cx37, Cx40, Cx43 and Cx45 (Christ et al., 1992; Saez et al., 2003). The amount and type of Cxs expressed are cell-type specific. For instance, some, but not all, studies have shown that Cx40 is not expressed in SMCs (van Kempen and Jongma, 1999; Yamamoto et al., 2001; Alonso et al., 2010). Some type of SMCs has been shown to coexpress Cx43 with Cx40 (Gustafsson et al., 2003; Kanagaratnam et al., 2002; van Kempen and Jongma, 1999). One of the consequences of Cx43 and Cx40 coexpression is that, these proteins may form GJs and channels with mixed connexin composition, hence display distinct permeability and selectivity properties than GJs composed of a single Cx isoform (Burt et al., 2001; Goldberg et al., 2004; Harris, 2007; Kanaporis et al., 2008). The physiological consequences of such coexpression have not been thoroughly explored.

To study the mechanisms of intercellular Ca^{2+} transmission from one cell to another via GJs, we chose to perform experiments with A7r5 cells, a rat aortic SMC line that has been well characterized and extensively used for studying calcium homeostasis in vascular smooth muscles (Rüegg et al., 1985; Moore et al., 1991; Blatter and Wier, 1992; Byron, 1996). Surprisingly,

local mechanical stimulation induced a Ca²⁺ wave in the stimulated A7r5 cell, but the Ca²⁺ wave did not propagate to adjacent cells. In contrast, in primary cultured rat mesenteric smooth muscle cells (pSMCs), local mechanical stimulation of one pSMC evoked an increase in [Ca²⁺]_i that propagated to neighboring pSMCs. GJ uncouplers inhibited the propagation. Using the scrape-loading and dye transfer technique with Lucifer Yellow (LY), pSMCs proved to be better dye-coupled than A7r5 cells.

The aim of this chapter is to understand the reason(s) behind the difference in cell-cell communication between A7r5 and pSMCs. Since some studies, but not all, have shown that Ca²⁺ waves are mediated through GJs composed of Cx43 (Charles et al., 1992; Toyofuku et al., 1998), we hypothesized that Ca²⁺ waves in pSMCs are also mediated through Cx43 GJs. Also, A7r5 cells are known to coexpress Cx43 and Cx40 (Moore et al., 1991), but there are no results concerning the expression of these proteins in pSMCs. For this purpose, we examined these cells for expression of the connexin isoforms: Cx40 and Cx43. We have also studied pSMCs in terms of Cx expression for the other two predominant Cxs in vascular tissue: Cx37 and Cx45. To validate our hypothesis that Cx43 GJs are primarily involved in the propagation of Ca²⁺ waves in pSMCs, and better understand the functional consequences of Cx43 and Cx40 coexpression at different ratios, we used 6B5N cells, a clone of A7r5 cells with an elevated Cx43:Cx40 protein expression ratio (Burt et al., 2001). Our results demonstrate that Cx43 GJs are primarily responsible for mediating intercellular Ca²⁺ waves between pSMCs and the coexpression of Cx43 and Cx40 may interfere in clustering of Cx43 into gap junction plaques, affecting cell-cell communication.

4.2 Results

4.2.1 Intercellular communication in A7r5 cells and in pSMCs

We induced Ca²⁺ waves by local mechanical stimulation of one single SMC, and then observed the propagation of the signal to adjacent cells. The stimulation was restricted to a small region of one cell, the furthest possible from the neighboring cells.

Local mechanical stimulation of A7r5 cells gave rise to a $[Ca^{2+}]_i$ increase in the stimulated cell ($n = 20$). In 15 experiments (out of 20), this Ca^{2+} signal was transmitted to only few adjacent cells, but with much smaller amplitude (Fig. 4.1 A). In the remaining 5 experiments the induced Ca^{2+} signal did not propagate to any adjacent cell. Because of the weak coupling between A7r5 cells we used pSMCs. Local mechanical stimulation of pSMCs evoked a Ca^{2+} rise that propagated to neighboring cells ($n = 16$) (Fig. 4.1 B). Quantitative assessment of the average peak fluorescence amplitude of the Ca^{2+} rise in neighboring cells relative to the stimulated cell (cell 1) further demonstrated that the transmission of the Ca^{2+} signal was significantly higher in pSMCs compared to A7r5 cells (Fig. 4.1 D).

To test whether the intercellular Ca^{2+} wave propagation in pSMCs was mediated through GJs, experiments were performed in buffer solution containing carbenoxolone (CBX) or octanol. Both GJ uncouplers inhibited the propagation of Ca^{2+} waves to adjacent cells. In the presence of 100 μ M CBX, Ca^{2+} wave propagation was diminished ($n = 4$, Fig. 4.2 upper row), whereas 1 mM octanol completely abolished the propagation ($n = 4$, Fig. 4.3 upper row). A decrease in Ca^{2+} peak amplitude in the stimulated pSMCs in presence of CBX and octanol was also observed.

In order to compare the difference in dye-coupling between A7r5 cells and pSMCs, we tested the intercellular diffusion of Lucifer Yellow (LY) in confluent monolayer cultures with the scrape-loading and dye transfer technique. The spread of LY was significantly greater in pSMCs ($n = 9$) than in A7r5 cells ($n = 9$). In A7r5 cells usually only the first rank of cells, adjacent to the scrape, showed LY signal (Fig. 4.4).

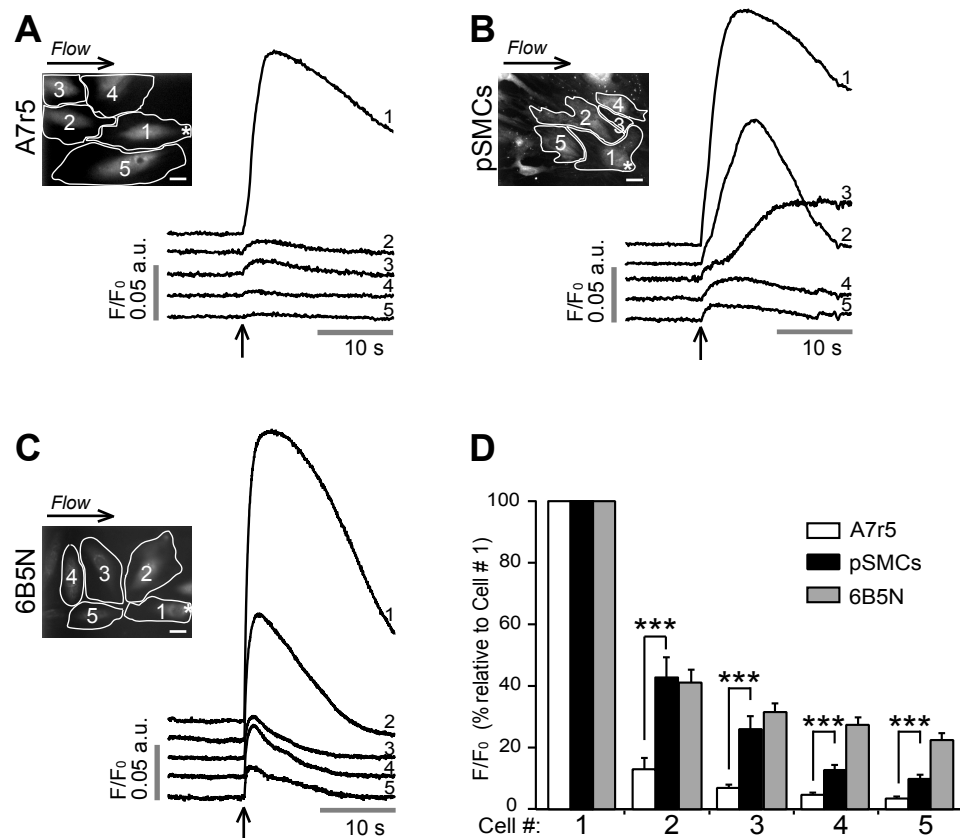


Figure 4.1: Representative fluorescence ratio (F/F_0) profiles of local mechanical stimulation-induced Ca^{2+} response. Site of stimulation is marked by an asterisk on cell 1. To exclude the possibility that soluble factors released due to mechanical stimulation may induce a Ca^{2+} increase, a counter perfusion flow was applied. The direction of the flow is indicated above the fluorescence images. Time of stimulation is indicated by an arrow. **A)** In A7r5 cells stimulation evoked a Ca^{2+} increase in the stimulated cell (cell 1) that failed to propagate to neighboring cells. In pSMCs **B** and 6B5N cells **C** the Ca^{2+} transient evoked in the stimulated cell propagated to neighboring cells. Scale bars: 25 μm . **D)** A data summary of average peak fluorescence amplitude of the Ca^{2+} rise in neighboring cells relative to the Ca^{2+} rise in the stimulated cell.

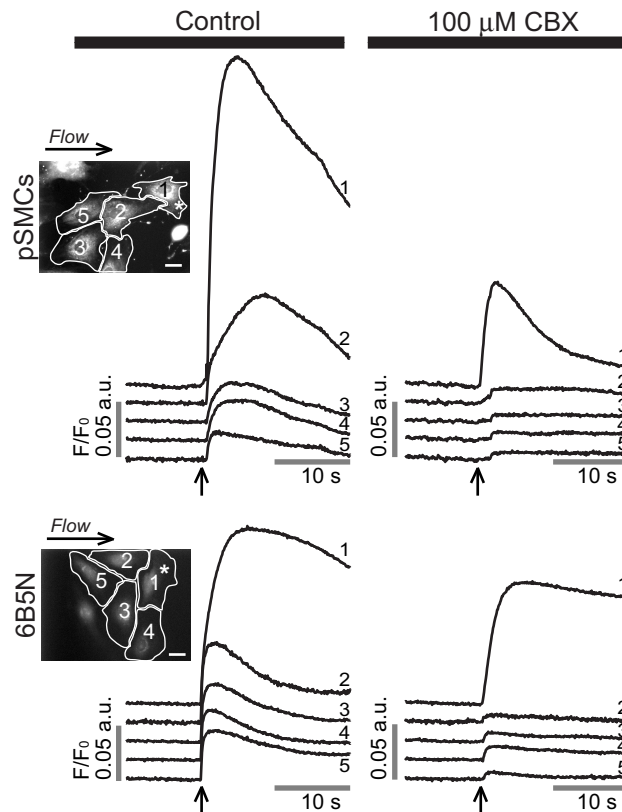


Figure 4.2: Effects of the gap junction inhibitor carbenoxolone (CBX) on the propagation of a Ca^{2+} wave in pSMCs and 6B5N cells. The same cell (cell 1) is stimulated before and after inhibitors were applied. CBX remarkably diminished the propagation of Ca^{2+} waves to neighboring cells. Scale bar: 25 μm .

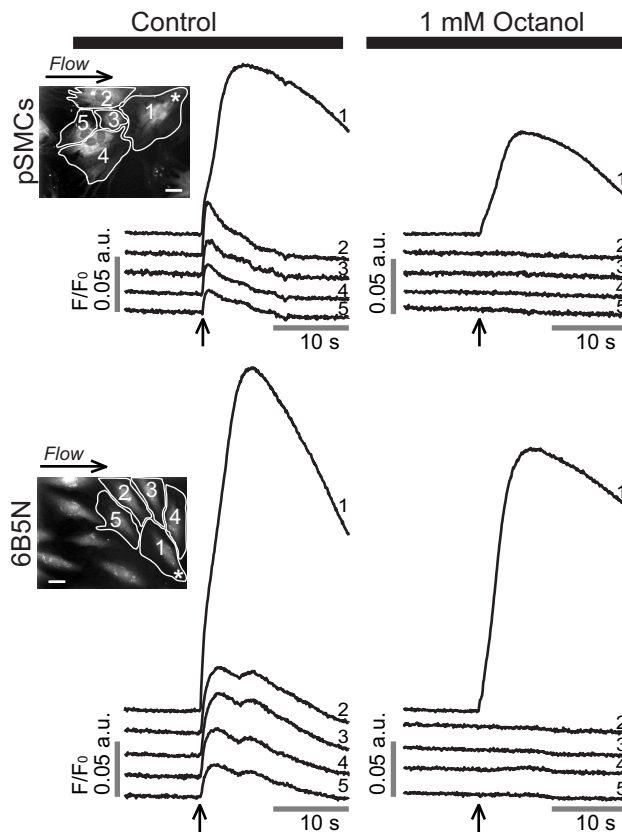


Figure 4.3: Effects of the gap junction inhibitor octanol on the propagation of a Ca^{2+} wave in pSMCs and 6B5N cells. Octanol blocked the propagation of Ca^{2+} waves to neighboring cells. Scale bar: 25 μm .

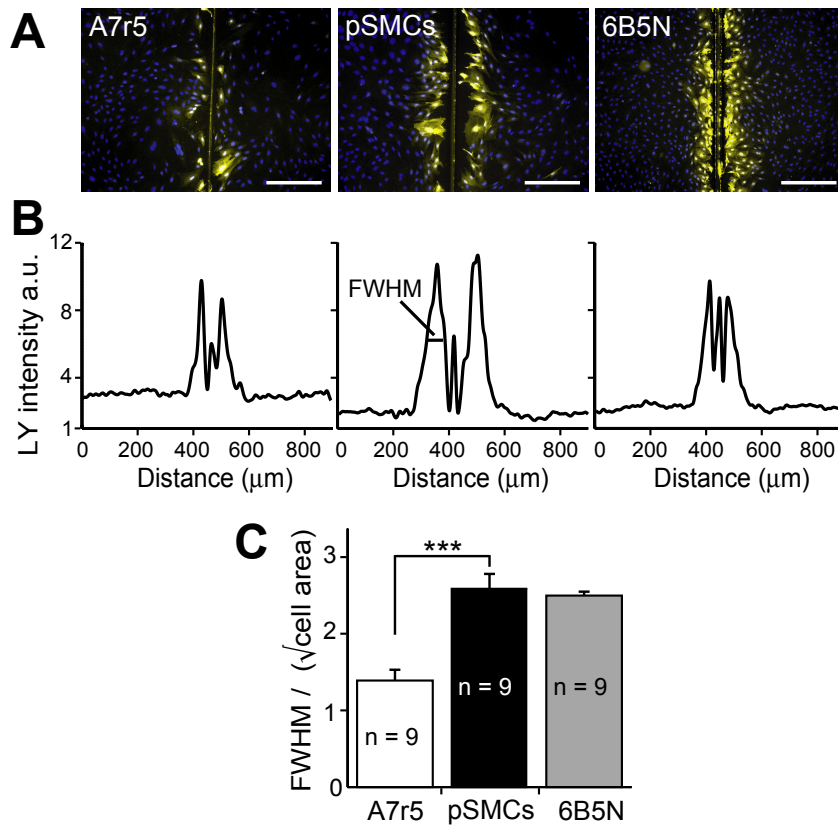


Figure 4.4: Quantification of gap junction dye-coupling by intercellular Lucifer Yellow diffusion. **A)** Scrape-loading and dye transfer of LY (yellow) in A7r5, pSMCs and 6B5N cells (nuclei in blue). The vertical line in the middle of the image is the mark of the scalpel blade used for scrape-loading. Scale bars: 200 μm . **B)** Plot of average LY fluorescence intensity in each pixel along the rows within the images in **A**. **C)** The distance of LY diffusion was quantified by taking the full width at half maximum (FWHM) of the plots in **B** divided by the square root of the average cell area. The spread of LY in pSMCs was significantly higher than in A7r5 cells and similar as in 6B5N cells.

4.2.2 Connexin expression in A7r5 cells and in pSMCs

To understand the difference in the gap junctional Ca²⁺ signal transmission between A7r5 and pSMCs, we analyzed the expression of Cx37, Cx40, Cx43 and Cx45. Cx expression was tested in terms of mRNA content, protein expression and immunofluorescence staining. Results of quantitative RT-PCR showed that expression of Cx43 mRNA was significantly higher in pSMCs compared to A7r5 cells, and that Cx40 is not expressed in pSMCs. Cx37 mRNA content was significantly lower in pSMC than in A7r5 cells, whereas, expression of Cx45 was not different (Fig. 4.5 A). Western blot analysis also showed that expression of Cx43 was significantly higher in pSMCs compared to A7r5 cells, and the absence of Cx40 in pSMCs. Cx45 protein level was significantly higher in pSMCs compared to 6B5N cells (Fig. 4.5 B). Quantification of the Cx protein expression levels are summarized in Fig. 4.5 C.

Cx43 and Cx40 had been previously shown to mediate Ca²⁺ waves. Therefore, to compare their expression patterns, immunofluorescence for Cx43 and Cx40 was performed in both cell types. In A7r5 cells, immunostaining demonstrated that Cx43 was mainly localized in the cytoplasm with few immunofluorescent dots at the regions of cell-to-cell contact (arrows in Fig. 4.6 upper row, n = 12). Cx40 was also present, but mostly in the cytoplasm and, even with higher magnification, was difficult to observe at the sites of cell-cell contact. In pSMCs, however, Cx43 was strongly expressed as shown by punctate staining at the regions of cell-cell contact corresponding to gap junction plaques, with negligible amount in the cytoplasm (Fig. 4.6 middle row, n = 8).

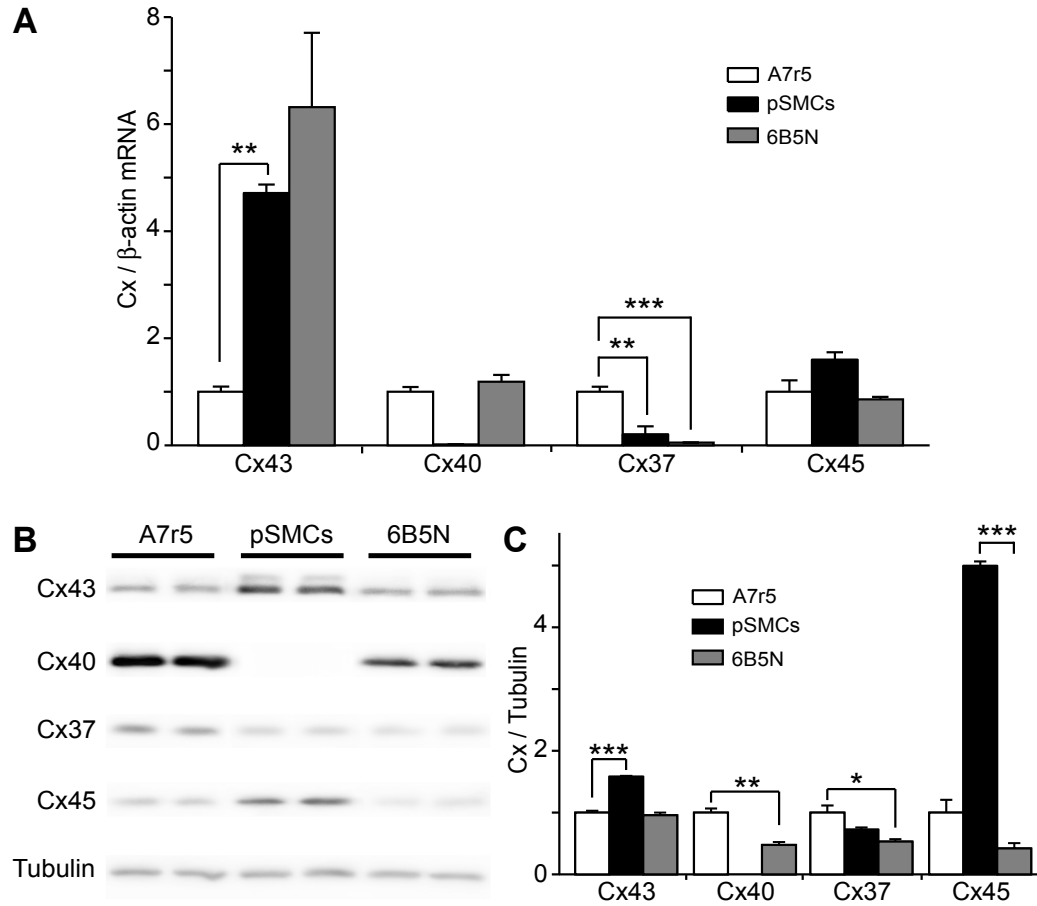


Figure 4.5: Expression of Cx37, Cx40, Cx43 and Cx45. **A)** RT-PCR analysis of Cx mRNA expression in A7r5 and pSMCs cells demonstrates a higher expression of Cx43 in pSMCs than in A7r5 cell, and the absence of Cx40 in pSMCs. The mean value of A7r5 cells, control, is presented as 1. Western blot analysis in **B** and densitometric analysis of Cx protein levels in **C** also showed the higher expression of Cx43 and the absence of Cx40 in pSMCs. Surprisingly, Cx45 expression was ~4-fold higher in pSMCs than A7r5 or 6B5n cells. 6B5N cells express the same amount of Cx43, but lower Cx40 compared to A7r5 cells.

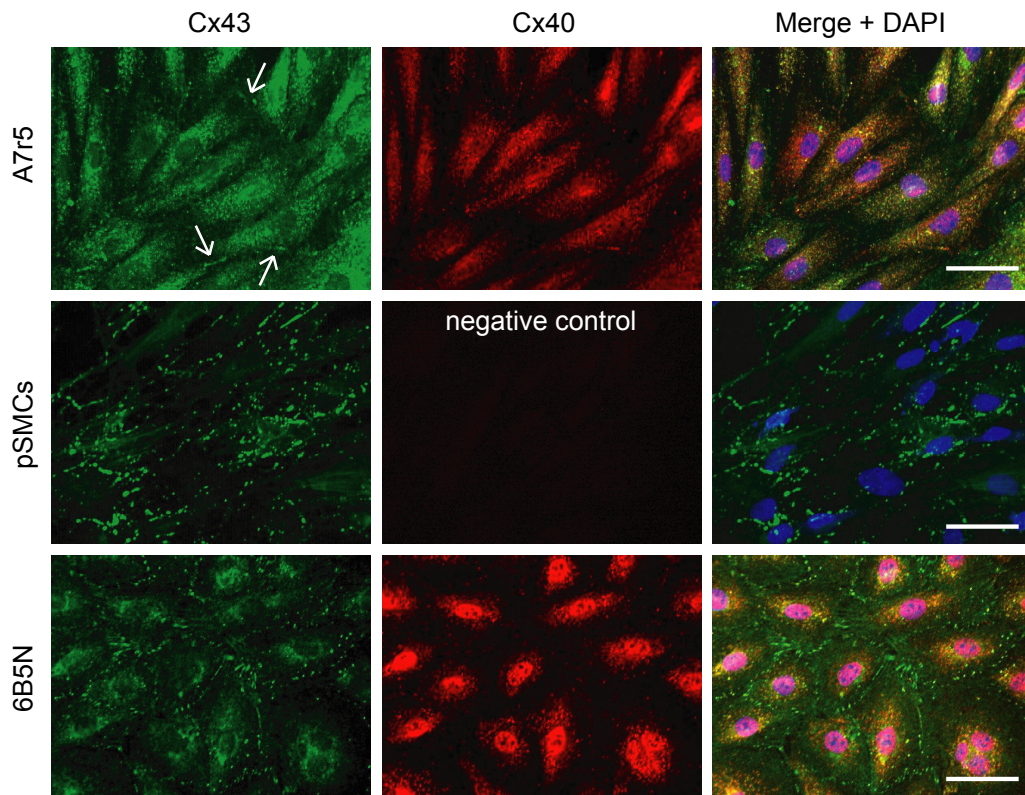


Figure 4.6: Expression patterns of Cx43 and Cx40 in A7r5, pSMCs and 6B5N cells. In A7r5 cells (upper row) Cx43 (green) was rarely localized at the site of cell-cell contact (arrows in upper row right). Most of the Cx43 was localized in the cytoplasm. PSMCs (middle row) showed punctate patterns of Cx43 immunoreactivity at the regions of cell-cell contact corresponding to gap junction plaques (nuclei in blue). In 6B5N cells (bottom row) distinct Cx43 immunoreactivity was detectable at the regions of cell-cell contact with fewer Cx43 in the cytoplasm compared to A7r5 cells. Scale bar: 50 μm .

4.2.3 Intercellular communication in 6B5N cells

To determine whether cells expressing a higher Cx43:Cx40 expression ratio than A7r5 cells would exhibit increased cell-cell coupling, we used 6B5N cells. 6B5N cells are a clone of A7r5 cells that expresses a higher Cx43:Cx40 ratio: 0.67 compared to 0.37 in A7r5 cells (Burt et al., 2001). This higher ratio is a result of decreased Cx40, but similar Cx43 expression levels to A7r5 cells as demonstrated in Burt et al. (2001). To test whether Ca^{2+} waves propagate between 6B5N cells, we applied local mechanical stimulation as described for A7r5 and pSMCs. Stimulation evoked a Ca^{2+}

rise that propagated to neighboring cells ($n = 26$) (Fig. 4.1 C). Quantitative assessment of the average peak fluorescence amplitude of the Ca^{2+} rise in neighboring cells relative to the stimulated cell (cell 1) is summarized in Fig. 4.1 D. To show that this propagation was mediated through gap junction channels, experiments were performed in presence of CBX or octanol. Both GJ uncouplers inhibited the propagation, similarly to pSMCs. (CBX: Fig. 4.2 bottom row, $n = 5$; octanol: Fig. 4.3 bottom row, $n = 5$). Scrape-loading and dye transfer with LY experiments showed that coupling between 6B5N cells is higher compared to A7r5 cells, as expected from an earlier study (Burt et al., 2001), but statistically not different from pSMCs ($P = 0.71$) (Fig. 4.4).

Cx37, Cx40, Cx43 and Cx45 expression, measured as mRNA content and protein expression, was also evaluated. 6B5N cells expressed lower protein levels of Cx40 and similar levels of Cx43 to A7r5 cells, as expected from an earlier study (Burt et al., 2001). Expression of Cx37 at both mRNA and protein levels was significantly lower in 6B5N cells compared to A7r5 cells, but statistically not different from pSMCs. On the other hand, Cx45 protein levels was significantly lower than in pSMCs (Fig. 4.5).

Immunostaining of 6B5N cells showed strong expression of Cx43 at the sites of cell-cell contact, but less strong than in pSMCs, and far less Cx43 was detected in the cytoplasm compared to A7r5 cells (Fig. 4.6 lower row, $n = 6$). Cx40 was also present mostly in the cytoplasm and, even with higher magnification, barely observable at the sites of cell-cell contact.

4.2.4 Effects of connexin-mimetic peptides on Ca^{2+} wave propagation

To test the hypothesis that the propagation of Ca^{2+} waves between pSMCs and 6B5N cells occurred through GJs composed of Cx43, we used the Cx-mimetic peptide $^{43}\text{Gap 26}$, that specifically blocks Cx43 in a concentration dependent manner (Chaytor et al., 1997). Both pSMCs ($n = 7$) and 6B5N cells ($n = 11$) were incubated for 40 min in buffer solution supplemented with $300 \mu\text{M}$ $^{43}\text{Gap 26}$. In both cell types, $^{43}\text{Gap 26}$ inhibited the propagation (Fig. 4.7 A & B). Data summary for mechanically-induced Ca^{2+} rise in pSMCs and 6B5N cells are shown in Fig. 4.7 C & D.

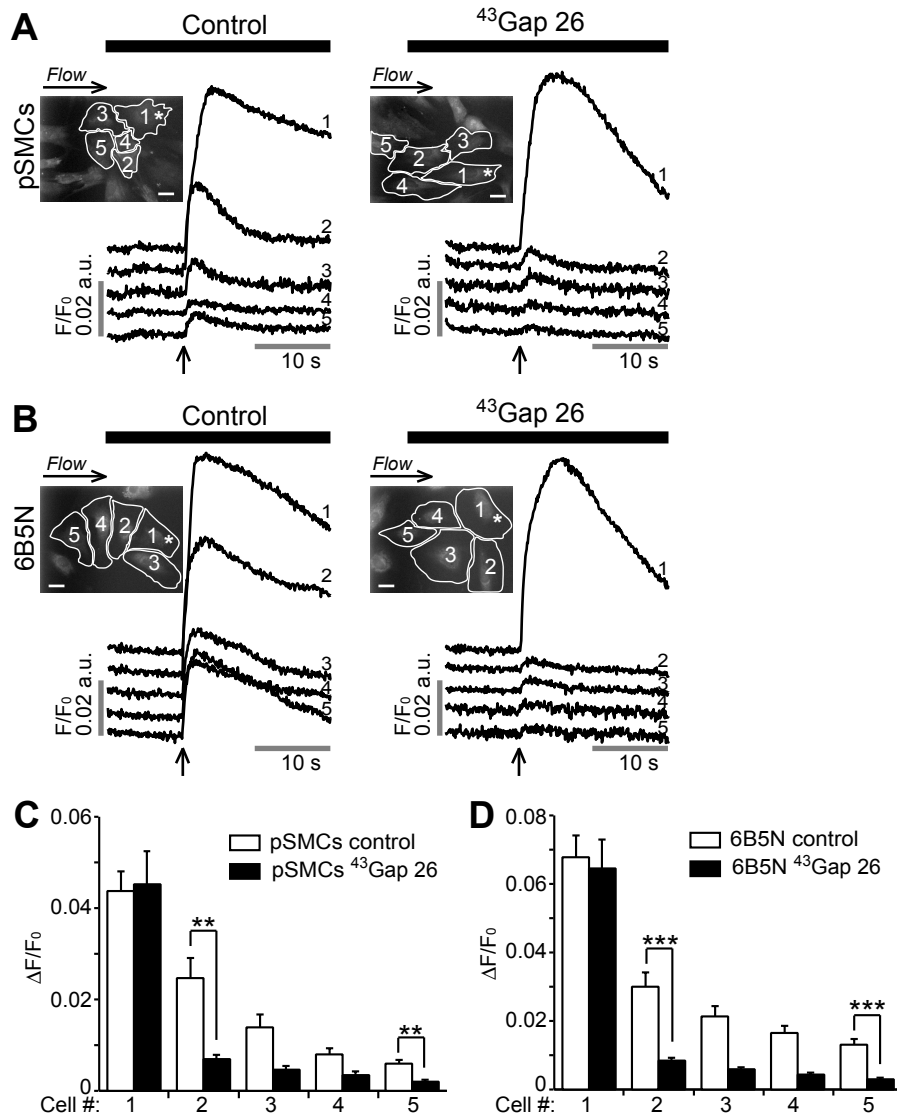


Figure 4.7: Effects of connexin-mimetic peptides on Ca^{2+} wave propagation. Experiments on the left panel are time-matched controls, whereas, the right panel shows experiments performed after 40 min incubation in buffer solution supplemented with the indicated connexin-mimetic peptide. $^{43}\text{Gap 26}$ significantly diminished the propagation of Ca^{2+} waves to neighboring cells in both pSMCs **A** and 6B5N cells **B**. Scale bars: 25 μm . Changes in fluorescence ratio ($\Delta F/F_0$) in control compared to $^{43}\text{Gap 26}$ treated cells are summarized in **C** for pSMCs and in **D** for 6B5N cells.

4.3 Discussion

The results of this study show that primary cultured rat mesenteric SMCs express Cx37, Cx43 and Cx45, but not Cx40, and that the mechanically-induced intercellular Ca^{2+} waves in pSMCs are mediated through Cx43 GJs. Comparison of results from cells coexpressing Cx43 and Cx40 demonstrates a direct correlation between higher Cx43:Cx40 expression ratios and successful propagation of Ca^{2+} waves, and suggests that coexpression of Cx43 with Cx40, depending on their relative expression levels, interferes with Ca^{2+} wave propagation between vascular smooth muscle cells.

A7r5 cells have been used as a SMC model in studies of calcium dynamics and intracellular calcium wave propagation (Rüegg et al., 1985; Moore et al., 1991; Blatter and Wier, 1992; Byron, 1996), yet, intercellular Ca^{2+} wave propagation studies, to the best of our knowledge, have not been conducted on these cells. To induce an intercellular Ca^{2+} wave between A7r5 cells, we applied local mechanical stimulation of one cell and followed signal propagation to adjacent cells. However, A7r5 cells showed very weak intercellular Ca^{2+} signal propagation. Using primary cultured SMCs from rat mesenteric artery instead, local mechanical stimulation evoked an increase in $[\text{Ca}^{2+}]_i$ that propagated to neighboring cells (Fig. 4.1 A & B). The use of gap junction inhibitors demonstrated that the propagation of intercellular Ca^{2+} waves was mediated by gap junctions. The decrease in Ca^{2+} amplitude in presence of the uncouplers is likely due to their non-specific actions as it has been demonstrated in previous studies (Coleman et al., 2001; Tare et al., 2002; Vessey et al., 2004). This effect was not observed when using the connexin-mimetic peptide $^{43}\text{Gap} 26$.

The difference in gap junction functionality between A7r5 cells and pSMCs can be explained by their different gap junction channel composition. Since Cx43 and Cx40 had been previously shown to mediate Ca^{2+} waves in different cell types (Charles et al., 1992; Toma et al., 2008; Toyofuku et al., 1998; Tallini et al., 2007), we focused on the comparison of Cx43 and Cx40 expression in A7r5 cells and pSMCs, but the expression of Cx37 and Cx45 was also investigated. Our main findings are that Cx43 expression level in pSMCs is ~4-fold higher compared to A7r5 cells, and that Cx40 is not expressed in pSMCs. Lack of Cx40 expression in rat mesenteric pSMCs is in accordance with results obtained in guinea-pig mesenteric arterioles (Yamamoto et al., 2001), in the SMCs of the adult rat aorta (van

Kempen and Jongma, 1999), as well as mouse aorta (Alonso et al., 2010), but differs from the results of Gustafsson et al. (2003), where immunoreactivity of Cx40 was detected in the media of small mesenteric arterioles. On the other hand, these studies agreed that Cx40 is predominantly expressed in endothelial cells. The variability of connexin expression in arteries is likely due to the fact that different species and vascular beds were studied.

Previous studies have shown, that coexpression of Cx40 and Cx43, including in A7r5 cells, allows the formation of gap junction channels with mixed connexin composition. Such junctions display functional properties different from junctions formed of a single connexin isoform (Burt et al., 2001; Cottrell et al., 2001, 2002; Heyman et al., 2009). In our study, however, immunostaining images (Fig. 4.6) revealed that most of the Cx43 in A7r5 cells seemed to be trapped in the cytoplasm. Cx40 distribution was also concentrated in the cytoplasm. On the other hand, immunofluorescence staining for Cx43 in pSMCs demonstrated strong immunoreactivity of Cx43 at the sites of cell-cell contact indicating the formation of Cx43 gap junction plaques. Based on our experimental results, we hypothesized that expression of Cx40 in A7r5 cells may have interfered with cell-to-cell communication. To test this hypothesis, we aimed to use cells that express higher Cx43 than Cx40; hence, we used the 6B5N cell line, which is a clone of A7r5 cells that expresses a higher Cx43:Cx40 ratio (Burt et al., 2001). In the 6B5N cells the higher Cx43:Cx40 ratio was obtained by decreased Cx40 expression levels, with no difference in Cx43 expression levels compared to the parental A7r5 cells. In 6B5N cells, local mechanical stimulation induced intercellular Ca²⁺ wave propagation. 6B5N cells also exhibited better LY dye-coupling than A7r5 cells, consistent with previously published data (Burt et al., 2001). The functional results obtained with 6B5N cells were comparable to those obtained with pSMCs.

By comparing Cx45 and Cx37 expression between pSMCs and 6B5N cells, Cx45 expression levels are significantly lower in 6B5N cells than in pSMCs, but no significant difference was found in Cx37 expression levels. These results suggest that neither Cx45 nor Cx37 was significantly involved in the observed experimental differences.

Immunostaining experiments showed that Cx43 in 6B5N cells was localized at the sites of cell-cell contact with few Cx43 in the cytoplasm. Therefore, based on the Cx expression and immunostaining images, it

seems that there exists an inverse relationship between Cx40 expression and the presence of Cx43 at the cell surface; in absence of Cx40 expression, as in pSMCs, Cx43 is exclusively present at the cell surface; in case of a medium expression of Cx40, as in 6B5N cells, Cx43 is present at the cell surface and in the cytoplasm; whereas, in case of a high expression of Cx40, as in A7r5 cells, Cx43 is mainly present in the cytoplasm. The possible mechanism by which Cx40 affects Cx43 trafficking and the level of interaction between those two proteins is not readily apparent. Further studies are necessary to resolve these possibilities.

To prove the involvement of Cx43 in mediating intercellular Ca^{2+} waves in pSMCs and in 6B5N cells, we used short connexin-mimetic peptides homologous to the extracellular loop of Cx43 (⁴³Gap 26) (Chaytor et al., 1997), designed to specifically inhibit Cx43. ⁴³Gap 26 inhibited Ca^{2+} wave propagation in both pSMCs and 6B5N cells. Thus, the inhibitory action of ⁴³Gap 26 demonstrated the involvement of Cx43 gap junction channels in the propagation of intercellular Ca^{2+} waves. The mechanisms underlying the propagation of Ca^{2+} waves in pSMCs and the molecules that diffuse through GJs remain to be determined and identified.

4.4 Conclusion

In summary, we have provided evidence for the first time that primary cultured rat mesenteric smooth muscle cells express Cx37, Cx43 and Cx45, but not Cx40. We showed that intercellular Ca^{2+} waves in these cells are mediated by Cx43 gap junction channels. Coexpression of Cx43 and Cx40 may be a relevant factor in determining the efficiency of cell-cell communication. The significance of this observation is rather high when considering the potential contribution of gap junctions to general circulatory homeostasis and the regulation of vascular tone. Further studies are needed to explore the possible mechanisms by which Cx40 affects Cx43 trafficking.

Chapter

5

Fast and slow intercellular Ca^{2+} waves

5.1 Introduction

A change in intracellular Ca^{2+} concentration ($[\text{Ca}^{2+}]_i$) is a key step in several functions that SMCs perform, including contraction. An increase in $[\text{Ca}^{2+}]_i$ in one cell, in response to chemical, electrical or mechanical stimuli, may propagate to neighboring SMCs along the arterial wall, as an intercellular Ca^{2+} wave (Karaki et al., 1997). Cytoplasmic Ca^{2+} increase is a result of either Ca^{2+} influx from the outside of the cell and/or Ca^{2+} release from the sarcoplasmic reticulum (SR). Voltage-operated calcium channels (VOCCs) mediate Ca^{2+} influx across the plasma membrane, whereas Ca^{2+} release from the SR occurs through the activation of two families of Ca^{2+} channels: inositol 1,4,5-trisphosphate (IP_3) and ryanodine (Ry) receptors. IP_3 receptors (IP_3Rs) are activated by Ca^{2+} itself and IP_3 (Foskett et al., 2007), a second messenger generated by the activation of phospholipase C (PLC) in response to stimuli (Berridge, 1993). Ry receptors (RyRs), are activated by Ca^{2+} (Zalk et al., 2007). A small increase in $[\text{Ca}^{2+}]_i$ may induce further Ca^{2+} release from the SR, a process known as Ca^{2+} -induced Ca^{2+} -release (CICR), which results in a Ca^{2+} wave that progresses throughout the cell and may propagate to neighboring cells. The mechanisms underlying the propagation of intra- and intercellular Ca^{2+} waves in SMCs, however, have yet to be clarified.

Already at the single cell level, the mechanisms involved in intracellular Ca^{2+} wave propagation are controversial. Some previous investigations have reported that RyRs are the major channels responsible for

Ca^{2+} wave propagation (Boittin et al., 1999; Ruehlmann et al., 2000; Straub et al., 2000; Ji et al., 2006). Other studies, however, have reported that CICR through IP_3Rs is sufficient to mediate a Ca^{2+} wave (Iino et al., 1993; Lamont and Wier, 2004; McCarron et al., 2004; Bai et al., 2009; McCarron et al., 2010). The reason for this controversy is that the mechanisms involved in Ca^{2+} wave propagation depend on the SMC type and condition (cultured or not). A better understanding of the mechanisms underlying intercellular Ca^{2+} waves is important, because Ca^{2+} waves play an important role in the propagation of contraction of SMCs along the arterial wall, and thus modulate local vascular resistance and blood flow.

To investigate the propagation mechanisms of Ca^{2+} waves at the cellular level, we used primary cultured rat mesenteric SMCs (pSMCs) loaded with the fluorescent Ca^{2+} dye Fluo-4. These cells were derived from the same tissue in which Ca^{2+} wave propagation was observed in arterial segments (Seppey et al., 2010). We applied the microcontact printing technique to culture pSMCs on collagen lines. The aligned arrangement of the cells facilitates local stimulation of a single cell at a restricted site, away from neighboring cells and the observation of Ca^{2+} wave progression from one cell to another. To induce an intercellular Ca^{2+} wave, a single pSMC was locally stimulated with a micropipette or by microinjection of KCl. Inhibitors of gap junctions, VOCCs, Ry and IP_3 receptors were applied to assess the involvement of these channels in the propagation of Ca^{2+} waves. Our results show that the propagation of intercellular Ca^{2+} waves depend on membrane depolarization-induced Ca^{2+} entry and require a SR with functional IP_3 receptors. Moreover, we show the effects of subsequent stimuli on the appearance of Ca^{2+} waves.

5.2 Results

5.2.1 Characteristics of mechanically-induced Ca^{2+} response in pSMCs: propagation of fast and slow Ca^{2+} waves

pSMCs grown on μCP collagen lines were mechanically stimulated in presence of a perfusion flow. The stimulation was restricted to a small region of the first cell, the furthest possible from the neighboring cell (marked by an asterisk in Fig. 5.1). Local mechanical stimulation evoked a $[\text{Ca}^{2+}]_i$

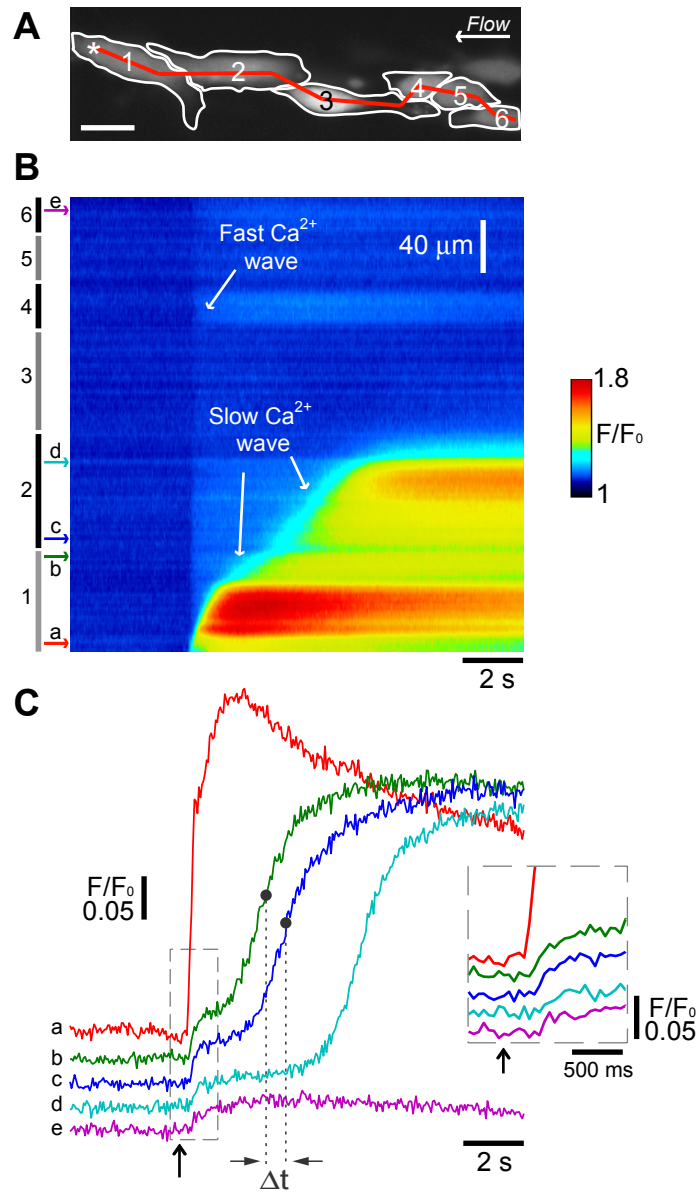


Figure 5.1: Local mechanical stimulation induced intercellular Ca²⁺ waves. **A)** Fluorescence image of pSMCs on μ CP collagen line. Place of stimulation is indicated by an asterisk in cell 1. Arrow indicates the direction of perfusion flow. Scale bar: 40 μ m. **B)** Kymograph of Ca²⁺ dependent fluorescence, with distance derived from the red trajectory in **A**, vertically and time running from left to right. The numbers and the black/grey vertical lines to the left of the kymograph correspond to the cells through which the red trajectory passes in **A**. Increasing fluorescence ratio (F/F_0) (thus free $[Ca^{2+}]_i$) is denoted by increasingly warm colors, see color bar. **C)** The traces show fluorescence profiles (F/F_0 , averaged over 4 pixels) measured at the sites indicated by the correspondingly colored horizontal arrows to the left of the kymograph in **B**. Time of stimulation is marked by a vertical arrow below the fluorescence profiles. The inset is a zoom of the profiles around the time of stimulation (marked with a rectangle). Δt between profiles b & c correspond to the transjunctional delay. Local mechanical stimulation evoked two distinct Ca²⁺ waves: 1) a fast Ca²⁺ wave that rapidly propagated to neighbouring cells, and 2) a slow Ca²⁺ wave that was spatially limited in propagation.

increase, followed by the propagation of the [Ca²⁺]_i transient that progressed throughout the stimulated cell. With an acquisition rate of 20 Hz and by analyzing the [Ca²⁺]_i response through a kymograph drawn along a line of pSMCs, images revealed that stimulation induced two distinct Ca²⁺ waves, that propagated with different velocities: 1) a fast Ca²⁺ wave, that propagated with a high velocity, but a small amplitude, and 2) a slow Ca²⁺ wave, consisting of a large amplitude, slowly travelling spatial [Ca²⁺]_i gradient. A representative response of pSMCs to local mechanical stimulation is shown in Fig. 5.1.

The fast Ca²⁺ wave propagated rapidly to all observed neighboring cells with a velocity of $2310 \pm 210 \mu\text{m/s}$ ($n = 25$). The propagation of the slow Ca²⁺ wave was most often spatially limited; it was always induced in the stimulated cell, but in only 28 % of the experiments propagated to a neighboring cell. The velocity of the slow Ca²⁺ wave was relatively constant through the cell, away from the stimulating site; in the first cell (stimulated cell): $19.8 \pm 1.6 \mu\text{m/s}$ ($n = 25$); in the second cell: $21.4 \pm 2.2 \mu\text{m/s}$ ($n = 7, P = 0.62$ compared to the first cell).

The amplitude of the Ca²⁺ signal at the site of stimulation (marked by "a" in Fig. 5.1 B) reached a peak value 1.2 – 1.6 s after stimulation. By plotting the [Ca²⁺]_i profile towards the end of the stimulated cell and in neighboring cells, a biphasic rise of [Ca²⁺]_i could be observed (Fig. 5.1 C, profiles b & c). The first increase, fast phase, is the fast Ca²⁺ response. The second delayed increase, the slow phase, is due to the arrival of the slow Ca²⁺ wave. This biphasic rise of [Ca²⁺]_i was not visible at the stimulation site. The amplitude of the Ca²⁺ transients varied in different regions of the cell, presumably due to the inhomogeneous distribution of release channels on the SR (Foskett et al., 2007). Likely for the same reason, as the Ca²⁺ transient progressed to neighboring cells its amplitude decreased; in few experiments, however, the Ca²⁺ increase was larger than in the stimulated cell (e.g., control experiments in Fig. 5.4 and 5.5).

When the slow Ca²⁺ wave passed from one cell to another, the wave experienced a delay before appearing in the next cell (transjunctional delay (Δt)). The wave front actually disappeared at this site, which corresponds to the gap junctional cleft (Fig. 5.1 B). Transjunctional delays were measured by taking the time difference between the points where F/F_0 is 50 % of maximum for each profile; the base of the profile was taken after the first Ca²⁺ increase, the fast phase, reaches a plateau (Fig. 5.1 C, profiles

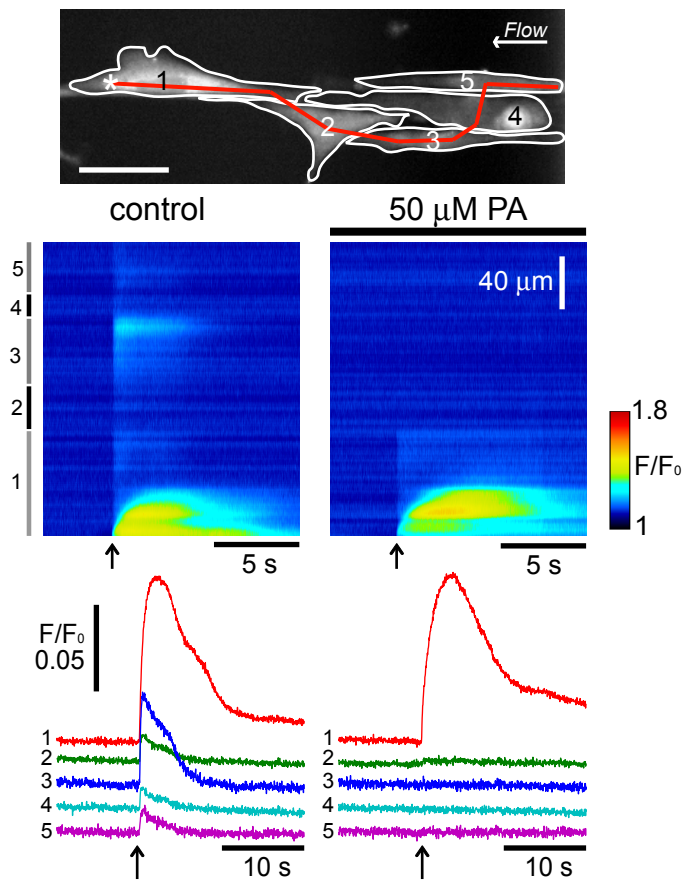


Figure 5.2: Intercellular fast Ca^{2+} wave propagation was mediated through gap junction channels. Gap junction uncoupler palmitoleic acid (PA) abolished fast Ca^{2+} wave propagation to neighboring cells. The right and the left kymographs are the same cells, taken from the same red trajectory in the fluorescence image, whereas, the fluorescence profiles correspond to changes in F/F_0 in the entire cell (ROI). Top image scale bar: 40 μm .

b & c). Transjunctional delays were 0.84 ± 0.16 s ($n = 7$). By measuring the distance between those two points the velocity across the junction was found to be 10.4 ± 0.9 $\mu\text{m}/\text{s}$ ($n = 7$).

To test whether the fast Ca^{2+} wave propagation was mediated through gap junction channels and not due to membrane stretching during mechanical stimulation, experiments were performed in buffer solution containing the gap junction uncoupler, palmitoleic acid (PA) (Lavado et al., 1997). Incubation of pSMCs in 50 μM PA for 20 min suppressed fast Ca^{2+} wave propagation to neighboring cells (Fig. 5.2) ($n = 5$).

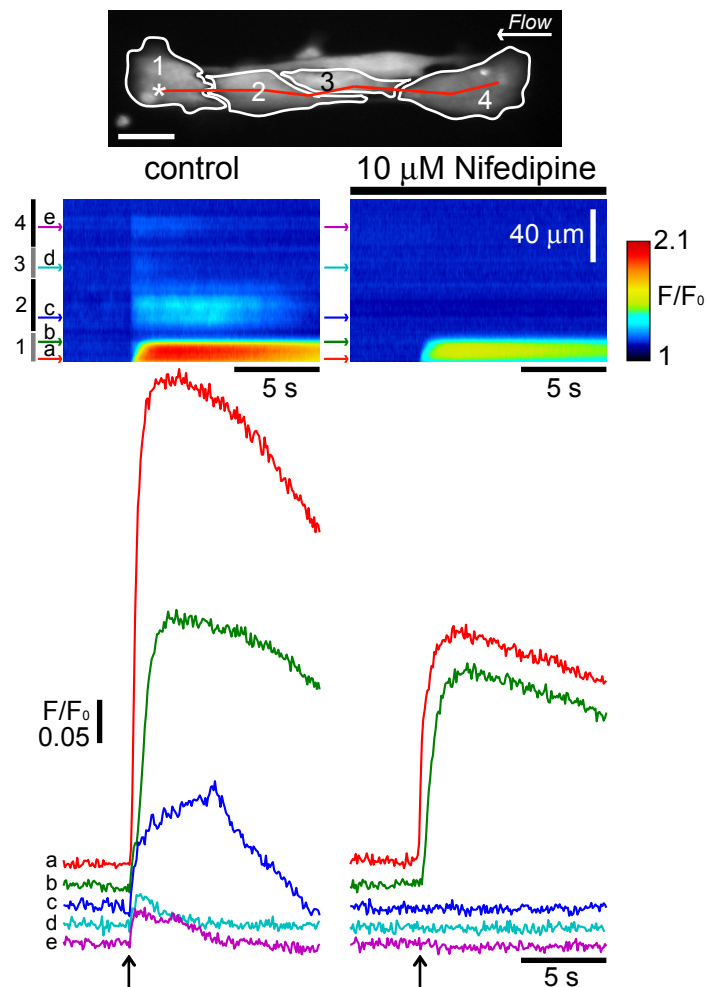


Figure 5.3: Contribution of VOCCs to the propagation of the fast Ca^{2+} wave. The VOCCs inhibitor nifedipine abolished the fast Ca^{2+} wave and caused a decrease in $[\text{Ca}^{2+}]_i$ amplitude without affecting slow wave velocity in the stimulated cell. Top image scale bar: $20\ \mu\text{m}$.

5.2.2 Role of L-type voltage-operated Ca^{2+} channels in the propagation of fast Ca^{2+} waves

To test the hypothesis that the fast Ca^{2+} wave was the result of Ca^{2+} influx through VOCCs, we used nifedipine, an L-type VOCCs inhibitor (Wang et al., 2000) and Bay K8644, a VOCCs activator (Zahradníková et al., 2007). Preincubation of pSMCs in $10\ \mu\text{M}$ nifedipine for 5 min completely abolished the fast Ca^{2+} waves. The propagation of the slow Ca^{2+} wave in the

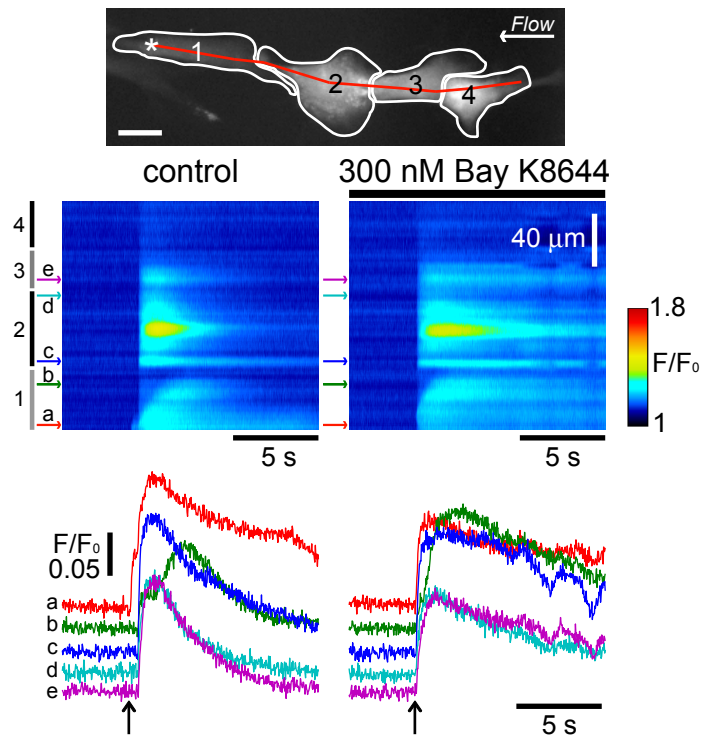


Figure 5.4: Contribution of VOCCs to the propagation of the fast Ca^{2+} wave. Bay K8644, which prolongs the opening of VOCCs, prolonged Ca^{2+} influx, and caused an earlier onset for the slow Ca^{2+} wave without affecting slow wave velocity in the stimulated cell. Top image scale bar: $20 \mu\text{m}$.

stimulated cell was not inhibited (Figure 5.3). In the stimulated cell, average Ca^{2+} amplitude decreased by $43 \pm 11 \%$ ($n = 7$) compared to control experiments with no change to slow wave velocity: $v = 22.04 \pm 3.3 \mu\text{m/s}$, $P = 0.41$, $n = 7$.

Experiments were then performed in presence of Bay K8644, which is known to prolong the opening of VOCCs in a concentration dependent manner (Zahradníková et al., 2007). Stimulation in presence of 300 nM Bay K8644, after a 5 min preincubation period, resulted a longer Ca^{2+} increase (Fig. 5.4) without change to average peak amplitude ($P = 0.63$, $n = 7$). Ca^{2+} wave velocity was statistically not different from control ($v_{\text{fast}} = 2306 \pm 439 \mu\text{m/s}$, $P = 0.99$, $v_{\text{slow}} = 18.81 \pm 2.25 \mu\text{m/s}$, $P = 0.90$, $n = 7$), however, the slow wave was triggered earlier than in control experiments (Fig. 5.4).

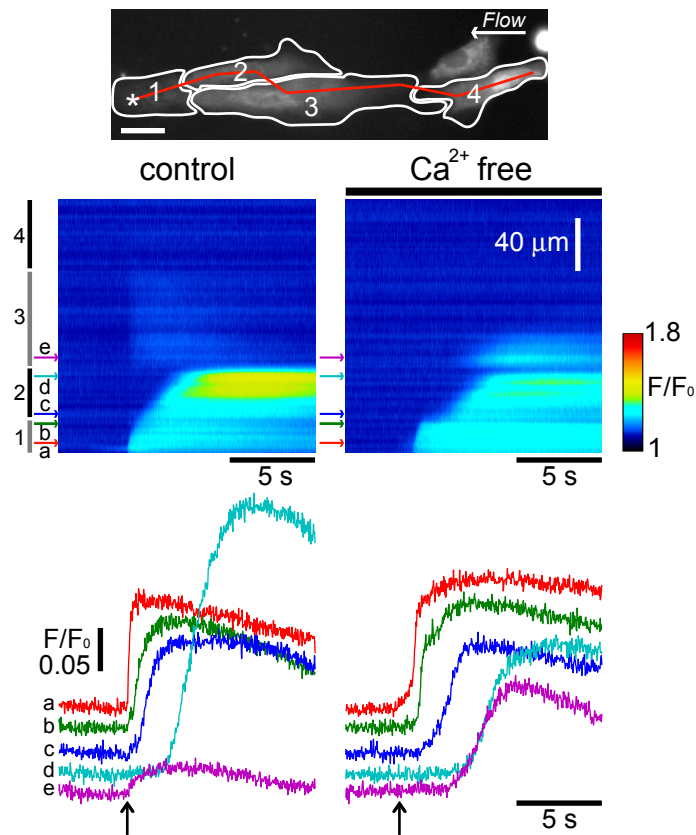


Figure 5.5: Effects of extracellular Ca^{2+} free medium. Fast Ca^{2+} waves were not observed when stimulation was performed in Ca^{2+} free medium (+0.5 mM EGTA). The transjunctal delay was longer compared to control. Top image scale bar: 20 μm .

5.2.3 Role of extracellular calcium in the propagation of slow Ca^{2+} waves

To test the influence of extracellular Ca^{2+} on the propagation of the slow Ca^{2+} wave, we performed experiments within 3 min after the application of Ca^{2+} free medium supplemented with 0.5 mM EGTA. Only experiments demonstrating a slow Ca^{2+} wave propagation to neighboring cells in the control experiment were considered.

As expected from previous experiments using nifedipine, fast Ca^{2+} waves were never observed in Ca^{2+} free medium. On the opposite, slow calcium waves were still elicited upon mechanical stimulation, and their propagation to neighboring cells was not inhibited in the absence of ex-

tracellular calcium. As a result of the absence of the fast Ca^{2+} wave, the kinetics of $[\text{Ca}^{2+}]_i$ increase changed; the biphasic Ca^{2+} rise changed to a one phase increase. At the time of stimulation the $[\text{Ca}^{2+}]_i$ started to gradually increase until a sharp start of the upstroke (Fig. 5.5).

Average peak amplitude decreased by $26 \pm 8.4\%$ compared to control in the second cell ($P = 0.04$, $n = 4$). Slow wave velocity neither in the first cell, nor in the second cell was statistically different in the absence of extracellular Ca^{2+} compared to control ($17.9 \pm 4.4 \mu\text{m/s}$, $P = 0.39$, $n = 4$, calculated for the slow Ca^{2+} wave in the second cell). The transjunctional delay was ~ 2 -fold longer than in control experiments.

5.2.4 Local KCl-induced Ca^{2+} response

In another series of experiments, local KCl stimulation was applied instead of local mechanical stimulation. Experiments were performed in a configuration of cells where at least 6 cells were connected on the μCP line. KCl stimulation is known to induce membrane depolarization causing Ca^{2+} entry through VOCCs (Bolton, 1979; Ganitkevich V and Isenberg, 1991). Local KCl stimulation induced fast intercellular Ca^{2+} wave propagation, but no slow Ca^{2+} waves were observed, not even in the stimulated cell (Fig. 5.6).

The amplitude of the fast wave induced by local KCl stimulation was statistically not different from that obtained by local mechanical stimulation ($P = 0.62$, $n_{\text{KCl}} = 8$, $n_{\text{mechanical}} = 11$). The fast intercellular wave propagation velocity was $2170 \pm 189 \mu\text{m/s}$ ($n = 8$), which was statistically not different from those obtained by local mechanical stimulation ($P = 0.73$).

5.2.5 Calcium release from intracellular stores; IP_3 receptors and Ryanodine receptors

To explore the role of the IP_3Rs and RyRs in the propagation of Ca^{2+} waves, responses to Xes C and ryanodine, that inhibit IP_3Rs and RyRs respectively, were examined. Only experiments demonstrating a slow Ca^{2+} wave propagation to neighboring cells in the control experiment were considered.

Inhibition of IP_3 receptors with Xes C caused a significant decrease

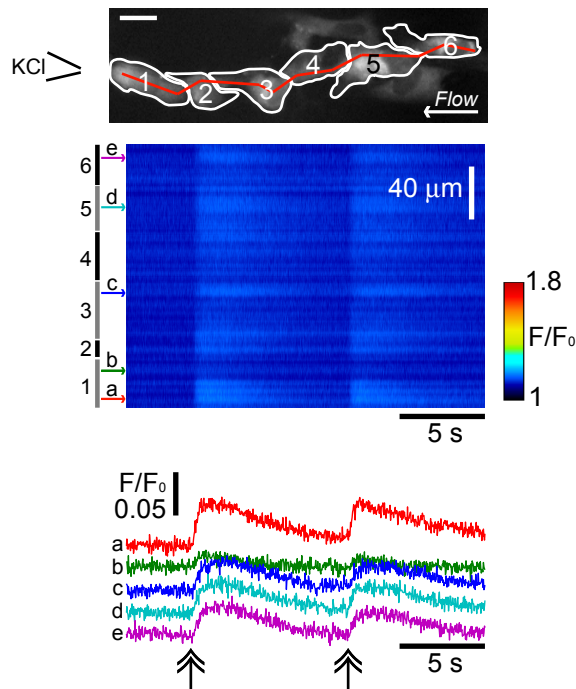


Figure 5.6: Local KCl stimulation evoked a fast Ca^{2+} wave that propagated with the same velocity as the fast waves initiated with local mechanical stimulation; but no slow Ca^{2+} wave was observed. Top image scale bar: 20 μm .

in average Ca^{2+} increase ($80.4 \pm 9.2\%$, $n = 4$, measured at the first cell) and suppressed the propagation of the slow Ca^{2+} wave, including in the stimulated cell (Fig. 5.7). On the other hand, pSMCs exposed to 20 μM ryanodine for 20 min showed a small decrease in average Ca^{2+} amplitude ($6.7 \pm 1.7\%$, $n = 3$, measured at the second cell), which was statistically not different from control experiments. However, ryanodine changed the appearance of the Ca^{2+} increase within one cell (Fig. 5.8). Ryanodine had no effect on the slow Ca^{2+} wave velocity compared to control; control first cell: $23.94 \pm 0.87 \mu\text{m/s}$, Ry first cell: $23.36 \pm 0.42 \mu\text{m/s}$, $P = 0.70$; control second cell: $22.52 \pm 1.02 \mu\text{m/s}$, Ry second cell: $21.93 \pm 0.54 \mu\text{m/s}$, $P = 0.61$, $n = 3$.

5.2.6 Effects of multiple stimuli

As mentioned earlier, the stimulated cell could be repetitively and reproducibly stimulated without change in the rate of Ca^{2+} increase for sub-

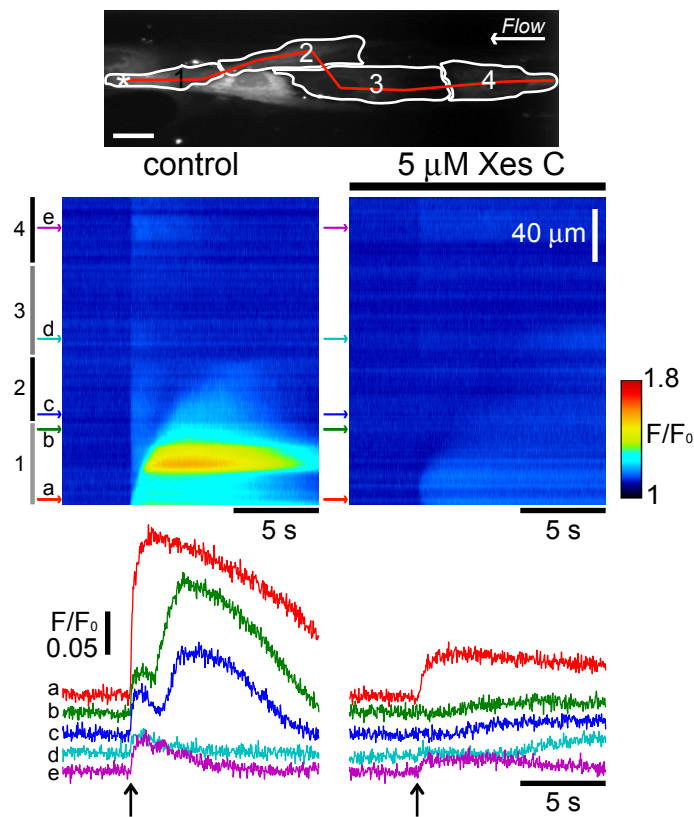


Figure 5.7: Role of IP_3Rs in Ca^{2+} wave propagation. *Xestospongin C* (*Xes C*) suppressed the propagation of the slow Ca^{2+} waves, including in the stimulated cell. The amplitude of the fast Ca^{2+} wave decreased. Top image scale bar: 20 μm .

sequent stimuli. However, if a second stimulation occurs just before the stimulated cell $[Ca^{2+}]_i$ goes back to basal level, the probability that the slow Ca^{2+} wave propagates to a neighboring cell was increased to 67 % ($n = 8$ out of 12) (Fig. 5.9 A).

This time window during which slow wave propagation could be enhanced, was measured to be between 35 and 60 s from the first stimulation, but more importantly; the second stimulation must happen before $[Ca^{2+}]_i$ goes back to basal level. If the second stimulation occurred earlier than this time window, the pSMCs were still in a refractory period and no changes were observed in neighboring cells. If the second stimulation occurs after the time window, then the second Ca^{2+} response was a replica of the first one. The second stimulation had no effect on the propagation velocity. A third stimulation did not result in any further communication

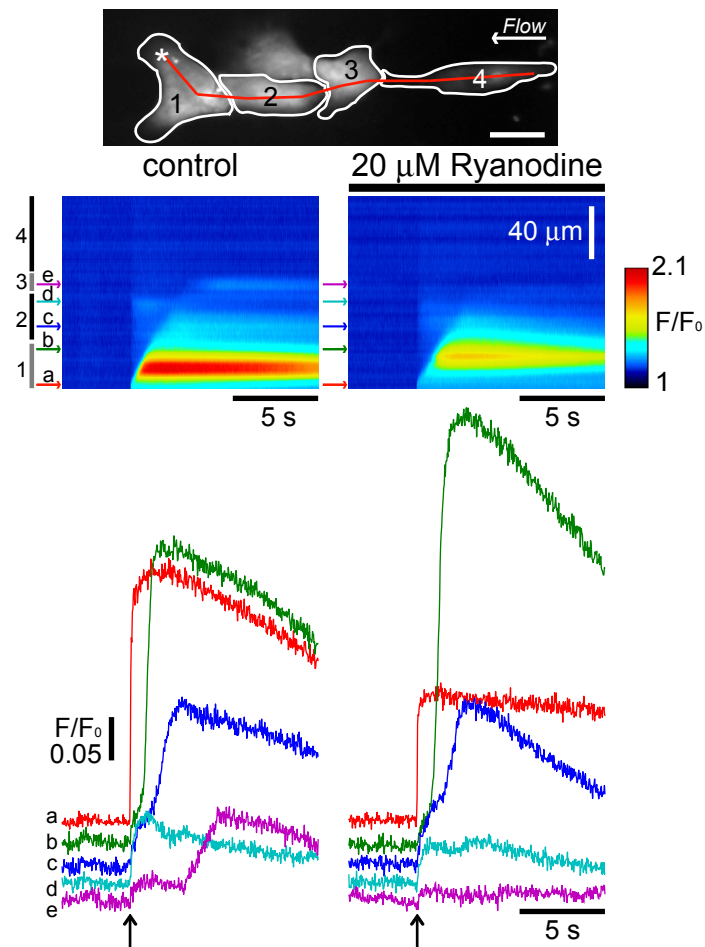


Figure 5.8: Role of RyRs in Ca^{2+} wave propagation. Ryanodine had no significant effect on the fast Ca^{2+} waves. A small decrease in the amplitude of the slow Ca^{2+} wave was observed without change in their velocity. Top image scale bar: 20 μm .

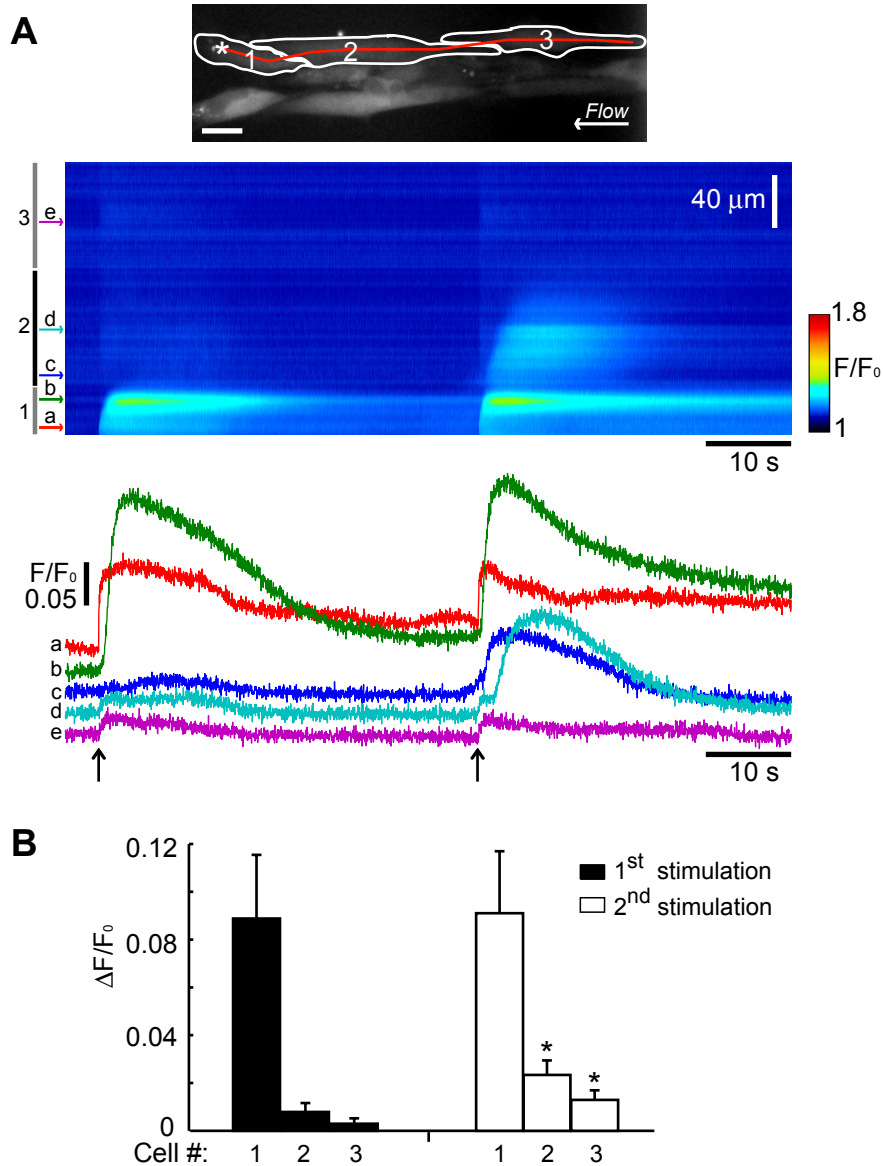


Figure 5.9: Effects of a second mechanical stimulation. **A)** The stimulated cell was exposed to a second stimulation shortly after the first one. Applying a second stimulation within a time window after the first one increased the probability of initiating slow intercellular Ca^{2+} waves in adjacent cells. Top image scale bar: $20\ \mu\text{m}$. **B)** Comparison of $\Delta F/F_0$ in pSMCs subject to two subsequent mechanical stimulations.

enhancement. In Fig. 5.9 B, we compare the Ca^{2+} rise between the first and the second stimulation which was applied within the required time window ($n = 8$). The fast Ca^{2+} rise was subtracted from the data of $\Delta F/F_0$ for the second and the third cell.

Adding a small concentration of phenylephrine (PE) to the extracellular medium, as a background stimulation, increases the IP_3 concentration and subsequently the $[\text{Ca}^{2+}]_i$, rendering the cells more sensitive to CICR (Seppey et al., 2010; Koenigsberger et al., 2010). We expected that, applying a background stimulation to pSMCs would mimic the effect of a second stimulation and would increase the range of slow Ca^{2+} wave propagation. However, pSMCs in culture substantially lost their sensitivity to PE. Replacing PE with vasopressin (AVP) induced spontaneous-like Ca^{2+} oscillations in pSMCs. We have also performed experiments with local AVP stimulation, but AVP induced only a slow Ca^{2+} wave in the stimulated cell, which did not propagate to neighboring cells (data are shown in Appendix A).

5.3 Discussion

5.3.1 Propagation of fast and slow Ca^{2+} waves: a general characterization

Using primary cultured mesenteric SMCs, we investigated the mechanisms underlying gap junction mediated propagation of intercellular Ca^{2+} waves, induced by local mechanical stimulation. Local mechanical stimulation of a single pSMC induced two distinct intercellular Ca^{2+} waves; a fast Ca^{2+} wave and a slow Ca^{2+} wave. The fast Ca^{2+} wave propagated to all observed neighboring cells with a low $[\text{Ca}^{2+}]_i$ amplitude, whereas the slow Ca^{2+} wave propagated with a high amplitude, but was spatially limited to the first cell and in only 28 % of the experiments propagated to a neighboring cell. Previous studies have shown that light mechanical stimulation, even in extracellular Ca^{2+} free medium, can induce $[\text{Ca}^{2+}]_i$ release from internal stores (Boitano et al., 1994; Charles et al., 1991). In our experiments, mechanical stimulation, in absence of external Ca^{2+} also induced an increase in $[\text{Ca}^{2+}]_i$ and a propagating Ca^{2+} wave, indicating that the source of the intracellular Ca^{2+} was from internal stores. The velocity

of the slow intracellular Ca^{2+} wave ($\sim 19 \mu\text{m/s}$) is typical of those reported in many studies of different systems (for a review see (Jaffe, 2010)). Those waves are found to be based on the regenerative CICR mechanism.

5.3.2 Propagation of fast Ca^{2+} waves depends on the propagation of membrane depolarization

In our experiments, we did not measure membrane potential; however, inhibition (activation) of VOCCs with nifedipine (Bay K8644), experiments in Ca^{2+} -free medium and with gap junction inhibitors demonstrate that the fast intercellular Ca^{2+} wave was a consequence of Ca^{2+} influx due to the propagation of membrane depolarization. Local membrane depolarization with KCl induced fast intercellular Ca^{2+} waves propagating with the same velocity and amplitude. These results strongly suggest that the propagation of mechanically-induced and KCl-induced fast Ca^{2+} waves is based on the same mechanism. Therefore, what appears as a fast intercellular Ca^{2+} wave is a rapid electrotonic propagation of membrane depolarization mediated through gap junctions that triggers Ca^{2+} increase through VOCCs opening in all connected pSMCs. In arteries, this likely represents a major mechanism by which a local stimuli can synchronize large numbers of smooth muscle cells for integrated vasomotor responses (Bény, 1999).

5.3.3 Propagation of the slow Ca^{2+} waves requires functional IP_3 receptors

Inhibition of IP_3 Rs with Xes C caused a significant decrease in average peak $[\text{Ca}^{2+}]_i$ and completely abolished slow Ca^{2+} wave propagation, including in the stimulated cell. In presence of ryanodine, that inhibits RyRs, both fast and slow Ca^{2+} waves were still observed. Ca^{2+} amplitude, compared to control, varied in different regions of the cell, but the change in average peak amplitude was statistically not different from control. Slow Ca^{2+} wave velocity was also unaffected in presence of ryanodine. These results were expected based on results of previous reports. It has been demonstrated by Berra-Romani et al. (2008), by using the same cell type as in this study, that rat arterial SMCs in primary culture express higher levels of IP_3 Rs compared to freshly dissociated SMCs. Increased expres-

sion of IP_3Rs was also observed in rat aortic SMCs in culture (Tasker et al., 2000). On the other hand, of the three RyR subtypes, RyR-II expression was downregulated, whereas, RyR-III was upregulated in primary cultured arterial myocytes (Berra-Romani et al., 2008). RyR-I is expressed abundantly in skeletal muscle (Takeshima et al., 1989), whereas, vascular SMCs express mainly RyR-II and RyR-III (Sanders, 2001). RyR-II, unlike RyR-III, is involved in the CICR mechanism (Sonnleitner et al., 1998; Coussin et al., 2000). Co-operativity between IP_3Rs and RyRs may occur depending on their expression ratio. This co-operativity, however, can be absent in cells expressing low or no RyRs (Boittin et al., 2000). Thus, the induced Ca^{2+} release is mainly mediated through IP_3Rs . This explains why IP_3Rs , rather than RyRs were primarily involved in the propagation of the slow Ca^{2+} waves.

In presence of Xes C, the fast Ca^{2+} wave was still observed, but with a substantially decreased amplitude. According to our results, we conclude that 1) propagation of slow Ca^{2+} waves requires functional IP_3Rs , and 2) the amplitude of the fast Ca^{2+} wave was not solely due to Ca^{2+} influx from the extracellular medium through VOCCs, but also involved Ca^{2+} release primarily through IP_3Rs . An illustration for the possible mechanisms involved in the propagation of fast and slow Ca^{2+} waves is presented in Fig. 5.10.

5.3.4 Transmission of the slow Ca^{2+} waves to neighboring cells through gap junctions: transjunctional delay

From the discussions above, the slow Ca^{2+} wave propagation was probably driven by a positive-feedback mechanism by Ca^{2+} . Requirement of IP_3 is also evident, since IP_3Rs require IP_3 besides Ca^{2+} for their activation (Foskett et al., 2007). Production of IP_3 is a result of phospholipase C activation, which can also be $[\text{Ca}^{2+}]_i$ and membrane-depolarization sensitive (Itoh et al., 1992; Berridge, 1993; Hirose et al., 1999). Considering IP_3 as the required component for the propagation of slow Ca^{2+} waves, could explain the transjunctional delay. The transjunctional delay measured in the current study (~ 0.8 s) is within the range measured previously (0.5 – 1 s) (Sanderson et al., 1990; Sneyd et al., 1994). This delay is presumably related to the time it takes to build up enough IP_3 at the trans side of the gap junction to reach the threshold for IP_3R activation. The longer transjunc-

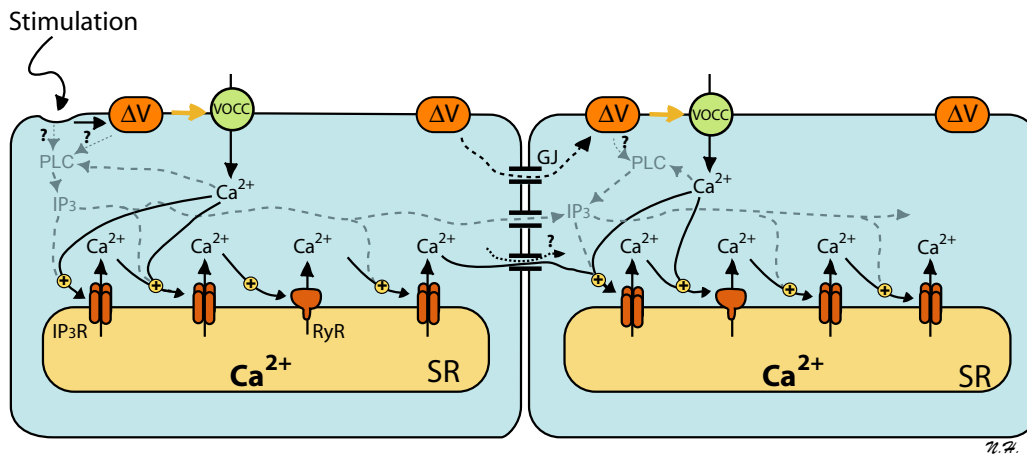


Figure 5.10: Schematic illustration of the propagation of fast and slow intercellular Ca^{2+} waves in pSMCs. Stimulation induces membrane-depolarization (ΔV), that is transmitted rapidly to the neighboring cell through gap junction channels (GJ). In the meantime, stimulation also activates phospholipase C (PLC) to produce IP_3 . IP_3 production may also be voltage- and $[\text{Ca}^{2+}]_i$ -sensitive. Diffusion of IP_3 and/or Ca^{2+} to SR calcium release channels (mainly IP_3Rs) causes further Ca^{2+} release and initiates the process of CICR (slow Ca^{2+} wave). IP_3 , Ca^{2+} and other, yet unknown, second messenger(s) propagate through GJ and may initiate a CICR based slow Ca^{2+} wave in the neighboring cell.

tional delay observed in Ca^{2+} free medium (also observed in (Sanderson et al., 1990; Sneyd et al., 1994)), could be explained by the lack of IP_3 on the trans side of the gap, which was produced during the fast Ca^{2+} wave in control conditions.

5.3.5 Role of the second stimulation in enhancing the range of slow Ca^{2+} wave propagation

Previous reports demonstrated that waves that exclusively rely on gap junction mediated IP_3 movement propagate over a limited distance, generally not much more than 2 – 4 cells (Braet et al., 2001, 2003; Fry et al., 2001), although this depends on the amount of IP_3 produced and the permeability of the gap junction channels. In the current study, slow Ca^{2+} wave propagation was spatially limited to the first cell, and in only 28 % of the experiments propagated to the second cell. A second stimulation increased the probability of the propagation to the second cell to 67 %.

This second stimulation had to be applied within a certain time window. It is likely, that the second stimulation induced a slow Ca^{2+} wave in the neighboring cell because the basal level of IP_3 and Ca^{2+} was slightly elevated due to the first stimulation. The first stimulation rendered the cells and IP_3 Rs more sensitive to CICR. In the cytosol, Ca^{2+} can diffuse to $< 1 \mu\text{m}$ distances before being buffered, whereas IP_3 can diffuse up to $24 \mu\text{m}$ (Allbritton et al., 1992). Therefore, a propagating intracellular Ca^{2+} wave that primarily depends on Ca^{2+} release through IP_3 Rs cannot rely on passive diffusion of IP_3 , but should also be synthesized throughout the cell. Otherwise, the slow intracellular Ca^{2+} wave would diminish halfway through the cell.

5.4 Conclusion

In this chapter, we imaged the spatiotemporal patterns of calcium waves induced by local mechanical and local KCl stimulation in primary cultured rat mesenteric SMCs. Cells were aligned with the microcontact printing technique to facilitate the observation of wave propagation. Mechanical stimulation induced two distinct intercellular Ca^{2+} waves with different velocities, a fast and a slow Ca^{2+} wave. We have shown that the fast intercellular Ca^{2+} wave was due to gap junction mediated membrane depolarization and subsequent Ca^{2+} entry, whereas, the slow Ca^{2+} wave was due to Ca^{2+} release, primarily through IP_3 receptors. Our results suggest a mechanism by which intercellular Ca^{2+} waves can propagate in SMCs of the arterial wall.

Chapter

6

Conclusions

The research work presented in this thesis focuses on gap junction mediated intercellular communication in arterial SMCs, with a particular focus on intercellular Ca^{2+} wave propagation.

In the first part of the thesis, we characterized three types of vascular SMCs, A7r5, pSMCs and 6B5N cells, in terms of connexin expression and the involvement of Cx43 gap junction channels in mediating intercellular Ca^{2+} waves. To the best of our knowledge, connexin expression in pSMCs has not yet been characterized. The main findings of this study is that pSMCs – unlike the A7r5 cell line – do not express Cx40, and that intercellular Ca^{2+} waves in pSMCs are mediated by Cx43. Comparison of results from cells coexpressing Cx43 and Cx40 demonstrated a direct correlation between higher Cx43:Cx40 expression ratios and successful propagation of Ca^{2+} waves to neighboring cells. The results of this study suggests that coexpression of Cx43 with Cx40, depending on their relative expression levels, affects trafficking and assembly of Cx43 into gap junctions. Further studies are needed to explore the level of interaction between those two proteins and the possible mechanisms by which Cx40 regulates Cx43 gap junction assembly. We also conclude that, while A7r5 cells may not be suitable, pSMCs are appropriate as an *in vitro* model to study the underlying mechanisms of intercellular Ca^{2+} wave propagation in mesenteric arterial SMCs.

In the second part of the thesis, we studied the mechanisms underlying intercellular Ca^{2+} waves in pSMCs. Cells were aligned with the microcontact printing technique to facilitate Ca^{2+} wave observation and analysis. The main finding of this study is that local mechanical stimulation induced two intercellular Ca^{2+} waves with different velocities, a fast (~ 2 mm/s) and a slow (~ 20 $\mu\text{m/s}$) intercellular Ca^{2+} wave. From the re-

sults obtained, we concluded that the fast Ca^{2+} wave was due to the electrotonic propagation of membrane depolarization via gap junctions and subsequent Ca^{2+} entry through VOCCs. The slow Ca^{2+} wave, however, was due to intracellular Ca^{2+} release from the SR through primarily IP_3 receptors. Together, our results suggest a mechanism by which intercellular Ca^{2+} waves can propagate between SMCs of the arterial wall.

7.1 Experimental perspectives

7.1.1 Characterization of Cx43 and Cx40 protein interaction

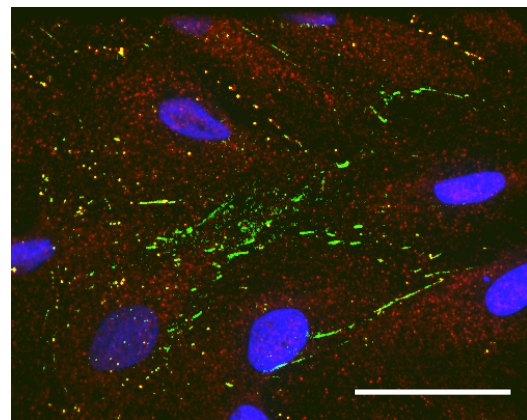
In Chapter 4 we have shown that there exists an interaction between Cx40 and Cx43 that affects Cx43 trafficking. Previous studies showed that Cx43 and Cx40 can form gap junctions of heteromeric connexons (Fig. 2.4 D) (He et al., 1999; Cottrell et al., 2001). To detect this interaction in our A7r5 and 6B5N cells, we propose to perform co-immunoprecipitation analysis. This technique works when the proteins involved are bound to each other tightly, such as Cx43 and Cx40 when forming a heteromeric channel. We also propose to use pSMCs as control for these experiments. If the interaction is confirmed, the level of interaction could be also determined. The next question to address would be why these connexons are trapped within the cytoplasm?

It is important to note, that based on functional data, it appears that Cx37 and Cx43 can also form heteromeric channels (Brink et al., 1997). In Chapter 4, in Fig. 4.5 B & C, we show that Cx37 protein expression in both pSMCs and 6B5N cells is reduced compared to A7r5 cells. Even Cx43 and Cx45 can form heteromeric channels (Martinez et al., 2002). In the same figure, we show that in pSMCs Cx45 protein expression is much higher than in A7r5 cells. The involvement of Cx37 or Cx45 in intercellular communication is not readily apparent. We could conclude from our results that neither Cxs are significantly involved in the propagation of gap junction mediated Ca^{2+} waves, however, further studies are needed to elucidate whether Cx37 or Cx45 regulate Cx43 expression or trafficking.

7.1.2 Regulation of Cx43 gap junction assembly by cAMP

Depending on the cell type, many different agents that increase intracellular cyclic AMP (cAMP) levels have been shown to increase Cx43 phosphorylation. Such enhancement has been shown to result from increased synthesis (Mehta et al., 1992) and/or increased trafficking of connexons to the plasma membrane, resulting in an increase in the cluster size and number of gap junctions (Burghardt et al., 1995; Wang et al., 1995; Paulson et al., 2000). Some studies demonstrated that cAMP increases gap junctional coupling and channel gating activity (Mehta et al., 1992; Chanson et al., 1996). Other studies, however, showed no effect of cAMP on gap junction communication (Kwak and Jongsma, 1996). cAMP may enhance cell-cell communication in A7r5 cells. To address this problem, we propose to use 8-Br-cAMP, an activator of cAMP-dependent protein kinases. Because of the modification by bromine, this compound is more lipophilic than cAMP, and it is membrane permeant. Therefore, 8-Br-cAMP should increase Cx43 trafficking and enhance Cx43 gap junction channel assembly in A7r5 cells, and thus may enhance cell-cell communication and intercellular Ca^{2+} wave propagation. In a test experiment, immunostaining of Cx43 was detectable at the sites of cell-cell contact in A7r5 cells within 1 hour of 1 mM 8-Br-cAMP application, with negligible amount detected in the cytoplasm (Fig. 7.1). Further experiments (scrape-load dye transfer and Ca^{2+} experiments) are needed to test whether the formed Cx43 gap junctions are functional.

Figure 7.1: Increase of Cx43 (green) gap junction channel clustering by cAMP. Incubation of A7r5 in 8-Br-cAMP increased trafficking of Cx43 to the plasma membrane resulting in the formation of Cx43 gap junction clusters. Cx40 in red and nuclei in blue. Scale bar: 40 μm .

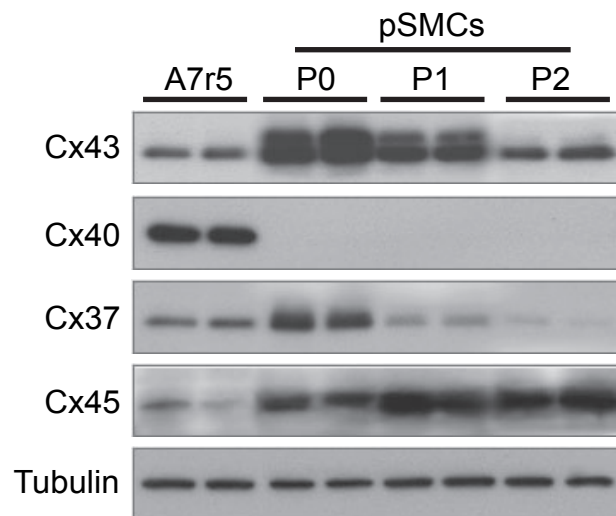


7.1.3 Expression of Cx43 in pSMCs at different passages and implication on function

In this thesis, we used pSMCs exclusively from passage one (P1, see Chapter 3.1). The reason is primarily technical; to increase the number of cells, and to facilitate the local stimulation of a single cell. To our knowledge, pSMCs in terms of Cx expression had not been studied yet. We showed in Chapter 4 that pSMCs in P1 express Cx37, Cx43 and Cx45, but not Cx40. However, in separate experiments, we have observed a difference in Cx expression between the passages P0, P1 and P2. We stopped at P2, since P3 cells showed morphological changes. Fig. 7.2 demonstrates the changes in protein expression in function of passage.

Therefore, we propose first to perform protein analysis on an arterial segment from which pSMCs are derived to understand the tendency in protein expression from the arterial segment to P2. Then, one can test whether this difference has any implication on the functionality of gap junctions on cell-cell communication between the cells in P0 to P2. To test the functionality, perhaps application of microinjection of e.g. Lucifer Yellow, or other tracers would be easier to perform on P0 cells than the scrape-load technique used in Chapter 4.

Figure 7.2: Western blot analysis of connexin expression in pSMCs at different passages, compared to A7r5 cells.



7.1.4 Propagation of depolarization and its influence on the slow Ca^{2+} waves

In Chapter 5, we have shown that the fast intercellular Ca^{2+} wave was due to the propagation of membrane depolarization and subsequent Ca^{2+} entry. In our experiments, however, we did not measure membrane potential. We propose to simultaneously measure changes in $[\text{Ca}^{2+}]_i$ and changes in membrane potential in a configuration of cells where 2 or at most 3 cells are connected with each other on the μCP line. Perhaps a better method to monitor changes in membrane potential and changes in $[\text{Ca}^{2+}]_i$, is to use the commercially available micro-electrode arrays. With such a device, conduction velocities and propagation patterns could also be measured, even from a cluster of several pSMCs. It would be also interesting to replace mechanical stimulation with electrical stimulation.

From the experiments in Chapter 5 the question arises as to whether inhibition of VOCCs with nifedipine would completely abolish slow wave propagation to neighboring cells? Because the slow Ca^{2+} wave progresses to the neighboring cell with a $\sim 28\%$ probability, more experiments are needed to prove this. Ideally, these experiments should be performed in cells that show intercellular slow wave propagation in the corresponding control experiment.

Nifedipine blocks Ca^{2+} entry through VOCCs, but the electrotonic propagation of membrane potential to neighboring cells is preserved. Therefore, to test whether intercellular slow Ca^{2+} wave propagation is depolarization dependent, we propose to inhibit Ca^{2+} -activated chloride channels. These channels are activated following an intracellular Ca^{2+} increase. By inhibiting these channels the membrane potential will not be further depolarized and regenerated, thus if slow waves are depolarization dependent, their range of propagation would be limited compared to control experiments.

In Chapter 5, Fig. 5.5, cell #3 displayed a slow Ca^{2+} wave in absence of extracellular Ca^{2+} , that did not progress throughout the cell. Such an enhanced Ca^{2+} signal propagation was observed in all experiments performed in Ca^{2+} -free medium. The reason of this enhancement is not clear, and could be related to the fact that the propagation of membrane depolarization was not inhibited. This phenomenon can be important for the understanding of intercellular slow Ca^{2+} wave propagation.

7.1.5 Ca^{2+} release in arterial segments: IP_3Rs vs. RyRs

Our results in Chapter 5 demonstrated that slow Ca^{2+} wave propagation requires functional IP_3Rs . This result was expected since Berra-Romani et al. (2008) had demonstrated that pSMCs express more IP_3Rs compared to freshly isolated cells and RyRs expression was switched from RyR-II to RyR-III . RyR-III is not involved in CICR. Because of this change in expression of the two important Ca^{2+} release channels, we propose to perform experiments with ryanodine and Xes C on rat mesenteric arterial segments and applying local PE and KCl stimulation (Seppey et al., 2010). These experiments would also demonstrate the contribution of either IP_3Rs or RyRs (or both) to contraction.

7.1.6 The effect of temperature

Mechanical performance of muscles is greatly influenced by temperature. Moderate cooling (from 37 to 20 °C) has been known to have a strong modulatory effect on the mechanical activity of different types of SMCs (Nasu, 1990). For example, studies on pressurized cerebral arteries at 37°C demonstrated that application of ryanodine caused an immediate contraction compared to arteries at room temperature (Knot et al., 1998). In intact, pressurized rat mesenteric small arteries, a decrease of temperature from 37°C to room temperature caused a decrease in the frequency of vasomotion (Mauban et al., 2001). It is suggested that arteries in myogenic tone at mammalian temperature are more depolarized (Jaggar, 2001). Also, membrane conductance increased with rising temperature and decreased with cooling in the smooth muscle of guinea-pig taenia coli (Brading et al., 1969). Based on these results, it is likely that cultured pSMCs in 37°C would be more sensitive to stimulation, thus respond faster and perhaps with an increased Ca^{2+} wave velocity. Therefore, stimulation at a higher temperature may be more efficient in triggering an intercellular Ca^{2+} wave, and the propagation of the slow Ca^{2+} wave might extend to few more cells.

7.1.7 PSMCs can contract if cultured on deformable substrates

In our studies we did not detect contraction of pSMCs, A7r5 or 6B5N cells. It is believed that SMCs in culture differentiate into a non-contractile phe-

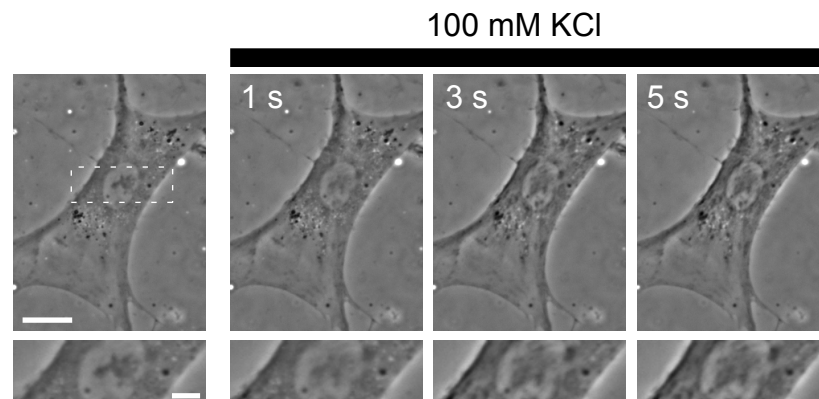


Figure 7.3: Global KCl stimulation induced contraction of pSMCs cultured on deformable substrates. Scale bars: 20 μ m, zoom: 6 μ m

notype (Chamley-Campbell et al., 1979; Golovina and Blaustein, 2006). We tested whether pSMCs would be able to contract if cultured on a soft, deformable substrate. For this purpose, we used culture dishes coated with silicone substrates, with a stiffness of 10 kPa, a kind gift from Dr. Lysianne Follonier Castella and Dr. Charles Godbout, as discussed in Castella et al. (2010).

PSMCs were cultured on the silicone substrates as described for Ca²⁺ experiments in Chapter 3.1. To induce contraction we used global AVP and KCl stimulation. As shown in Appendix A, pSMCs are very sensitive to AVP. Already a concentration of 100 pM induces Ca²⁺ response. However, stimulation did not induce contraction, not even with 500 nM AVP. On the other hand, 100 mM KCl induced a rapid contraction in pSMCs ($n = 6$) (Figure 7.3). It is important to note, that we did not detect contraction with 50 mM KCl. These experiments suggest that pSMCs cannot contract if cultured on a stiff substrate but not because they lose their contractile phenotype in culture.

Culturing pSMCs on soft substrates allows to study Ca²⁺ variations and contractions simultaneously at the cellular level. Data from pSMCs cultured in such an environment could better explain the results obtained in *in vitro* experiments of arterial segments.

7.2 Model perspectives

For this thesis a mathematical model describing intercellular Ca²⁺ wave propagation in SMCs has been developed. The validity of this model was

tested in a semester project by Marco Salathe (a physics Masters student, under my supervision). The model could reproduce intercellular Ca^{2+} waves propagating from one cell to another cell through gap junctions. The description of this model is included in Appendix B. The main purpose of constructing the model was to predict the reason of the enhanced Ca^{2+} intercellular communication after a second mechanical stimulation.

According to the results in Chapter 5, when the cell was stimulated for the second time, the wave propagated to 1 or 2 more cells. However, if the second stimulation occurred rapidly after the first one no enhancement was observed. Moreover, if the second stimulation occurred more than 1 min after the first stimulation, no enhancement was observed either. This shows that there exists a refractory period that has significant effects on the CICR mechanism, also, that there is a time window, after the first stimulation where the cell is still excitable. A possible explanation for this is that the IP_3 concentration is still elevated in the cell after the first stimulation.

To model the enhanced communication and predict the mechanisms involved, we will probably need to incorporate an equation modeling the time evolution of the opening probability of the activated channels at the membrane of the SR. Also, by adjusting the model parameters we may arrive to the case where the asymptotic state of the cell is non-oscillatory, but the cell is not in a stable steady state, i.e., we may find bistability in the system. In this state a small perturbation (a second stimulation) may excite the cell to produce a new Ca^{2+} transient. Such behavior is characteristic for excitable state.

Appendix A

Chemical stimulation

A.1 Background stimulation

The following are supplementary data for the experiments referred to in Section 5.2.6. To test the Ca^{2+} response of pSMCs due to PE stimulation, we applied global stimulation with $0.8 \mu\text{M}$ PE (Seppey et al., 2008). Neither this concentration value nor $50 \mu\text{M}$ induced any Ca^{2+} rise. Increasing PE up to $100 \mu\text{M}$ induced a small Ca^{2+} rise ($n = 3$, Fig. A.1 A). On the other hand, pSMCs were sensitive to global AVP stimulation. Already 100 pM AVP induced spontaneous-like Ca^{2+} oscillations in $\sim 40\%$ cells ($n = 5$, Fig. A.1 B).

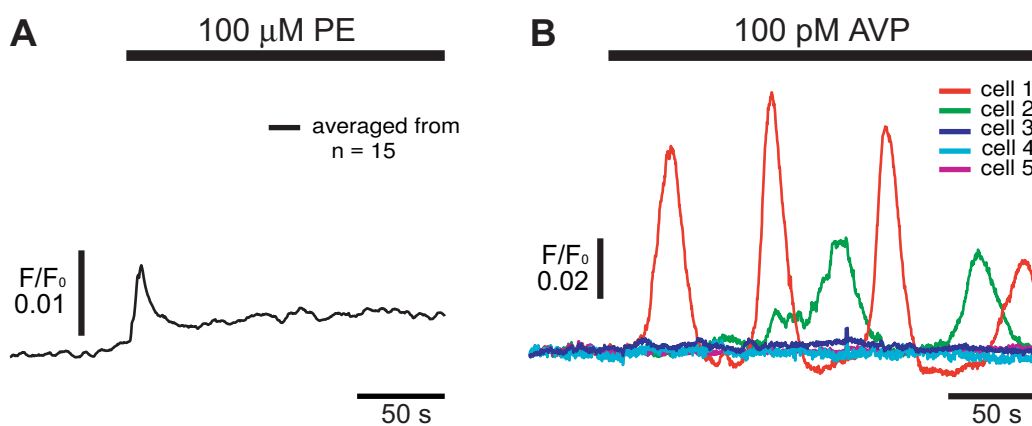


Figure A.1: **A)** Global PE stimulation. pSMCs in culture substantially lost their sensitivity to PE. **B)** Global AVP stimulation. Stimulation induced spontaneous-like Ca^{2+} oscillations already at pM concentration values.

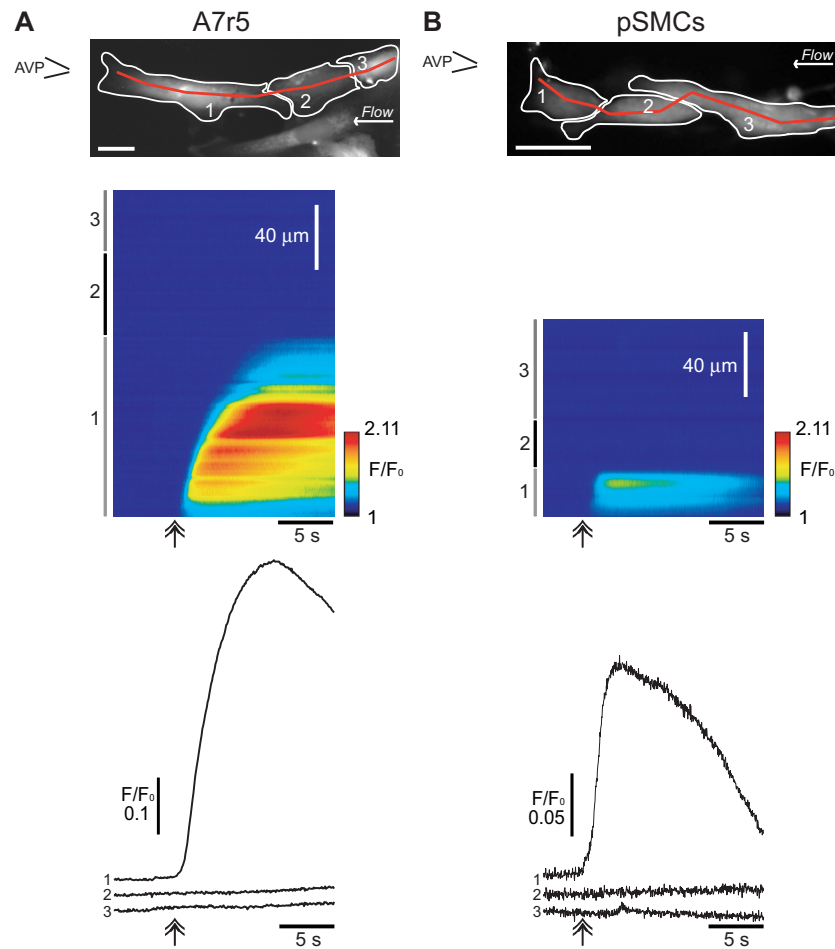


Figure A.2: Local AVP stimulation in pSMCs and A7r5 cells. Stimulation induced a slow Ca^{2+} wave in the stimulated cell, that did not propagate to neighboring cells. Top image scale bar: $25\mu\text{m}$.

A.2 Local AVP stimulation

The following are supplementary data for the experiments referred to in Section 5.2.6. We have performed local AVP stimulation on all three cell types, pSMCs ($n = 5$), A7r5 ($n = 12$) and 6B5N cells ($n = 9$). Stimulation induced only a slow Ca^{2+} wave in the stimulated cell that did not propagate to neighboring cells. Fig. A.2 demonstrates Ca^{2+} response due to local AVP stimulation in pSMCs and A7r5 cells, and see Fig. A.3 for 6B5N cells. Fig. A.3 also demonstrates that extracellular diffusion of AVP induces Ca^{2+} response in all observed cells. Therefore, the cells are responsive, but with local AVP stimulation, for some reason, the signal was not transmitted.

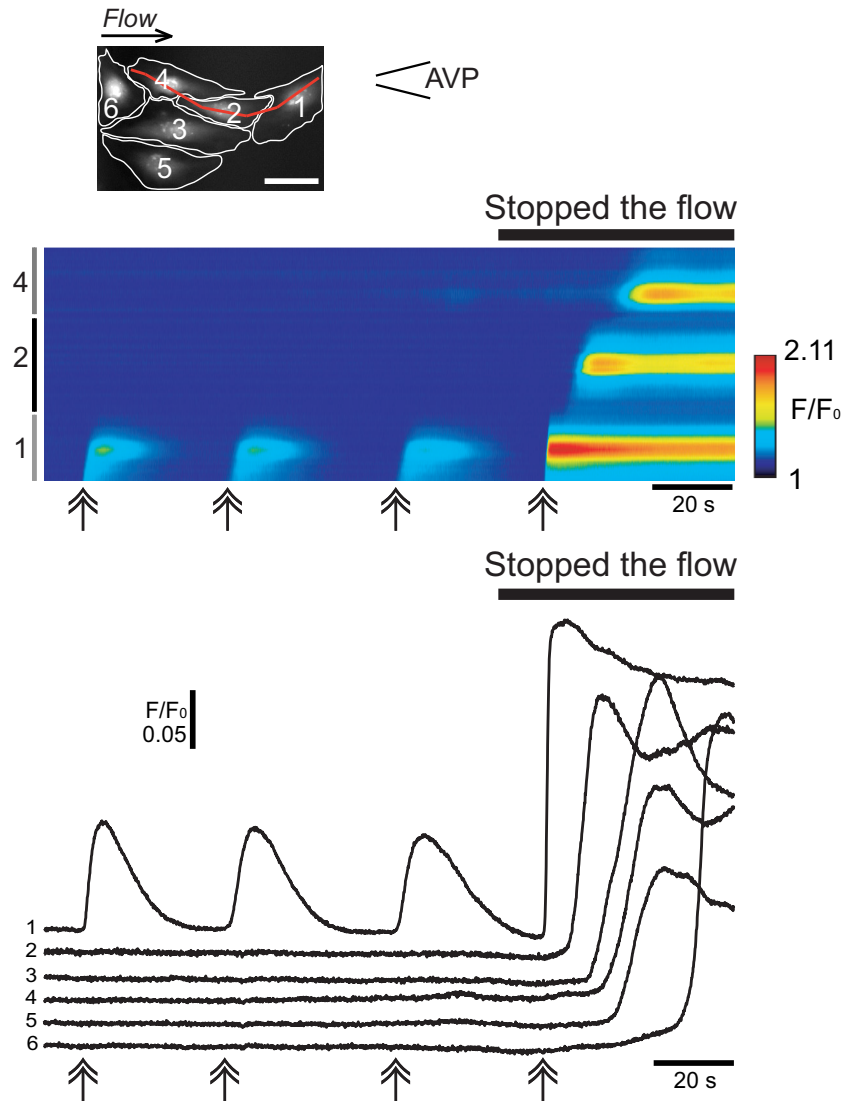


Figure A.3: Local AVP stimulation in 6B5N cells. Stimulation induced a slow Ca^{2+} wave in the stimulated cell, that did not propagate to neighboring cells. If the counter flow was stopped, however, all observed cells responded to the diffusing AVP. Top image scale bar: $25\mu\text{m}$.

Appendix

B

Model equations

B.1 A model for Ca^{2+} waves

The equations describing the calcium dynamics in SMCs referred to in Section 7.2 are adapted from Koenigsberger et al. (2004). This model takes into account the most important cellular components involved in the regulation of SMC calcium dynamics. The equations has been extended by diffusional terms with effective diffusion coefficients D_c for Ca^{2+} and D_{ip} for IP_3 . The values of D_c and D_{ip} (see Table B.1) are taken from Allbritton et al. (1992). A one-dimensional arrangement of cells is considered since cells are seeded along a line and we follow changes in $[\text{Ca}^{2+}]_i$ along a line on a kymograph, as demonstrated in Fig. 5.1 A & B.

The model has the following variables: the calcium concentration in the cytosol c_i , the IP_3 concentration I_i , the calcium concentration in the SR s_i , the cell membrane potential v_i and the open state probability w_i of calcium activated potassium channels in cell i :

$$\frac{\partial c_i}{\partial t} = D_c \frac{\partial^2 c_i}{\partial x^2} + J_{\text{CICR}_i} - J_{\text{SRuptake}_i} + J_{\text{leak}_i} + J_{\text{extrusion}_i} + J_{I_i} - J_{\text{VOCC}_i} + J_{\text{Na/Ca}_i} \quad (\text{B.1})$$

$$\frac{\partial I_i}{\partial t} = D_{ip} \frac{\partial^2 I_i}{\partial x^2} + J_{\text{PLCagonist}_i} + J_{\text{PLC}\delta_i} - J_{\text{degrad}_i}, \quad (\text{B.2})$$

$$\frac{ds_i}{dt} = J_{\text{SRuptake}_i} - J_{\text{CICR}_i} - J_{\text{leak}_i}, \quad (\text{B.3})$$

$$\frac{dv_i}{dt} = \gamma(-J_{\text{Na/K}_i} - J_{\text{Cl}_i} - 2J_{\text{VOCC}_i} - J_{\text{Na/Ca}_i} - J_{\text{K}_i}) + V_{\text{coupling}_i}, \quad (\text{B.4})$$

$$\frac{dw_i}{dt} = \lambda(K_{\text{activation}_i} - w_i). \quad (\text{B.5})$$

The various terms appearing in this set of nonlinear differential equations are detailed in (Parthimos et al., 1999). Equation (B.5) could be disregarded for modeling simplification. The quantity J_{I_i} represents the calcium release from the stores possessing IP_3 receptors. The term

$$J_{VOCC_i} = G_{Ca} \frac{v_i - v_{Ca_1}}{1 + e^{-[(v_i - v_{Ca_2})/R_{Ca}]}} \quad (B.6)$$

models the calcium influx through VOCCs,

$$J_{Na/Ca_i} = G_{Na/Ca} \frac{c_i}{c_i + c_{Na/Ca}} (v_i - v_{Na/Ca}) \quad (B.7)$$

is the Na^+/Ca^{2+} exchange,

$$J_{SRuptake_i} = B \frac{c_i^2}{c_i^2 + c_b^2} \quad (B.8)$$

represents the SR uptake,

$$J_{CICR_i} = C \frac{s_i^2}{s_c^2 + s_i^2} \frac{c_i^4}{c_c^4 + c_i^4} \quad (B.9)$$

is the calcium induced calcium release (CICR),

$$J_{extrusion_i} = D c_i \left(1 + \frac{v_i - v_d}{R_d}\right) \quad (B.10)$$

models the calcium extrusion from the SMC by Ca^{2+} -ATPase pumps,

$$J_{leak_i} = L s_i \quad (B.11)$$

is the leak from the SR,

The constant $J_{PLC_{agonist_i}}$ is the rate of the PLC activated by receptor-ligand agonists, while the term

$$J_{PLC_{ff_i}} = E \frac{c_i^2}{K_{Ca}^2 + c_i^2} \quad (B.12)$$

models the PLC- δ (Höfer et al., 2002). Finally, $J_{degrad_i} = k I_i$ expresses IP_3 degradation. The term $J_{IP_3_i}$ in Eq. B.1 is directly related to the IP_3 concen-

tration (Miyakawa et al., 1999):

$$J_{IP_3i} = F \frac{I_i^2}{K_I^2 + I_i^2}. \quad (B.13)$$

The term

$$J_{Na/Ki} = F_{Na/K} \quad (B.14)$$

describes the Na^+ - K^+ -ATPase,

$$J_{Cl_i} = G_{Cl}(v_i - v_{Cl}) \quad (B.15)$$

models the chloride channels,

$$J_{K_i} = G_K w_i (v_i - v_K) \quad (B.16)$$

models the K^+ efflux,

$$V_{coupling_i} = -g \sum_j (v_i - v_j) \quad (B.17)$$

models the electrical coupling between cells and

$$K_{activation_i} = \frac{(c_i + c_w)^2}{(c_i + c_w)^2 + \beta e^{-[(v_i - v_{Ca_3})/R_K]}} \quad (B.18)$$

represents the calcium and voltage activation of K^+ channels. All parameter values are given in Table 1. Several parameter values are subject to change with respect to the results obtained in order to be able to reproduce the experimental results.

B.2 Gap junctional communication

The attempt to incorporate IP_3 and Ca^{2+} diffusion through gap junction was based on Sneyd et al. (1995) (Sneyd et al., 1995) which is given in terms of the flux of IP_3 and Ca^{2+} from cell to cell. Cells are coupled by diffusive gap junctional fluxes of IP_3 and Ca^{2+} . For example, if cell i has $[IP_3] = I_i$, it is assumed that the flux of IP_3 from cell i to cell j is given by $P_{ip}(I_i - I_j)$, where P_{ip} is the gap junctional permeability to IP_3 . The same

equation will hold for the flux of Ca^{2+} between two adjacent cells after changing P_{ip} to P_c .

Assuming Fick's law, the intercellular flux conditions read:

$$D_c \frac{\partial c_i}{\partial x} = P_c (I_i - I_j) \quad (\text{B.19})$$

$$D_{ip} \frac{\partial I_i}{\partial x} = P_{ip} (I_i - I_j) \quad (\text{B.20})$$

The values of the parameters P_c and P_{ip} may differ because of the intrinsic properties of gap junction channels (e.g., charge and size selectivity) and because of the effect of fast Ca^{2+} buffering included in P_c (Höfer et al., 2001). Because of calcium buffering $P_c \ll P_{ip}$. There are no values for the gap junctional permeability P_c or P_{ip} of the SMCs in the literature, the coupling coefficients were treated as a free parameter.

B.3 Parameters

Input parameters in Table B.1 can be changed to fit experimental conditions and results.

Table B.1: Parameter values for the SMC model

Parameter	Description	Value	Source ¹
F	Maximal rate of activation dependent calcium influx	0.23 $\mu\text{M}/\text{s}$	ME
K_I	Half saturation constant for agonist-dependent calcium entry	1 μM	ME
G_{Ca}	Whole cell conductance for VOCCs	0.00129 $\mu\text{M mV}^{-1} \text{s}^{-1}$	ME
v_{Ca_1}	Reversal potential for VOCCs	100.0 mV	[PEG]
v_{Ca_2}	Half-point of the VOCC activation sigmoidal	-24.0 mV	[PEG]
R_{Ca}	Maximum slope of the VOCC activation sigmoidal	8.5 mV	[PEG]
$G_{Na/Ca}$	Whole cell conductance for $\text{Na}^+/\text{Ca}^{2+}$ exchange	0.007 $\mu\text{M mV}^{-1} \text{s}^{-12}$	ME
$c_{Na/Ca}$	Half-point for activation of $\text{Na}^+/\text{Ca}^{2+}$ exchange by Ca^{2+}	0.5 μM	[PEG]
$v_{Na/Ca}$	Reversal potential for the $\text{Na}^+/\text{Ca}^{2+}$ exchanger	-30.0 mV ²	[PEG]
B	SR uptake rate constant	2.025 $\mu\text{M}/\text{s}$	ME
c_b	Half-point of the SR ATPase activation sigmoidal	1.0 μM	[PEG]
C	CICR rate constant	55 $\mu\text{M}/\text{s}$	ME
s_c	Half-point of the CICR Ca^{2+} efflux sigmoidal	2.0 μM	[PEG]
c_c	Half-point of the CICR activation sigmoidal	0.9 μM	[PEG]
D	Rate constant for Ca^{2+} extrusion by the ATPase pump	0.08 s^{-12}	ME
v_d	Intercept of voltage dependence of extrusion ATPase	-100.0 mV	[PEG]
R_d	Slope of voltage dependence of extrusion ATPase	250.0 mV	[PEG]
L	Leak from SR rate constant	0.025 s^{-1}	[PEG]
$G_{stretch}$	Whole cell conductance for SACs	0.0061 $\mu\text{M mV}^{-1} \text{s}^{-1}$	ME
E_{SAC}	Reversal potential for SACs	-18 mV	[WD]
α	Slope of stress dependence of the SAC activation sigmoidal	0.0074 mmHg ⁻¹	ME
σ_0	Half-point of the SAC activation sigmoidal	500 mmHg	ME
γ	Scaling factor relating net movement of ion fluxes to the membrane potential (inversely related to cell capacitance)	1970 mV/ μM	[PEG]
$F_{Na/K}$	Net whole cell flux via the Na^+/K^+ -ATPase	0.2 $\mu\text{M}/\text{s}^2$	ME
G_{Cl}	Whole cell conductance for Cl^- current	0.00134 $\mu\text{M mV}^{-1} \text{s}^{-1}$	ME
v_{Cl}	Reversal potential for Cl^- channels	-25.0 mV	[PEG]
G_K	Whole cell conductance for K^+ efflux	0.002 $\mu\text{M mV}^{-1} \text{s}^{-12}$	ME
v_K	Reversal potential for K^+	-94.0 mV	[PEG]
λ	Rate constant for net K_{Ca} channel opening	45.0	[PEG]
c_w	Translation factor for Ca^{2+} dependence of K_{Ca} channel activation sigmoidal	0 μM	[PEG]
β	Translation factor for membrane potential dependence of K_{Ca} channel activation sigmoidal	0.13 μM^2	[PEG]
v_{Ca_3}	Half-point for the K_{Ca} channel activation sigmoidal	-27.0 mV	[PEG]
R_K	Maximum slope of the K_{Ca} activation sigmoidal	12.0 mV	[PEG]
$J_{PLC_{agonist_i}}$	Rate of PLC activated by agonists	free	
k	Rate constant of IP_3 degradation	0.1 s^{-1}	[WAT]
E	Maximal rate of PLC- δ	0 $\mu\text{M}/\text{s}^2$	[HVC]
K_{Ca}	Half-saturation constant for calcium activation of PLC- δ	0.3 μM	[HVC]
g	Homocellular electrical coupling coefficient	1000 s^{-1}	ME
P_c	Junctional permeability for Ca^{2+}		ME
P_{ip}	Junctional permeability for IP_3		ME
D_c	Effective diffusion coefficient of Ca^{2+}	20 $\mu\text{m}/\text{s}^2$	
D_{ip}	Diffusion coefficient of Ca^{2+}	280 $\mu\text{m}/\text{s}^2$	

¹ME \equiv Model Estimation; [PEG] \equiv Parthimos et al. (1999); [WAT] \equiv Wang et al. (1995); [WD] \equiv Wu and Davis (2001); [HVC] \equiv Höfer et al. (2002)

Bibliography

- Aalkjaer, C., Danielsen, H., Johannesen, P., Pedersen, E. B., Rasmussen, A., and Mulvany, M. J. (1985). Abnormal vascular function and morphology in pre-eclampsia: a study of isolated resistance vessels. *Clin Sci (Lond)*, 69:477–482.
- Aalkjaer, C. and Nilsson, H. (2005). Vasomotion: cellular background for the oscillator and for the synchronization of smooth muscle cells. *Br J Pharmacol*, 144:605–616.
- Akata, T., Kodama, K., and Takahashi, S. (1995). Role of endothelium in oscillatory contractile responses to various receptor agonists in isolated small mesenteric and epicardial coronary arteries. *Jpn J Pharmacol*, 68:331–343.
- Allbritton, N. L., Meyer, T., and Stryer, L. (1992). Range of messenger action of calcium ion and inositol 1,4,5-trisphosphate. *Science*, 258:1812–1815.
- Alonso, F., Krattinger, N., Mazzolai, L., Simon, A., Waeber, G., Meda, P., and Haefliger, J. A. (2010). An angiotensin ii- and nf-kappab-dependent mechanism increases connexin 43 in murine arteries targeted by renin-dependent hypertension. *Cardiovasc Res*, 87:166–176.
- Bai, Y., Edelmann, M., and Sanderson, M. J. (2009). The contribution of inositol 1,4,5-trisphosphate and ryanodine receptors to agonist-induced Ca²⁺ signaling of airway smooth muscle cells. *Am J Physiol Lung Cell Mol Physiol*, 297:347–361.

- Balemba, O. B., Heppner, T. J., Bonev, A. D., Nelson, M. T., and Mawe, G. M. (2006). Calcium waves in intact guinea pig gallbladder smooth muscle cells. *Am J Physiol Gastrointest Liver Physiol*, 291:717–727.
- Bandick, N. R. and Sparks, H. V. (1970). Contractile response of vascular smooth muscle of renal hypertensive rats. *Am J Physiol*, 219:340–344.
- Bartlett, I. S. and Segal, S. S. (2000). Resolution of smooth muscle and endothelial pathways for conduction along hamster cheek pouch arterioles. *Am J Physiol Heart Circ Physiol*, 278:604–612.
- Bayliss, M. (1902). On the local reactions of the arterial wall to changes in internal pressure. *J Physiol*, 28:220–231.
- Bény, J. L. (1999). Information networks in the arterial wall. *News Physiol Sci*, 14:68–73.
- Berra-Romani, R., Mazzocco-Spezia, A., Pulina, M. V., and Golovina, V. A. (2008). Ca²⁺ handling is altered when arterial myocytes progress from a contractile to a proliferative phenotype in culture. *Am J Physiol Cell Physiol*, 295:779–790.
- Berridge, M. J. (1993). Inositol trisphosphate and calcium signalling. *Nature*, 361:315–325.
- Berridge, M. J. (2009). Inositol trisphosphate and calcium signalling mechanisms. *Biochim Biophys Acta*, 1793:933–940.
- Berridge, M. J., Bootman, M. D., and Roderick, H. L. (2003). Calcium signalling: dynamics, homeostasis and remodelling. *Nat Rev Mol Cell Biol*, 4:517–529.
- Berridge, M. J., Lipp, P., and Bootman, M. D. (2000). The versatility and universality of calcium signalling. *Nat Rev Mol Cell Biol*, 1:11–21.
- Blatter, L. A. and Wier, W. G. (1992). Agonist-induced [Ca²⁺]_i waves and Ca²⁺-induced Ca²⁺ release in mammalian vascular smooth muscle cells. *Am J Physiol*, 263:576–586.
- Boitano, S., Sanderson, M. J., and Dirksen, E. R. (1994). A role for Ca²⁺-conducting ion channels in mechanically-induced signal transduction of airway epithelial cells. *J Cell Sci*, 107 (Pt 11):3037–3044.

- Boittin, F. X., Coussin, F., Morel, J. L., Halet, G., Macrez, N., and Mironneau, J. (2000). Ca^{2+} signals mediated by $\text{ins}(1,4,5)\text{p}_3$ -gated channels in rat ureteric myocytes. *Biochem J*, 349:323–332.
- Boittin, F. X., Macrez, N., Halet, G., and Mironneau, J. (1999). Norepinephrine-induced Ca^{2+} waves depend on IP_3 and ryanodine receptor activation in vascular myocytes. *Am J Physiol*, 277:139–151.
- Bolton, T. B. (1979). Mechanisms of action of transmitters and other substances on smooth muscle. *Physiol Rev*, 59:606–718.
- Brading, A., Bülbiring, E., and Tomita, T. (1969). The effect of temperature on the membrane conductance of the smooth muscle of the guinea-pig taenia coli. *J Physiol*, 200:621–635.
- Braet, K., Paemeleire, K., D'Herde, K., Sanderson, M. J., and Leybaert, L. (2001). Astrocyte-endothelial cell calcium signals conveyed by two signalling pathways. *Eur J Neurosci*, 13:79–91.
- Braet, K., Vandamme, W., Martin, P. E., Evans, W. H., and Leybaert, L. (2003). Photoliberating inositol-1,4,5-trisphosphate triggers atp release that is blocked by the connexin mimetic peptide gap 26. *Cell Calcium*, 33:37–48.
- Braverman, I. M., Keh, A., and Goldminz, D. (1990). Correlation of laser doppler wave patterns with underlying microvascular anatomy. *J Invest Dermatol*, 95:283–286.
- Brink, P. R., Cronin, K., Banach, K., Peterson, E., Westphale, E. M., Seul, K. H., Ramanan, S. V., and Beyer, E. C. (1997). Evidence for heteromeric gap junction channels formed from rat connexin43 and human connexin37. *Am J Physiol*, 273:1386–1396.
- Bund, S. (2001). Spontaneously hypertensive rat resistance artery structure related to myogenic and mechanical properties. *Clinical Science*, 101:385–393.
- Burghardt, R. C., Barhoumi, R., Sewall, T. C., and Bowen, J. A. (1995). Cyclic amp induces rapid increases in gap junction permeability and changes in the cellular distribution of connexin43. *J Membr Biol*, 148:243–253.

- Burt, J. M., Fletcher, A. M., Steele, T. D., Wu, Y., Cottrell, G. T., and Kurjika, D. T. (2001). Alteration of cx43:cx40 expression ratio in a7r5 cells. *Am J Physiol Cell Physiol*, 280:500–508.
- Byron, K. L. (1996). Vasopressin stimulates Ca^{2+} spiking activity in a7r5 vascular smooth muscle cells via activation of phospholipase a2. *Circ Res*, 78:813–820.
- Castella, L. F., Buscemi, L., Godbout, C., Meister, J. J., and Hinz, B. (2010). A new lock-step mechanism of matrix remodelling based on subcellular contractile events. *J Cell Sci*, 123:1751–1760.
- Chamley-Campbell, J., Campbell, G. R., and Ross, R. (1979). The smooth muscle cell in culture. *Physiol Rev*, 59:1–61.
- Chanson, M., White, M. M., and Garber, S. S. (1996). camp promotes gap junctional coupling in t84 cells. *Am J Physiol*, 271:533–539.
- Charles, A. C., Merrill, J. E., Dirksen, E. R., and Sanderson, M. J. (1991). Intercellular signaling in glial cells: calcium waves and oscillations in response to mechanical stimulation and glutamate. *Neuron*, 6:983–992.
- Charles, A. C., Naus, C. C., Zhu, D., Kidder, G. M., Dirksen, E. R., and Sanderson, M. J. (1992). Intercellular calcium signaling via gap junctions in glioma cells. *J Cell Biol*, 118:195–201.
- Chaytor, A. T., Evans, W. H., and Griffith, T. M. (1997). Peptides homologous to extracellular loop motifs of connexin 43 reversibly abolish rhythmic contractile activity in rabbit arteries. *J Physiol*, 503 (Pt 1):99–110.
- Chemtob, S., Inayatulla, A., and Varma, D. R. (1992). Eicosanoid-dependent and endothelium-independent oscillations of rat aorta. *J Vasc Res*, 29:270–280.
- Chen, Z. P., Levy, A., and Lightman, S. L. (1995). Nucleotides as extracellular signalling molecules. *J Neuroendocrinol*, 7:83–96.
- Christ, G. J., Moreno, A. P., Melman, A., and Spray, D. C. (1992). Gap junction-mediated intercellular diffusion of Ca^{2+} in cultured human cor-poral smooth muscle cells. *Am J Physiol*, 263:373–383.

- Clapham, D. E. (2007). Calcium signaling. *Cell*, 131:1047–1058.
- Coleman, H. A., Tare, M., and Parkington, H. C. (2001). K⁺ currents underlying the action of endothelium-derived hyperpolarizing factor in guinea-pig, rat and human blood vessels. *J Physiol*, 531:359–373.
- Cottrell, G. T., Wu, Y., and Burt, J. M. (2001). Functional characteristics of heteromeric cx40-cx43 gap junction channel formation. *Cell Commun Adhes*, 8:193–197.
- Cottrell, G. T., Wu, Y., and Burt, J. M. (2002). Cx40 and cx43 expression ratio influences heteromeric/ heterotypic gap junction channel properties. *Am J Physiol Cell Physiol*, 282:1469–1482.
- Coussin, F., Macrez, N., Morel, J. L., and Mironneau, J. (2000). Requirement of ryanodine receptor subtypes 1 and 2 for Ca²⁺-induced Ca²⁺ release in vascular myocytes. *J Biol Chem*, 275:9596–9603.
- Dora, K. A. (2010). Coordination of vasomotor responses by the endothelium. *Circ J*, 74:226–232.
- Evans, W. H., De Vuyst, E., and Leybaert, L. (2006). The gap junction cellular internet: connexin hemichannels enter the signalling limelight. *Biochem J*, 397:1–14.
- Fagrell, B., Fronek, A., and Intaglietta, M. (1977). A microscope-television system for studying flow velocity in human skin capillaries. *Am J Physiol*, 233:318–321.
- Figuroa, X. F. and Duling, B. R. (2009). Gap junctions in the control of vascular function. *Antioxid Redox Signal*, 11:251–266.
- Fill, M. and Copello, J. A. (2002). Ryanodine receptor calcium release channels. *Physiol Rev*, 82:893–922.
- Follonier, L., Schaub, S., Meister, J. J., and Hinz, B. (2008). Myofibroblast communication is controlled by intercellular mechanical coupling. *J Cell Sci*, 121:3305–3316.
- Foskett, J. K., White, C., Cheung, K. H., and Mak, D. O. (2007). Inositol trisphosphate receptor Ca²⁺ release channels. *Physiol Rev*, 87:593–658.

- Freeman, K. A., Mao, A., Nordberg, L. O., Pak, J., and Tallarida, R. J. (1995). The relationship between vessel wall tension and the magnitude and frequency of oscillation in rat aorta. *Life Sci*, 56:129–134.
- Fry, T., Evans, J. H., and Sanderson, M. J. (2001). Propagation of intercellular calcium waves in c6 glioma cells transfected with connexins 43 or 32. *Microsc Res Tech*, 52:289–300.
- Ganitkevich V, Y. and Isenberg, G. (1991). Depolarization-mediated intracellular calcium transients in isolated smooth muscle cells of guinea-pig urinary bladder. *J Physiol*, 435:187–205.
- Goffin, J. M., Pittet, P., Csucs, G., Lussi, J. W., Meister, J., and Hinz, B. (2006). Focal adhesion size controls tension-dependent recruitment of α -smooth muscle actin to stress fibers. *JCB*, 172:259–268.
- Goldberg, G. S., Valiunas, V., and Brink, P. R. (2004). Selective permeability of gap junction channels. *Biochim Biophys Acta*, 1662:96–101.
- Golovina, V. A. and Blaustein, P. M. (2006). Preparation of primary cultured mesenteric artery smooth muscle cells for fluorescent imaging and physiological studies. *Nature Protocols*, 1:2681–2687.
- Gonzalez-Fernandez, J. M. and Ermentrout, B. (1994). On the origin and dynamics of the vasomotion of small arteries. *Math Biosci*, 119:127–167.
- Griffith, T. M. and Edwards, D. H. (1993). Modulation of chaotic pressure oscillations in isolated resistance arteries by edrf. *Eur Heart J*, 14 Suppl I:60–67.
- Gustafsson, F., Mikkelsen, H. B., Arensbak, B., Thuneberg, L., Neve, S., Jensen, L. J., and Holstein-Rathlou, N. H. (2003). Expression of connexin 37, 40 and 43 in rat mesenteric arterioles and resistance arteries. *Histochem Cell Biol*, 119:139–148.
- Gustafsson, H., Mulvany, M., and Nilsson, H. (1993). Rhythmic contractions of isolated small arteries from rat: influence of the endothelium. *Acta Physiol Scand.*, 148:153–163.
- Haddock, R. E., Grayson, T. H., Brackenbury, T. D., Meaney, K. R., Neylon, C. B., Sandow, S. L., and Hill, C. E. (2006). Endothelial coordination of

- cerebral vasomotion via myoendothelial gap junctions containing connexins 37 and 40. *Am J Physiol Heart Circ Physiol*, 291:2047–2056.
- Hamada, H., Damron, D. S., Hong, S. J., Van Wagoner, D. R., and Murray, P. A. (1997). Phenylephrine-induced Ca^{2+} oscillations in canine pulmonary artery smooth muscle cells. *Circ Res*, 81:812–823.
- Harris, A. L. (2007). Connexin channel permeability to cytoplasmic molecules. *Prog Biophys Mol Biol*, 94:120–143.
- He, D. S., Jiang, J. X., Taffet, S. M., and Burt, J. M. (1999). Formation of heteromeric gap junction channels by connexins 40 and 43 in vascular smooth muscle cells. *Proc Natl Acad Sci U S A*, 96:6495–6500.
- Heyman, N. S., Kurjiaka, D. T., Ek Vitorin, J. F., and Burt, J. M. (2009). Regulation of gap junctional charge selectivity in cells coexpressing connexin 40 and connexin 43. *Am J Physiol Heart Circ Physiol*, 297:450–459.
- Hilgers, R. H. and Webb, R. C. (2005). Molecular aspects of arterial smooth muscle contraction: focus on rho. *Exp Biol Med (Maywood)*, 230:829–835.
- Hill, C. E., Eade, J., and Sandow, S. L. (1999). Mechanisms underlying spontaneous rhythmical contractions in irideal arterioles of the rat. *J Physiol*, 521 (Pt 2):507516.
- Hirose, K., Kadowaki, S., Tanabe, M., Takeshima, H., and Iino, M. (1999). Spatiotemporal dynamics of inositol 1,4,5-trisphosphate that underlies complex Ca^{2+} mobilization patterns. *Science*, 284:1527–1530.
- Höfer, T., Politi, A., and Heinrich, R. (2001). Intercellular Ca^{2+} wave propagation through gap-junctional Ca^{2+} diffusion: a theoretical study. *Biophys J*, 80:75–87.
- Höfer, T., Venance, L., and Giaume, C. (2002). Control and plasticity of intercellular calcium waves in astrocytes: a modeling approach. *J Neurosci*, 22:4850–4859.
- Iino, M., Kasai, H., and Yamazawa, T. (1994). Visualization of neural control of intracellular Ca^{2+} concentration in single vascular smooth muscle cells in situ. *EMBO J*, 13:5026–5031.

- Iino, M., Yamazawa, T., Miyashita, Y., Endo, M., and Kasai, H. (1993). Critical intracellular Ca^{2+} concentration for all-or-none Ca^{2+} spiking in single smooth muscle cells. *EMBO J*, 12:5287–5291.
- Imtiaz, M. S., Smith, D. W., and van Helden, D. F. (2002). A theoretical model of slow wave regulation using voltage-dependent synthesis of inositol 1,4,5-trisphosphate. *Biophys J*, 83:1877–1890.
- Isakson, B. E., Ramos, S. I., and Duling, B. R. (2007). Ca^{2+} and inositol 1,4,5-trisphosphate-mediated signaling across the myoendothelial junction. *Circ Res*, 100:246–254.
- Itoh, T., Seki, N., Suzuki, S., Ito, S., Kajikuri, J., and Kuriyama, H. (1992). Membrane hyperpolarization inhibits agonist-induced synthesis of inositol 1,4,5-trisphosphate in rabbit mesenteric artery. *J Physiol*, 451:307–328.
- Jackson, W. F. (1988). Oscillations in active tension in hamster aortas: role of the endothelium. *Blood Vessels*, 25:144–156.
- Jacobsen, J. C., Aalkjaer, C., Nilsson, H., Matchkov, V. V., Freiberg, J., and Holstein-Rathlou, N. H. (2007). A model of smooth muscle cell synchronization in the arterial wall. *Am J Physiol Heart Circ Physiol*, 293:229–237.
- Jaffe, L. F. (2010). Fast calcium waves. *Cell Calcium*, 48:102–113.
- Jaggar, J. H. (2001). Intravascular pressure regulates local and global Ca^{2+} signaling in cerebral artery smooth muscle cells. *Am J Physiol Cell Physiol*, 281:439–448.
- Ji, G., Feldman, M., Doran, R., Zipfel, W., and Kotlikoff, M. I. (2006). Ca^{2+} -induced Ca^{2+} -release through localized Ca^{2+} uncaging in smooth muscle. *J Gen Physiol*, 127:225–235.
- Jones, T. W. (1852). Discovery that the veins of the bat's wing (which are furnished with valves) are endowed with rythmical contractility, and that the onward flow of blood is accelerated by each contraction. *Phil. Trans. R. Soc. Lond.*, 142:131–136.
- Kanagaratnam, P., Rothery, S., Patel, P., Severs, N. J., and Peters, N. S. (2002). Relative expression of immunolocalized connexins 40 and 43

- correlates with human atrial conduction properties. *J Am Coll Cardiol*, 39:116–123.
- Kanaporis, G., Mese, G., Valiuniene, L., White, T. W., Brink, P. R., and Valiunas, V. (2008). Gap junction channels exhibit connexin-specific permeability to cyclic nucleotides. *J Gen Physiol*, 131:293–305.
- Kangasniemi, K. and Opas, H. (1997). *Suomalainen lkriekeskus 1. Toinen painos*. WSOY, Porvoo.
- Karaki, H., Ozaki, H., Hori, M., Mitsui-Saito, M., Amano, K., Harada, K., Miyamoto, S., Nakazawa, H., Won, K., and Sato, K. (1997). Calcium movements, distribution, and functions in smooth muscle. *Pharmacol Rev.*, 49:157–230.
- Knot, H. J., Standen, N. B., and Nelson, M. T. (1998). Ryanodine receptors regulate arterial diameter and wall $[Ca^{2+}]$ in cerebral arteries of rat via Ca^{2+} -dependent k^+ channels. *J Physiol*, 508 (Pt 1):211–221.
- Koenigsberger, M., Sauser, R., Lamboley, M., Bény, J. L., and Meister, J. J. (2004). Ca^{2+} dynamics in a population of smooth muscle cells: Modeling the recruitment and synchronization. *Biophys J*, 87:92–104.
- Koenigsberger, M., Seppey, D., Bény, J. L., and Meister, J. J. (2010). Mechanisms of propagation of intercellular calcium waves in arterial smooth muscle cells. *Biophys J*, 99:333–343.
- Kvandal, P., Stefanovska, A., Veber, M., Kvermmo, H. D., and Kirkebø en, K. A. (2003). Regulation of human cutaneous circulation evaluated by laser doppler flowmetry, iontophoresis, and spectral analysis: importance of nitric oxide and prostaglandines. *Microvascular Research*, 65(3):160 – 171.
- Kwak, B. R. and Jongsma, H. J. (1996). Regulation of cardiac gap junction channel permeability and conductance by several phosphorylating conditions. *Mol Cell Biochem*, 157:93–99.
- Lamboley, M., Schuster, A., Bény, J. L., and Meister, J. J. (2003). Recruitment of smooth muscle cells and arterial vasomotion. *Am J Physiol Heart Circ Physiol*, 285:562–569.

- Lamont, C. and Wier, W. G. (2004). Different roles of ryanodine receptors and inositol (1,4,5)-trisphosphate receptors in adrenergically stimulated contractions of small arteries. *Am J Physiol Heart Circ Physiol*, 287:617–625.
- Lavado, E., Sanchez-Abarca, L. I., Tabernero, A., Bolaños, J. P., and Medina, J. M. (1997). Oleic acid inhibits gap junction permeability and increases glucose uptake in cultured rat astrocytes. *J Neurochem*, 69:721–728.
- Lee, C. H., Poburko, D., Kuo, K. H., Seow, C. Y., and van Breemen, C. (2002). Ca^{2+} oscillations, gradients, and homeostasis in vascular smooth muscle. *Am J Physiol Heart Circ Physiol*, 282:1571–1583.
- Lewis, R. S. (2003). Calcium oscillations in t-cells: mechanisms and consequences for gene expression. *Biochem Soc Trans*, 31:925–929.
- Mahler, F., Muheim, M. H., Intaglietta, M., Bollinger, A., and Anliker, M. (1979). Blood pressure fluctuations in human nailfold capillaries. *Am J Physiol*, 236:888–893.
- Marchenko, S. M. and Sage, S. O. (1994). Smooth muscle cells affect endothelial membrane potential in rat aorta. *Am J Physiol*, 267:804–811.
- Martinez, A. D., Hayrapetyan, V., Moreno, A. P., and Beyer, E. C. (2002). Connexin43 and connexin45 form heteromeric gap junction channels in which individual components determine permeability and regulation. *Circ Res*, 90:1100–1107.
- Matchkov, V. V., Rahman, A., Peng, H., Nilsson, H., and Aalkjaer, C. (2004). Junctional and nonjunctional effects of heptanol and glycyrrhetic acid derivatives in rat mesenteric small arteries. *Br J Pharmacol*, 142:961–972.
- Mauban, J. R., Lamont, C., Balke, C. W., and Wier, W. G. (2001). Adrenergic stimulation of rat resistance arteries affects Ca^{2+} sparks, Ca^{2+} waves, and Ca^{2+} oscillations. *Am J Physiol Heart Circ Physiol*, 280:2399–2405.
- McCarron, J. G., Chalmers, S., MacMillan, D., and Olson, M. L. (2010). Agonist-evoked Ca^{2+} wave progression requires Ca^{2+} and IP_3 . *J Cell Physiol*, 224:334–344.

- McCarron, J. G., MacMillan, D., Bradley, K. N., Chalmers, S., and Muir, T. C. (2004). Origin and mechanisms of Ca^{2+} waves in smooth muscle as revealed by localized photolysis of caged inositol 1,4,5-trisphosphate. *J Biol Chem*, 279:8417–8427.
- Meşe, G., Richard, G., and White, T. W. (2007). Gap junctions: basic structure and function. *J Invest Dermatol*, 127:2516–2524.
- Mehta, P. P., Yamamoto, M., and Rose, B. (1992). Transcription of the gene for the gap junctional protein connexin43 and expression of functional cell-to-cell channels are regulated by camp. *Mol Biol Cell*, 3:839–850.
- Mirieli, V. A., Mauban, J. R., Blaustein, M. P., and Wier, W. G. (1999). Local and cellular Ca^{2+} transients in smooth muscle of pressurized rat resistance arteries during myogenic and agonist stimulation. *J Physiol*, 518 (Pt 3):815–824.
- Miyakawa, T., Maeda, A., Yamazawa, K., Hirose, K., Kurosaki, T., and Lino, M. (1999). Encoding of Ca^{2+} signals by differential expression of IP_3 receptor subtypes. *Embo J*, 18:1303–1308.
- Moore, L. K., Beyer, E. C., and Burt, J. M. (1991). Characterization of gap junction channels in a7r5 vascular smooth muscle cells. *Am J Physiol*, 260:975–981.
- Nakano, A. (2002). Spinning-disk confocal microscopy - a cutting-edge tool for imaging membrane traffic. *Cell structure and function*, 27:394–355.
- Nasu, T. (1990). Effects of cooling on smooth muscle contraction. *Comp Biochem Physiol A Comp Physiol*, 95:201–207.
- Nilsson, H. and Aalkjaer, C. (2003). Vasomotion: mechanisms and physiological importance. *Mol Interv*, 3:79–89.
- Oishi, H., Schuster, A., Lambole, M., Stergiopoulos, N., Meister, J. J., and Bény, J. L. (2002). Role of membrane potential in vasomotion of isolated pressurized rat arteries. *Life Sci*, 71:2239–2248.
- Okazaki, K., Seki, S., Kanaya, N., Hattori, J., Tohse, N., and Namiki, A. (2003). Role of endothelium-derived hyperpolarizing factor in phenylephrine-induced oscillatory vasomotion in rat small mesenteric artery. *Anesthesiology*, 98:1164–1171.

- Omote, M. and Mizusawa, H. (1993). The role of sarcoplasmic reticulum in endothelium-dependent and endothelium-independent rhythmic contractions in the rabbit mesenteric artery. *Acta Physiol Scand*, 149:15–21.
- Parthimos, D., Edwards, D. H., and Griffith, T. M. (1999). Minimal model of arterial chaos generated by coupled intracellular and membrane Ca^{2+} oscillators. *Am J Physiol*, 277:1119–1144.
- Pascoal, I. F., Lindheimer, M. D., Nalbantian-Brandt, C., and Umans, J. G. (1998). Preeclampsia selectively impairs endothelium-dependent relaxation and leads to oscillatory activity in small omental arteries. *J Clin Invest*, 101:464–470.
- Paulson, A. F., Lampe, P. D., Meyer, R. A., TenBroek, E., Atkinson, M. M., Walseth, T. F., and Johnson, R. G. (2000). Cyclic amp and ldl trigger a rapid enhancement in gap junction assembly through a stimulation of connexin trafficking. *J Cell Sci*, 113 (Pt 17):3037–3049.
- Peng, H., Ivarsen, A., Nilsson, H., and Aalkjaer, C. (1998). On the cellular mechanism for the effect of acidosis on vascular tone. *Acta Physiol Scand.*, 164:517–525.
- Peng, H., Matchkov, V., Ivarsen, A., Aalkjaer, C., and Nilsson, H. (2001). Hypothesis for the initiation of vasomotion. *Circ Res*, 88:810–815.
- Porret, C. A. (1997). *Caractéristiques et contrôle de la vasomotricité artérielle: rôle de paramètres physiques*. PhD thesis, Thesis no.: 1721, EPFL, Switzerland.
- Porret, C. A., Stergiopulos, N., Hayoz, D., Brunner, H. R., and Meister, J. J. (1995). Simultaneous ipsilateral and contralateral measurements of vasomotion in conduit arteries of human upper limbs. *Am J Physiol*, 269:1852–1858.
- Rücker, M., Strobel, O., Vollmar, B., Roesken, F., and Menger, M. D. (2000). Vasomotion in critically perfused muscle protects adjacent tissues from capillary perfusion failure. *Am J Physiol Heart Circ Physiol*, 279:550–558.
- Rüegg, U. T., Doyle, V. M., Zuber, J. F., and Hof, R. P. (1985). A smooth muscle cell line suitable for the study of voltage sensitive calcium channels. *Biochem Biophys Res Commun*, 130:447–453.

- Ruehlmann, D. O., Lee, C. H., Poburko, D., and van Breemen, C. (2000). Asynchronous Ca^{2+} waves in intact venous smooth muscle. *Circ Res*, 86:72–79.
- Saez, J. C., Berthoud, V. M., Branes, M. C., Martinez, A. D., and Beyer, E. C. (2003). Plasma membrane channels formed by connexins: their regulation and functions. *Physiol Rev*, 83:1359–1400.
- Sanders, K. M. (2001). Invited review: mechanisms of calcium handling in smooth muscles. *J Appl Physiol*, 91:1438–1449.
- Sanderson, M. J., Charles, A. C., and Dirksen, E. R. (1990). Mechanical stimulation and intercellular communication increases intracellular Ca^{2+} in epithelial cells. *Cell Regul*, 1:585–596.
- Segal, S. S. and Kurjiaka, D. T. (1995). Coordination of blood flow control in the resistance vasculature of skeletal muscle. *Med Sci Sports Exerc*, 27:1158–1164.
- Sell, M., Boldt, W., and Markwardt, F. (2002). Desynchronising effect of the endothelium on intracellular Ca^{2+} concentration dynamics in vascular smooth muscle cells of rat mesenteric arteries. *Cell Calcium*, 32:105–120.
- Sepey, D., Sauser, R., Koenigsberger, M., Bény, J. L., and Meister, J. J. (2008). Does the endothelium abolish or promote arterial vasomotion in rat mesenteric arteries? explanations for the seemingly contradictory effects. *J Vasc Res*, 45:416–426.
- Sepey, D., Sauser, R., Koenigsberger, M., Bény, J. L., and Meister, J. J. (2010). Intercellular calcium waves are associated with the propagation of vasomotion along arterial strips. *Am J Physiol Heart Circ Physiol*, 298:488–496.
- Sneyd, J., Charles, A. C., and Sanderson, M. J. (1994). A model for the propagation of intercellular calcium waves. *Am J Physiol*, 266:293–302.
- Sneyd, J., Wetton, B. T., Charles, A. C., and Sanderson, M. J. (1995). Intercellular calcium waves mediated by diffusion of inositol trisphosphate: a two-dimensional model. *Am J Physiol*, 268:1537–1545.

- Sonnleitner, A., Conti, A., Bertocchini, F., Schindler, H., and Sorrentino, V. (1998). Functional properties of the ryanodine receptor type 3 (ryr3) Ca^{2+} release channel. *EMBO J*, 17:2790–2798.
- Stansberry, K. B., Shapiro, S. A., Hill, M. A., McNitt, P. M., Meyer, M. D., and Vinik, A. I. (1996). Impaired peripheral vasomotion in diabetes. *Diabetes Care*, 19:715–721.
- Straub, S. V., Giovannucci, D. R., and Yule, D. I. (2000). Calcium wave propagation in pancreatic acinar cells: functional interaction of inositol 1,4,5-trisphosphate receptors, ryanodine receptors, and mitochondria. *J Gen Physiol*, 116:547–560.
- Takeshima, H., Nishimura, S., Matsumoto, T., Ishida, H., Kangawa, K., Minamino, N., Matsuo, H., Ueda, M., Hanaoka, M., and Hirose, T. (1989). Primary structure and expression from complementary dna of skeletal muscle ryanodine receptor. *Nature*, 339(6224):439–445.
- Tallini, Y. N., Brekke, J. F., Shui, B., Doran, R., Hwang, S. M., Nakai, J., Salama, G., Segal, S. S., and Kotlikoff, M. I. (2007). Propagated endothelial Ca^{2+} waves and arteriolar dilation in vivo: measurements in cx40^{BAC}-gcamp2 transgenic mice. *Circ Res*, 101:1300–1309.
- Tare, M., Coleman, H. A., and Parkington, H. C. (2002). Glycyrrhetic derivatives inhibit hyperpolarization in endothelial cells of guinea pig and rat arteries. *Am J Physiol Heart Circ Physiol*, 282:335–341.
- Tasker, P. N., Taylor, C. W., and Nixon, G. F. (2000). Expression and distribution of IP₃ receptor subtypes in proliferating vascular smooth muscle cells. *Biochem Biophys Res Commun*, 273:907–912.
- Toma, I., Bansal, E., Meer, E. J., Kang, J. J., Vargas, S. L., and Peti-Peterdi, J. (2008). Connexin 40 and atp-dependent intercellular calcium wave in renal glomerular endothelial cells. *Am J Physiol Regul Integr Comp Physiol*, 294:1769–1776.
- Toyofuku, T., Yabuki, M., Otsu, K., Kuzuya, T., Hori, M., and Tada, M. (1998). Intercellular calcium signaling via gap junction in connexin-43-transfected cells. *J Biol Chem*, 273:1519–1528.

- Tsai, A. G. and Intaglietta, M. (1993). Evidence of flowmotion induced changes in local tissue oxygenation. *Int J Microcirc Clin Exp*, 12:75–88.
- Tsai, M. L., Watts, S. W., Loch-Caruso, R., and Webb, R. C. (1995). The role of gap junctional communication in contractile oscillations in arteries from normotensive and hypertensive rats. *J Hypertens*, 13:1123–1133.
- van Kempen, M. J. and Jongsma, H. J. (1999). Distribution of connexin37, connexin40 and connexin43 in the aorta and coronary artery of several mammals. *Histochem Cell Biol*, 112:479–486.
- Vessey, J. P., Lalonde, M. R., Mizan, H. A., Welch, N. C., Kelly, M. E., and Barnes, S. (2004). Carbenoxolone inhibition of voltage-gated ca channels and synaptic transmission in the retina. *J Neurophysiol*, 92:1252–1256.
- von der Weid, P. Y. and Bény, J. L. (1993). Simultaneous oscillations in the membrane potential of pig coronary artery endothelial and smooth muscle cells. *J Physiol*, 471:13–24.
- Walker-Caprioglio, H. M., Trotter, J. A., Mercure, J., Little, S. A., and McGuffee, L. J. (1991). Organization of rat mesenteric artery after removal of cells of extracellular matrix components. *Cell Tissue Res*, 264:63–77.
- Wang, R., Wu, Y., Tang, G., Wu, L., and Hanna, S. T. (2000). Altered l-type Ca^{2+} channel currents in vascular smooth muscle cells from experimental diabetic rats. *Am J Physiol Heart Circ Physiol*, 278:714–722.
- Wang, S. S., Alousi, A. A., and Thompson, S. H. (1995). The lifetime of inositol 1,4,5-trisphosphate in single cells. *J Gen Physiol*, 105:149–171.
- Wede, O. K., Löfgren, M., Li, Z., Paulin, D., and Arner, A. (2002). Mechanical function of intermediate filaments in arteries of different size examined using desmin deficient mice. *Journal of Physiol.*, 540:941–949.
- Wu, X. and Davis, M. J. (2001). Characterization of stretch-activated cation current in coronary smooth muscle cells. *Am J Physiol Heart Circ Physiol*, 280:1751–1761.
- Wynne, B. M., Chiao, C., and Webb, R. C. (2009). Vascular smooth muscle cell signaling mechanisms for contraction to angiotensin ii and endothelin-1. *J Am Soc Hypertens.*, 3:84–95.

- Yamamoto, Y., Klemm, M. F., Edwards, F. R., and Suzuki, H. (2001). Intercellular electrical communication among smooth muscle and endothelial cells in guinea-pig mesenteric arterioles. *J Physiol*, 535:181–195.
- Yao, J., Oite, T., and Kitamura, M. (2009). Gap junctional intercellular communication in the juxtaglomerular apparatus. *Am J Physiol Renal Physiol*, 296:939–946.
- Young, R. C., Schumann, R., and Zhang, P. (2002). The signaling mechanisms of long distance intercellular calcium waves (far waves) in cultured human uterine myocytes. *J Muscle Res Cell Motil*, 23:279–284.
- Zahradníková, A., Minarovic, I., and Zahradník, I. (2007). Competitive and cooperative effects of bay k8644 on the l-type calcium channel current inhibition by calcium channel antagonists. *J Pharmacol Exp Ther*, 322:638–645.
- Zalk, R., Lehnart, S. E., and Marks, A. R. (2007). Modulation of the ryanodine receptor and intracellular calcium. *Annu Rev Biochem*, 76:367–385.
- Zang, W. J., Balke, C. W., and Wier, W. G. (2001). Graded alpha1-adrenoceptor activation of arteries involves recruitment of smooth muscle cells to produce 'all or none' Ca²⁺ signals. *Cell Calcium*, 29:327–334.

Curriculum Vitæ

Name: Nadia Halidi
Born: 8th August 1977; Budapest (Hungary)
Nationality: Hungarian
Family status: Married
Language skills: English: fluent; French: intermediate; Italian: intermediate

Education

2007– PhD student at the Laboratory of Cell Biophysics, EPFL; Lausanne (Switzerland). Supervisor: Prof. Jean-Jacques Meister
2001–2006 Studies Chemistry at the Faculty of Natural Sciences, University of Pécs (M.Sc. in Chemistry 2006)
1997–2002 Studies Physics at the Faculty of Natural Sciences, University of Pécs; Pécs, Hungary (M.Sc. in Physics 2002)

Professional Experience

2009–2010 Supervising student projects, undergraduate level, EPFL

- 2007–2010 Teaching assistant: Laboratory practice in Physics; Deterministic chaos and ultrasound for 4th year physics students, Metrology for 1st year Physics and Life Science students, EPFL
- 2005–2006 Lecturer: Biophysics in both Hungarian and English (occasional)*
- 2005 Teaching assistant: Computational Neuroscience, at the Center for Complex Systems Studies, Kalamazoo College, Kalamazoo, MI, USA
- 2003–2006 Lecturer: Physical Basis of Biophysics, Hungarian and English programs*
- 2003–2006 Teaching assistant: Laboratory practice in Biophysics Hungarian and English programs*
- 2002–2006 Research assistant at the Department of Biophysics, Faculty of Medicine, University of Pécs. Supervisor: Prof. Béla Somogyi
- other training**
- 2003 Two weeks practice in electrophysiology at the Department of Biophysics and Cell Biology, Medical and Health Science Center, University of Debrecen, Debrecen (Hungary).

*at the University of Pécs, Faculty of Medicine

Scholarships and Awards

- 2010 Distinguished teaching assistant award, Ecole Polytechnique Fédérale de Lausanne; Lausanne (Switzerland)
- 2006 Best poster prize at the 36th Hungarian Membrane Transport Conference; Sümeg (Hungary)
- 2004 Full Scholarship for the 8th European Symposium on Calcium; Cambridge (UK)
- 2003 Best poster prize at the 33rd Hungarian Membrane Transport Conference; Sümeg (Hungary)
- 1999–2000 Erasmus Scholarship for 5 months at the University degli Studi L'Aquila; L'Aquila (Italy)

Publications

N. Halidi, F. Alonso, J. M. Burt, JL Bény, JA. Haefliger and JJ. Meister. *Intercellular calcium waves in primary cultured rat mesenteric smooth muscle cells are mediated by connexin43*. Submitted.

N. Halidi, FX. Boittin, JL. Bény and JJ. Meister. *Propagation of fast and slow intercellular Ca²⁺ waves in primary cultured arterial smooth muscle cells..* In preparation.

Refereed conference proceedings

N. Halidi, A. Formey, FX. Boittin, JL. Bény and JJ. Meister. *Propagation of fast and slow intercellular calcium waves in primary cultured smooth muscle cells*. Biophysical Journal 2009, vol. 96, issue 3, pp. 285a-285a.

N. Halidi, A. Visegrády, A. Volford, Z. Noszticzius, B. Somogyi. *Effects of inositol 1,4,5-trisphosphate concentration on intracellular calcium wave characteristics*. Cytometry Part A 2003, 56A:120-140.

Conference Activities

p: poster presentation, *o*: oral presentation

- p* N. Halidi, JL. Bény, JJ. Meister. (2010) *Propagation of intercellular Ca²⁺ waves in arterial smooth muscle cells*. **XXXIX European Muscle Conference**; Padova (Italy)
- p* F. Alonso, JA. Haefliger, JJ. Meister, N. Halidi. (2009) *Connexins mediate intercellular calcium waves between primary rat mesenteric smooth muscle cells*. **International Gap Junction Conference**; Sedona (AZ, USA)
- p* N. Halidi, A. Formey, FX. Boittin, JL. Bény, JJ. Meister. (2009) *Propagation of fast and slow intercellular calcium waves in primary cultured smooth muscle cells*. **The Biophysical Society's 53rd Annual Meeting**; Boston (MA, USA)

- o* N. Halidi. *Confocal Microscopy: Theoretical Considerations*. Second European Network of Excellence on Embryo Implantation Control (EMBIC) Summer School entitled **Molecular Mechanisms of Implantation**; July 2006, Pécs (Hungary)
- p & o* N. Halidi, A. Volford, Z. Noszticzius, B. Somogyi. (2006) *Initiation of local Ca^{2+} oscillations*. (In Hungarian) **36th Hungarian Membrane Transport Conference**; Sümeg (Hungary)
- p* N. Halidi, A. Volford, Z. Noszticzius, B. Somogyi. (2005) *Minimal Requirements for Ca^{2+} Wave Initiation with Local and Global Perturbation: Theoretical Study*. **Symposium on Quantitative Biology and Modeling**; East Lansing (MI, USA)
- p* N. Halidi, A. Visegrády, A. Volford, Z. Noszticzius, B. Somogyi. (2005) *Minimal requirements of perturbation for Ca^{2+} wave initiation*. **EMBO-HHMI Central European Scientists Meeting**; Budapest (Hungary)
- p* N. Halidi, A. Visegrády, A. Volford, Z. Noszticzius, B. Somogyi. (2004) *Modelling calcium waves initiated with local and global perturbation*. **8th European Symposium on Calcium**; Cambridge (UK)
- p* N. Halidi, A. Visegrády, A. Volford, Z. Noszticzius, B. Somogyi. (2003) *Initiation of intracellular Ca^{2+} waves with local and global perturbation: model calculations*. **Nonlinear phenomena in chemistry, ESF REACTOR workshop**; Budapest.
Hungarian version was presented at the **33rd Hungarian Membrane Transport Conference** (2003); Sümeg (Hungary) and **21st Hungarian Biophysical Society meeting** (2003); Szeged (Hungary)
- o* N. Halidi. *Investigating perturbation methods for intracellular calcium wave initiation*. (In Hungarian) **1st Doctoral Students' Symposium** Regional Committee of the Hungarian Academy of Sciences at Pécs, Molecular Biology Committee, December 2002; Pécs (Hungary)
- p* N. Halidi, A. Visegrády, A. Volford, Z. Noszticzius, B. Somogyi. (2002) *Propagation of intracellular calcium waves in a heterogeneous medium*. (In Hungarian) **32nd Hungarian Membrane Transport Conference**; Sümeg (Hungary)

- p* N. Halidi, A. Visegrády, A. Volford, Z. Noszticzius, B. Somogyi. (2002) *Effects of inositol 1,4,5-trisphosphate concentration on intracellular calcium wave characteristics. (In Hungarian) III. Cell Analysis Conference; Budapest (Hungary)*

Professional skills

Cellular biology	Cell culture; isolation and culture of primary smooth muscle cells (rat mesenteric arteries); immunofluorescence staining; fluorescent calcium imaging.
Microscopy	Phase contrast and differential interference contrast (DIC) microscopy; live cell imaging; fluorescence and confocal microscopy.
Other	Building flow chambers; micromanipulation; micro-contact printing of proteins for cell patterning.
Software skills	For image processing and analysis: ImageJ, MetaMorph, MATLAB. For mathematical modeling: MATLAB, GNU Octave, Maple.

Hobbies

Road cycling, geocaching, ballet, swimming, skiing, collecting stamps and painting.